Diss. ETH No. 14036

TAILORING MIXED SELF-ASSEMBLED MONOLAYERS (SAMS) FOR ADHESION STUDIES

DISSERTATION

submitted to the

EIDGENÖSSICHE TECHNISCHE HOCHSCHULE ZÜRICH

for the degree of

DOCTOR OF TECHNICAL SCIENCES

presented by

HENRIK PERSSON

M. Sc. Chemical Engineering, Lund University, Sweden
born July 18th, 1970
citizen of Sweden

accepted on the recommendation of

Prof. Dr. Ulrich W. Suter, examiner
Prof. Dr. Nicholas D. Spencer, co-examiner
PD. Dr. Walter Caseri, co-examiner

Zürich, 2000

This thesis deals with the application of self-assembled monolayers (SAMs) to the study of the influence of chemical interactions on adhesion. The basic mechanisms of adhesion, although of considerable scientific and technological interest, are not yet satisfactorily understood, mainly due to limited understanding of the adhesive-surface interactions. The study of such phenomena requires a detailed knowledge of the surfaces to be studied. Self-assembled monolayers and mixed monolayers with different terminal groups allow a convenient and well-established technique to produce thin layers with minimal effort and good reproducibility. These thin layers are excellent model systems with a unprecedented control in surface properties, and their composition of the surface groups can be varied easily by chemical reactions. Such modifications on pre-established monolayers are described in this thesis.

Till Mamma och Pappa

"This writing business. Pencils and what-not.
Overrated if you ask me. Silly stuff.
Nothing in it."

The old grey donkey Eeyore in
"*Winnie-the-Pooh*" by A. A. Milne

Table of Contents

Symbols and Notation

AFM	Atomic Force Microscopy
AR-XPS	Angle Resolved X-ray Photoelectron Spectroscopy
ATR	Attenuated Total Reflection
ar	aromatic
C	Celsius
CVD	Chemical Vapor Deposition
cm	centimetre
DDT	Dodecanethiol
DGEBA	Diglycidyl ether of bisphenol-A
DRIFT	Diffuse Reflection Infrared Fourier Transformation
d	thickness
ESCA	Electron Spectroscopy for Chemical Analysis
eV	electron Volts
FT-IR	Fourier Transformation Infrared Spectroscopy
GIR	Grazing Incidence Reflection
h	hours
IR	Infrared Spectroscopy
K	Kelvin
k_{sub}	extinction coefficient of the substrate
kcal	kilocalories
kJ	kiloJoules
LB	Langmuir-Blodgett
LFM	Lateral Force Microscopy
M	Molar
MBE	Molecular Beam Epitaxy
MHA	16-Mercapto-1-hexadecanoic acid
MHD	16-Mercapto-1-hexadecanol
MPA	3-Mercaptopropanoic acid
MUD	1-Mercapto-11-undecanol
mM	millimolar
mbar	millibar
mm	millimetre
n_{film}	real part of reflection index of the film
n_{sub}	real part of reflection index of the film
nm	nanometre
OTS	Octadecyltrichlorosilane
ODT	Octadecanthiol
PDI	Phenylenediisocyanate
PEI	Poly(ethylenimine)
PVD	Physical Vapor Deposition
QCM	Quartz Crystal Microbalance
R_a	average roughness
SA	Self-Assembly
SAM	Self-Assembled Monolayer
SAWD	Surface Acoustic Wave Device

SEM	Scanning Electron Microscopy
SFG	Sum Frequency Generation spectroscopy
STM	Scanning Tunnelling Microscopy
T_g	Glass transition temperature
ToF-SIMS	Time of Flight Secondary Ion Mass Spectroscopy
TPD	Temperature Programmed Desorption
UHV	Ultra High Vacuum
UV	Ultraviolet
UPS	Ultraviolet Photoelectron Spectroscopy
WA	Thermodynamic Work of Adhesion
XPS	X-ray Photoelectron Spectroscopy
y_{MUD}	MUD fraction in solution (relative mole fraction)
Å	Ångström
γ_{lv}	liquid vapour interfacial tension
γ_{sl}	solid liquid interfacial tension
γ_{sv}	solid vapour interfacial tension
δ	deformation vibration
ν_{as}	asymmetric stretch vibration
ν_s	symmetric stretch vibration
μCP	microcontact printing
Ξ_{MUD}	MUD fraction at the surface (relative surface fraction)

Abstract

This thesis deals with the application of self-assembled monolayers (SAMs) to the study of the influence of chemical interactions on adhesion. The basic mechanisms of adhesion, although of considerable scientific and technological interest, are not yet satisfactorily understood, mainly due to limited understanding of the adhesive-surface interactions. The study of such phenomena requires a detailed knowledge of the surfaces to be studied. Self-assembled monolayers and mixed monolayers with different terminal groups allow a convenient and well-established technique to produce thin layers with minimal effort and good reproducibility. These thin layers are excellent model systems with a unprecedented control in surface properties, and their composition of the surface groups can be varied easily.

In this thesis, the surface composition and wetting properties of mixed monolayers made of 1-dodecanethiol (DDT) and 1-mercapto-11-undecanol (MUD) are discussed together with the characterisation of the underlaying gold substrate (chapter 2). The surface fraction of MUD (Ξ_{MUD}), as determined by XPS, is below the related fraction in solution (y_{MUD}) if y_{MUD} is below 0.7-0.8, and this is an effect of the used solvent. At fractions of MUD above 0.7-0.8 in the solution, the surface fraction is found to be similar to the fraction in solution ($\Xi_{MUD} \approx y_{MUD}$). This is believed to be due to hydrogen bonding between adjacent hydroxyl groups of adsorbed MUD molecules. Comparison of XPS measurements with results derived from contact angle measurements and interpreted by the Cassie as well as the Israelachvili and Gee equation suggests that the resulting monolayers are randomly mixed for SAMs adsorbed from solutions with $0.2 \leq y_{MUD} \leq 0.7$. This assumption is based on the better fit of the data by the Israelachvili and Gee equation. For $y_{MUD} > 0.7$, the system might be separated into domains or patches according to the better fit to the Cassie equation.

The MUD monolayer and the mixed monolayers react under mild conditions with 1,4-phenylene diisocyanate (PDI) as confirmed by infrared spectroscopy, XPS, ellipsometry and contact angle measurements. The optimal reaction conditions were found at a temperature of 40 °C, a MUD concentration of 0.1 M, and a reaction time of 2 h. Higher reaction

temperatures result in desorption of the underlaying SAM. The derivatization of monolayers with PDI is accomplished by a reaction between hydroxyl groups in the SAM and one of the isocyanates in PDI. A carbamate group is formed, while the other isocyanate remains unaffected and reactive as confirmed by IR investigations. XPS measurements lead to the conclusion that the surface hydroxyl groups have been converted to a high extent (93 (±10)%), independent of Ξ_{MUD}. The carbamate groups and, consequently also the residual phenylene isocyanate moieties, are preferentially oriented with the carbonyl groups parallel and the 1,4-phenylene axis perpendicular to the surface.

The PDI-activated SAMs react under mild conditions with an extraordinarily broad variety of functional groups and, accordingly, we have performed model reactions with some substances, i.e., alcohols, amines, and water. The results from GIR spectroscopy imply high extents of reaction of the isocyanate groups under the reaction conditions applied here for all substances (water, methanol, hexanol, diethylamine, and 1,2-diaminoethane) except for 3,3-dimethylbutanol, probably due to a slow rate or insufficient space for completion of the reaction (steric hindrance of the bulky side groups). XPS measurements were undertaken of the modified surface to determine the composition of elements in the outermost surface layer. The O/N ratios are in fairly good agreement with theoretical values suggesting a high yield of the modification reactions.

Finally, self-assembled monolayers with tailored concentrations of functional groups were applied in adhesion studies performed with peel-tests. For both adhesive systems investigated (an epoxy adhesive as well as an acrylic acid copolymer adhesive), a higher concentration of functional groups in the substrate results in stronger peel forces. In the epoxy system, the monolayers terminating in NH_2-groups result in significantly higher adhesive forces than those found for monolayers terminating in OH-groups. This can be explained by the higher reactivity of amine-groups to form a covalent bond with the epoxy-ring. Hence, more covalent bonds between the adhesive and the substrate will be formed and these are accounting for the higher peel forces found. The suggested formation of covalent bonds at the interface are supported by XPS investigations where traces of sulphur and gold are found on the adhesive layer after peeling. In the copolymer system studied, the adhesive forces at the interface are suggested to rely upon physical interac-

tions such as van der Waals forces and hydrogen bonds. The difference between the two functional groups studied is barely significant and is believed to originate in the higher electronegativity of oxygen resulting in stronger hydrogen bonds and van der Waals forces at the interface.

Zusammenfassung

Diese Doktorarbeit beschäftigt sich mit der Verwendung von selbst-organisierenden Monoschichten (SAMs), um chemische Interaktionen im Zusammenhang mit Adhäsion zu untersuchen. Die grundlegenden Mechanismen der Haftfestigkeit, obwohl von beträchtlichem wissenschaftlichen und technologischen Interesse, wird noch nicht befriedigend verstanden. Das ist hauptsächlich auf das begrenzte Verständnis der Ereignisse an der Grenzfläche zwischen Substrat und Klebstoff zurückzuführen. Das Studium solcher Phänomene erfordert die vollständige Kenntnis der untersuchten Oberflächen. Selbst-organisierende Monoschichten erlauben ein günstiges Verfahren, um dünne Schichten mit minimalem Aufwand und guter Reproduzierbarkeit herzustellen. Diese dünnen Schichten sind ausgezeichnete Modell-Systeme, welche einzigartige Kontrollen ihrer Eigenschaften erlauben, die sich durch Adsorption von gemischtenMonoschichten weitläufig ändern lassen.

Diese Arbeit behandelt die Oberflächenkonzentration und die Benetzungseigenschaften für gemischte Monoschichten, die mit 1-Dodecanthiol (DDT) und 1-Mercapto-11-undecanol (MUD) hergestellt werden. Diese Themen werden zusammen mit der Beschaffenheit des Gold-Substrats im Kapitel 2 behandelt. Der Anteil von MUD (Ξ_{MUD}) auf den Oberflächen wurde mit Röntgenphotoelektronspektroskopie (XPS) bestimmt. Er liegt deutlich unter dem Anteil von MUD in der Lösung (y_{MUD}), wenn y_{MUD} unter als 0.7-0.8 liegt. Das kann auf das verwendete Lösungsmittel zurückgeführt werden. y_{MUD} über 0.7-0.8 ergeben Oberflächenanteile (Ξ_{MUD}) ähnlich wie die in der Adsorptionslösung. Das kann mit Wasserstoffbrücken zwischen adsorbierten benachbarten Hydroxylgruppen erklärt werden. Ergebnisse von XPS-Messungen, welche mit den Kontaktwinkelmessungen verglichen werden, die mit der Gleichung von Cassie, beziehungsweise Israelachvili und Gee ausgewertet wurden, legen nahe anhand der besseren Übereinstimmung mit der Israelachvili und Gee Gleichung, dass die Monoschichten aus Lösungen mit $0.2 \leq y_{MUD} \leq 0.7$ zufällig gemischt sind. Für $y_{MUD} > 0.7$ kann die adsorbierte Schicht möglicherweise getrennt in Domänen vorliegen, wie durch die bessere Übereinstimmung mit der Cassie Gleichung, suggeriert wird.

MUD-Monoschichten und gemischte Monoschichten reagieren unter milden Bedingungen mit 1,4-Phenylendiisocyanat (PDI), was mit Infrarot Spektroskopie, XPS, Ellipsometrie und Kontaktwinkel-Messungen bestätigt wurde. Die optimalen Reaktionsbedingungen werden bei einer Temperatur von 40 °C, einer Konzentration von 0.1 M bezüglich PDI und einer Reaktionszeit von 2 h gefunden. Höhere Reaktionstemperaturen führen zu Desorption der adsorbiereten Monoschichten. Die Modifizierung der Monoschichten erfolgt durch eine chemische Reaktion zwischen Hydroxylgruppen der Monoschichten und einer der Isocyanatgruppen des PDI, die eine Urethanbindung bilden. Die andere Isocyanatgruppe bleibt unbeeinflusst und reaktiv, wie mit IR Spektroskopie bestätigt wurde. XPS-Messungen fuhren zur Schlussfolgerung, dass die Hydroxylgruppen der Oberfläche zu einem hohen Grad mit PDI reagieren. Die Ausbeute beträgt 93 (±10)%, unabhängig von Ξ_{MUD}. Die Urethangruppen und somit auch die Phenylisocyanatgruppen sind mit der Ketogruppe vorzüglich parallell zur Oberfläche orientiert, und die 1,4-Phenylenachse befindet sich senkrecht zur Oberfläche.

Die PDI-aktivierten Monoschichten reagieren unter milden Bedingungen mit einer außergewöhnlich breiten Vielfalt funktioneller Gruppen. Dementsprechend haben wir Modell-Reaktionen mit einigen Substanzen, z. B. Alkoholen, Aminen und Wasser durchgeführt. Die Ergebnisse der Infrarot-Spektroskopie weisen auf eine hohe Aubeute bezüglich Umsetzung die Modifizierung der Isocyanatgruppen, ausgenommen für 3,3-Dimethylbutanol. Das ist möglicherweise auf eine langsame Reaktionsgeschwindig-keit oder ungenügend Platz für eine Vervollständigung der Reaktion (steriche Hinderung der grossen Seitengruppen) zurückzuführen. XPS-Messungen wurden von den modifizierten Oberflächen durchgeführt, um die Zusammensetzung der Elemente in der äussersten Schicht zu bestimmen. Die O/N Verhältnis stimmt gut mit theoretischen Werten überein, was eine hohe Ausbeute der Reaktionen impliziert.

Zuletzt wurden selbst-organisierte Monoschichten mit massgeschneiderten Konzentrationen der funktionellen Gruppen für Adhäsionsstudien durch Schältests verwendet. Für beide untersuchten Klebstoffsysteme (ein Epoxy-Klebstoff und ein Acrylsäureester-Copolymer-Klebstoff) führt eine höhere Konzentration von funktionellen Gruppen zu höheren Schälkräften. Mit dem Epoxy-Klebstoff wurde für Proben mit Aminogruppen eine

deutlich stärkere Haftung gefunden als für Schichten mit Hydroxylgruppen. Das kann durch die höhere Reaktivität der Aminogruppen bezüglich Epoxyringen erklärt werden. Mehr kovalente Bindungen werden gebildet als für die hydroxylterminierten Schichten, und demnach werden auch höhere Schälkräfte gefunden. Die vorgeschlagenen kovalenten Bindungen wurden von XPS-Messungen unterstützt, wo Gold und Schwefel in der Klebeschicht nach dem Schälversuch gefunden wurde. Für den untersuchten Acrylsäureester-Copolymer-Klebstoff werden die Kräfte an der Grenzfläche auf physikalische Interaktionen zurückgeführt (z. B. van der Waals Kräfte und Wasserstoffbrücken). Die Unterschiede der verschiedenen funktionellen Gruppen auf den Oberflächen sind kaum merkbar und beruhen auf der höhere Elektronegativität von Sauerstoff, was zu stärkeren van der Waals Kräften und Wasserstoffbrücken führt.

Seite Leer /
Blank leaf

1. Introduction

Some of the first evidence of the use of adhesives date back to 4000 B. C. in Mesopotamia. A mixture made out of animal skin and bones was used as a glue, the proteins present in the mixture (mainly mammalian collagen from skin and sinew) acted as the adherent [1][2]. With technical progress and the evolution of synthetic chemistry during the last century, the quality of adhesives improved although the understanding of the underlaying phenomena of adhesion remained inconclusive, mainly due to a limited understanding of the adhesive-surface interactions. This thesis deals with the physical and chemical interactions of organic molecules at inorganic surfaces and modification reactions at these surfaces to tailor their chemical composition. Such tailored and characterised surfaces are then applied for adhesion studies in an attempt to improve the basic understanding of adhesion.

1.1. Thin and Ultrathin Layers

Thin and ultrathin layers are films with a thickness ranging from micrometers down to a few Ångströms. They can be of both inorganic and organic nature depending on which precursors they are made of. When the layers are as thin as the molecule's dimensions they are called monolayers. There has been a growing interest in monolayers over the past 20 years as a result of the development of surface analytical tools, which allow to address structural issues of these monolayers in great detail and with unprecedented precision [3][4]. Thin layers with controlled characteristics are excellent model systems for a more fundamental understanding of phenomena in fields involving homogeneous surface modification, e. g., control of wetting [5][6][7][8], control of bio-compatibility [9][10][11], the electrical characteristics of solid-state electronic devices [12], optical properties of lenses and coatings [13], lubrication [14], corrosion inhibition [15][16], metal refining [17], adhesion [18][19][20][21][22][23] and passivation [24]. In a longer perspective commercial applications from thin layers such as biosensors, coatings for tribology and corrosion inhibition will probably also be available [25][26].

The production of thin and ultrathin layers can be achieved in many different ways e. g. physical vapour deposition (PVD) [27], chemical vapor deposition (CVD) [28], plasma deposition [29] and molecular beam epitaxy (MBE) [30]. These techniques are, however, limited in the control of thickness and order of the layers as in the cases of PVD, CVD and plasma deposition are slow and technically complicated as is MBE [3][31]. On the other hand adsorption from solution as described below is a versatile technique for making thin and ultrathin layers with less effort and better control.

1.2. Adsorption from Solution and Self-Assembled Monolayers (SAMs)

The Babylonians used to spread droplets of oil randomly onto water surfaces and by studying the behaviour of these thin films they made predictions about the future [32]. A less esoteric application of similar films was continued in the work of Benjamin Franklin in the 18th century [33]. He showed that a thin layer of oil had a calming effect on the water in a pond. The thickness of such films was decreased by Agnes Pockels who was the first to describe a monolayer at the water-air interface [34][35][36][37]. These films are named Langmuir films after Irving Langmuirs systematic study of amphiphilic molecules and their behaviour at the interface of a liquid and a gas [38].

Langmuir films were used by Katharine Blodgett in the thirties to deposit multilayers of long chain carboxylic acids onto various solid substrates such as glass, chromium, brass, steel and silver surfaces. Such films are referred to as Langmuir-Blodgett (LB) films [39][40]. They are produced typically by adding amphiphilic molecules to a trough with water where the amphiphiles congregate at the interface with the hydrophilic head towards the water and the hydrophobic tail facing the air. A moving barrier at the surface controls the surface pressure and thereby also the order of the amphiphilic molecules. By moving a substrate up and down in the trough, a film is deposited under appropriate conditions onto the substrate, and iterative deposition can result in multilayer films. The principle of the production of LB-films is shown in Figure 1.1. The properties of these films can be varied in abundance, e. g., depending on the nature of the substrate, the environment, the subphase, the amphiphilic molecules to be deposited and whether the deposition starts from a position of the substrate within or above the trough [4]. The technique allows

a good control of the films during the preparation whereas the long time stability is less controlled because of the thermodynamic inequlibrium of the films when they are deposited on the substrate and removed from the trough [41]. This is due to the nature of the films where the molecules are usually physisorbed onto the substrate. A more stable layer is produced when the molecules are chemisorbed onto the substrate which is often the case for the self-assembly (SA) techniques.

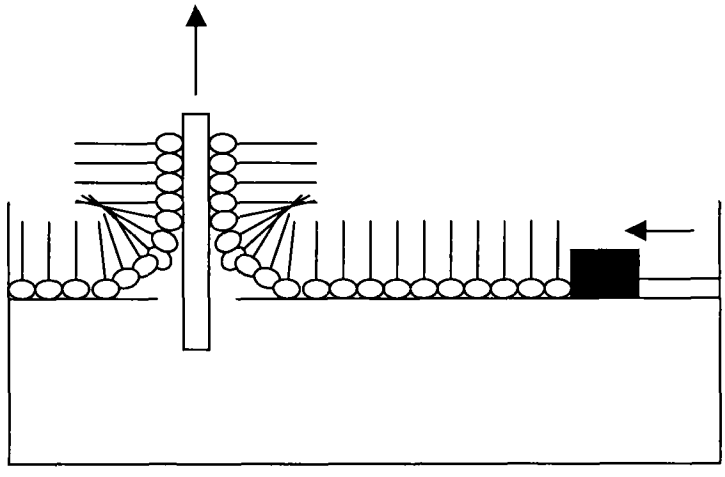

Figure 1.1. Schematic representation of the principle for the production of Langmuir-Blodgett films.

The self-assembly (SA) technique was first described by Zisman et al. [42]. By exposing glass surfaces to dilute solutions of long-chain alcohols in hexadecane as solvent, films of oriented monolayers formed. The resulting surfaces were not wetted by the solvent and exhibited wetting properties similar to those of Langmuir-Blodgett films. This system has later been extended to include various metal and metal oxide surfaces as well as different surfactant-like molecules such as long-chained amines, carboxylic acids and primary amides [43][44]. The driving force for the self-assembly is the large interfacial energy present between the inorganic surface and the hydrocarbon solvent phase that is reduced upon directed spontaneous adsorption of the amphiphilic species. The polar head group is adsorbed onto the solid substrate and the hydrophobic tail is oriented away from the substrate exposing a low energy surface of methyl groups. An extension of the SA technique was Zisman's demonstration of the preference of adsorption of one chemical group over another allowing the ability to produce oriented films from polar solvents such as water. The amine groups employed showed an affinity for platinum of more than 10^6 versus the

hydroxyl groups of water [43]. The biggest disadvantage of Zismans systems is that they are limited regarding to stability and that they only generate low-energy hydrophobic surfaces.

The SA-technique employing organosilicon derivatives introduced a method of producing self-assembled monolayers (SAMs) with various tail groups and by that means also generating high energy surfaces. Sagiv [45] described the technique in 1980 when he made SAMs of octadecyltrichlorosilane (OTS) on SiO_2. This was still a low-energy surface due to the hydrophobic tails but effectively described the driving force of this self assembly which is the in situ formation of poly(siloxane) when the orgoansilicon derivative is connected to surface hydroxyl groups (-OH) via Si-O bonds. SAMs with various ω-substituted alkyl silanes have later been reported showing high surface free energy with functional groups such as amines [46][47], halogens [47][48][49][50][51], cyanide and thiocyanide [47], methyl ether and acetate [48], thioacetate [48][52], α-haloacetate [49], vinyl [53][54][55][56][57][58][59][60][61][62], (trimethylsilyl)ethynyl [63], methyl ester [64][65], and p-chloromethylphenyl [49][66][67][68][69]. Monolayers with low surface free energy by octadecyltrichlorosilanes have been described (see above) as well as surfaces from partially fluorinated alkyl silanes [48][70][71][72]. The use of organosilicon derivatives provides a convenient technique to make SAMs with high free surface energy, however, they are still not simple to produce due to difficulties in controlling the amount of water in the adsorption solution [53][73][74]. A total absence of water causes incomplete monolayers [54][75] and an excess of water causes polymerization in solution and polysiloxane deposition at the surface [76]. A flexible alternative to organosilicon SAMs is the use of organosulphur compounds, especially those made of thiols which allows a straightforward preparation, and good long term stability.

1.3. Self-Assembled Monolayers (SAMs) of Thiols

In 1983 Nuzzo and Allara discovered that dialkyldisulfides (RS-SR) form oriented monolayers on gold surfaces with the tailgroup (R) facing the interface towards air [77]. This was later found to rely on the strong interaction of sulphur atoms with gold [78][79][80][81][82]. Oriented monolayers have also been described in relation to other metal surfaces such as silver [83], copper [84][85][86], and platinum [87]. However the drawback with these metals is that they form stable oxides in contrast to gold, and hence most of the related work has been performed on gold surfaces, which do not form stable oxides [88] with the exception of very specific treatment with ozone and UV irradiation [89].

Many other organosulphur compounds besides dialkyldisulfides have been reported to coordinate to gold in recent years. These include among others alkanethiols [90], dialkylsulfides [87][91], xanthates [92], thiocarbamates [93], and cysteines [94][95]. Due to the different head groups accounting for the bonding with the surface, the packing of the monolayers is expected to be different. This was also shown by Bain et al. when they compared the contact angles of water and hexadecane on monolayers of various adsorbed compounds with similar length of the alkyl chain but with different head groups. They compared the contact angles on monolayers of alkanethiols, dialkyldisulfides, dialkylsulfides, and xanthates (shown in Figure 1.1.) and found higher contact angles on monolayers produced from alkanethiols compared to the others, indicating a better packed monolayer due to the smaller head group [96].

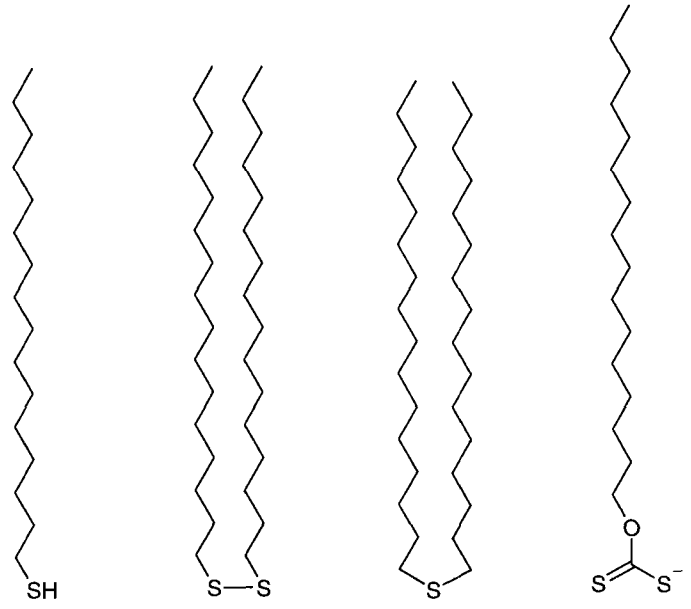

Figure 1.2. Organosulphur compounds used for comparing contact angles by Bain *et al.* From left to right: alkanethiol, dialkyldisulfide, dialkylsulfide and xanthate.

In the same study, Bain and coworkers also compared phosphorous compounds with alkanethiols in rival experiments. Gold slides immersed in solution of acetonitrile containing a 3:1 mixture of trioctylphosphine $[H_3C(CH_2)_7]_3P$ and 1-mercapto-11-undecanol $HO-(CH_2)_{11}-SH$, MUD, showed a water contact angle suggesting a 1:1 ratio of methyl and hydroxyl groups on the surface, although the ratio in the solution was 9:1. This indicates a preferred adsorption of the thiol group over the phosphine group from which Ulman later concluded, that thiol groups form the strongest interactions with gold surfaces over all other head groups that have been studied [4].

1.3.1. Adsorption Kinetics

The adsorption process of a self-assembled monolayer is characterized by two distinct phases of different kinetics. The initial formation of the monolayer is very rapid, within seconds. A clean gold slide immersed in a 1 mM solution of a long-chain alkanethiol is autophobic, meaning that the adsorbing solution peels back to leave a dry surface when

the slide is removed from the solvent. Within the initial formation, the contact angles reach their limiting values whilst the thickness reaches about 80-90% of its maximum. The first rapid step is followed by a slower second step lasting several hours during which the thickness slowly approaches its final value [97]. This behaviour can be explained by a rapid adsorption of an imperfect monolayer which is then followed by a slower process of additional adsorption and consolidation, displacement of contaminants as well as lateral diffusion on the surface to reduce defects and enhance the packing density of the monolayer.

The adsorption kinetics also depends on the concentration of thiols in the adsorption solution. For concentrations lower than 1 mM, a slower kinetics in the formation of the monolayer has been observed by studying the thickness of the monolayers as well as the contact angle with hexadecane [97]. For higher concentrations than 1 mM Ulman and coworkers found that functionalised thiols that form surfaces with high excess free surface energy, such as 1-mercapto-11-undecanol, MUD, tend to yield monolayers with excessive thicknesses, probably due to adsorption of the alcohol on the surface [98]. It thus can be concluded that a 1 mM solution is a very convenient concentration for formation of self-assembled monolayers.

Different head groups containing organosulphur moieties described above show differences in kinetics of the formation of the monolayers. In contrast to alkanethiols where the well-packed oriented monolayers are formed within hours, sulfides and disulfides need immersion times of several days to form packed monolayers [96].

The length of the alkyl chain and its influence on the kinetics of the formation of monolayers on gold was studied by Bain and coworkers for decanethiol HS-$(CH_2)_9$-CH_3 and dodecanethiol HS-$(CH_2)_{17}$-CH_3 [88]. It was found that the kinetics are faster for longer alkyl chains because of strong van der Waals interactions which are a function of the chain length, and thereby enhance the assembly of a longer alkyl chain.

The chemisorption of alkanethiols on gold gives monolayers; the commonly accepted mechanism attributes this to the formation of Au(I) thiolate (RS^-) species [4]. The reaction

can be considered as an oxidative addition of the S-H bond to the gold surface followed by a reductive elimination of hydrogen. When a clean surface is used, H_2 is expected to evolve. This is deduced from the fact that monolayers can be formed from the gas phase [100][101][102] in complete absence of oxygen:

$$\text{R-S-H} + \text{Au}^0_n \rightarrow \text{R-S}^-\text{Au}^+\cdot\text{Au}^0_{n-1} + \tfrac{1}{2}\,\text{H}_2$$

The formation of H_2 is thought to be exotermic which may be important in the chemisorption energetics. The bonding of the thiolate group is very strong and the homolytic bond strength has been estimated to be approximately 40 kcal per mol [78].

1.3.2. Order and Orientation of SAMs

The van der Waals forces between the alkyl chains in the SAM do not only affect the formation kinetics but also affect the order of the monolayer. Porter and coworkers studied the film thickness by ellipsometry as a function of the chain length for thiols $HS\text{-}(CH_2)_n\text{-}CH_3$ (Figure 1.3.) [90]. Two separate regions could be distinguished for values of n, below and above approximately 8. For $n < 8$ a lower slope than for $n \geq 9$ was observed. Linear regression for the region $n \geq 9$, results in a slope of 1.5 Å/CH_2 and an intercept of 3.8 Å. Infrared spectroscopic evidence from the same study indicated that the longest thiols assume an average tilt of 20-30° from the surface normal. These results suggest that for $n \geq 9$ the long-chain thiols form a densely packed crystalline-like assembly with fully extended alkyl chains in a trans zigzag conformation tilted from the surface normal by an angle of ~25°, allowing a better packing and a more ordered monolayer

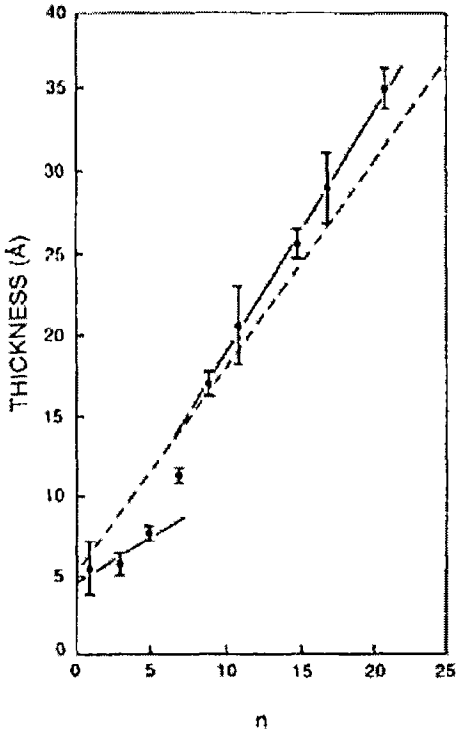

Figure 1.3. Film thickness of alkanethiols adsorbed on gold as a function of the number of CH_2 groups in the chain, determined by ellipsometry (——) and estimated for fully extended chains at an angle of 25° to the surface normal(---) [99].

The hypothesis stating that the order of the monolayer increases with the length of the alkyl chain has also been supported by contact angle measurements of methyl terminated SAMs [97]. For n >10, advancing contact angles $\theta(H_2O)$= 111-114° and θ(hexadecane)= 45-48 were consistently observed, for shorter chains the contact angles were progressively lower. This trend is assumed to be due to increasing disorder in the short-chain monolayers exposing methylene groups at the surface and thereby decreasing the contact angle.

The symmetry of monolayers of alkanethiolates on gold has been investigated by electron diffraction studies [103][104][105], helium diffraction [105], and atomic force microscopy (AFM) [106]. Due to the size of the sulphur atom not all the hollow sites on Au (111) can be occupied by a sulphur atom, and as a consequence a structure coincident with the underlaying gold lattice in a $\sqrt{3}$ x $\sqrt{3}$ R 30° overlayer is formed (see Figure 1.2.) where the

distance between two sulphur atoms is $\sqrt{3}$ times larger than between two gold atoms (2.88 Å) [107][108]. The symmetry of sulphur atoms is hexagonal with an S···S spacing of 4.97 Å and a calculated area per molecule of 21.4 $Å^2$ [3]. The tilt of ~30° of the alkyl chain (see above) can be explained by the smaller perpendicular area of the alkyl moiety compared to the surface area occupied by the sulphur atom. The tilt decreases the distance between the alkyl chains and thereby optimises the van der Waals attraction (Figure 1.2. lower part).

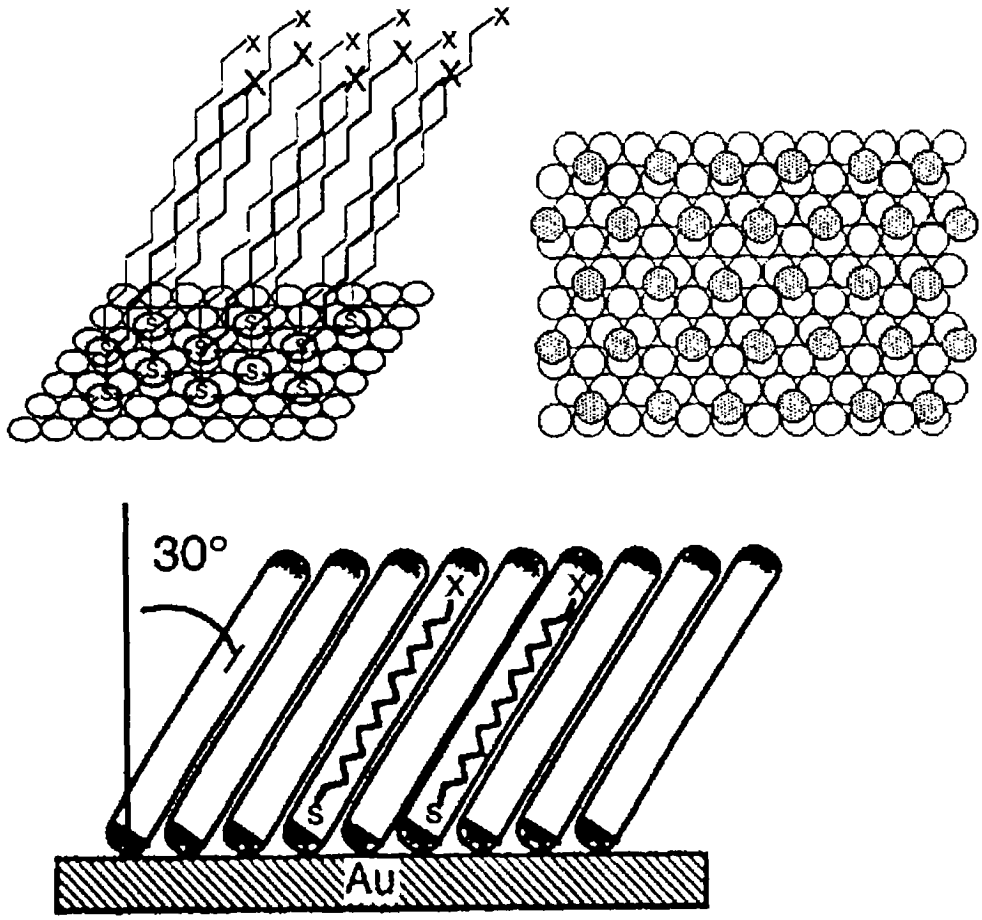

Figure 1.4. Hexagonal coverage scheme for alkanethiolates on Au(111). The open circles represent gold atoms and the shaded circles represent sulphur atoms organised in a $\sqrt{3}$ x $\sqrt{3}$ R30° overlayer (upper part). The upper part left and the lower part show the tilt of the SAM which optimises the van der Waals forces between the alkyl chains. The tilt is originating from the smaller perpendicular area of the alkyl moiety compared to the surface area occupied by the sulphur atom [41].

1.3.3. Stability of SAMs

The stability of alkanethiolates on gold has been addressed in a number of publications. Delamarche and coworkers studied the stability of dodeanethiol (DDT) in air at elevated temperatures and found no loss of thiols for samples exposed to temperatures of 100 °C for 10 h [104]. At higher temperatures, XPS revealed a loss of carbon and sulphur as well as a decrease in contact angles of water at an annealing time of 10 h. A decrease of the contact angle at 100 °C was observed for annealing times longer than 10 h but no indication of a loss of the methyl terminated monolayer was evident from XPS. The decrease of the contact angles observed could be due to contaminations.

When the monolayer is exposed to a solvent, the surface-bound thiols can desorb already at 70°C in a hydrocarbon. The desorption rate is not only dependent on the temperature but also on the characteristics of the solvent and the chain length of the adsorbate. The desorption is more rapid in hexadecane than in ethanol and with hexadecane as the solvent at 83 °C, the desorption rate decreases with the chain length of the alkanethiol [97].

Radio labelling of octadecanethiol has shown that a monolayer exposed to a solution of the same thiol will self-exchange and can be described by first order kinetics [105]. This study also showed a decrease of the relative coverage of the SAM of 20% after exposure to hexane for 24 h at 41 °C.

Photooxidation of the thiolate ($R\text{-}S^-$) to sulphonate ($R\text{-}SO_3^-$) is decreasing the strength of the interaction between sulphur and gold [106]. After photooxidation, the stability of the SAM is significantly decreased and ozone was recently shown to be the determining step in the photooxidation [109]. The photooxidation can easily be controlled by not exposing the SAM to UV-light in an oxygen atmosphere which is the crucial factor for the formation of ozone. Despite this, the photooxidation of SAMs has contributed a lot to studies of the stability of SAMs concerning functional tail groups.

Studies with photooxidized SAMs have shown an increased stability for SAMs formed from molecules with polar terminal groups that can form hydrogen bonds between the dif-

ferent alkane chains [110][111]. Photo-patterned short-chain thiols such as 3-mercapto-propanoic acid (MPA) are not eroded by a long-chain thiol such as ODT. A photo-patterned long-chain thiol such as DDT was however eroded by the short-chained MPA. These results give little information about the stability of SAMs in ambient conditions, but are at least an indication that not only the chain length is responsible for the stability of the monolayer.

The study of photooxidized SAMs suggests that the stability of HS-$(CH_2)_n$-X monolayers depends on the tail group or other stabilizing groups incorporated in the alkane chain. For the latter, no long-chain thiols are commercially available to our knowledge. In the case of functional tail groups, several short-chain thiols are available but for n >8 the only readily commercial available thiols with a functional tailgroup are 1-mercapto-11-undecanol (MUD) and 1-mercapto-16-hexadecanoic acid (MHA). These are both able to form hydrogen bonding. Compounds with other functional endgroups that could increase the stability of the monolayer, for example amine and amide groups, have to be synthesized.

1.3.4. Synthesis of Functional Thiols

The synthesis of thiols with different functional tail groups is laborious for the preparation of SAMs with tailored functional groups. In order to keep the SAM densely packed it is required to keep the functional tail group smaller than that for the oligomethylene chain (21.4 Å, see "Order and Orientation of SAMs" on page 26) so that the size of the tail group does not interfere with the packing of the hydrocarbon chains [112].

The packing density is also influenced by the length of the alkane chain as described above. Despite the less ordered monolayer obtained from short-chain, ω-functionalised hydrocarbons, many studies have focused on these thiols due to the greater availability of commercial precursors and synthetic accessibility. Functionalised thiols with $n \geq 9$, in the formula HS-$(CH_2)_n$-X, form densely packed monolayers. Those described in the literature with $n \geq 9$ are shown in table 1 with their references.

Table 1.1. Overview on functionalised alkanethiols ($HS-(CH2)_n-X$) described in the literature.

Tail group (X)	n	References
OH	11, 16, 19, 22	[6], [97], [113]
COOH	10, 15	[6], [97], [113], [114]
$B(OH)_2$	11	[115]
PO_3H_2	8, 10, 19	[116], [117], [118]
$CONH_2$	10, 15	[113]
$(OCH_2CH_2)_mOH$	11, m=1-7	[119], [120]
$(OCH_2CH_2)_6OCH_3$	11	[120]
Br	11	[97]
Cl	11	[97]
CN	10, 11, 16, 21	[6], [114]
$(SO(CH_2)_3)_3SOCH_3$	11	[121]
OCH_3	11, 16	[8], [97]
O_2CCH_3	11	[122]
$SCOCH_3$	11	[97]
CO_2CH_3	10, 15	[97], [113]
$CONHCH_3$	11	[6]
$O(CH_2)_mCH_3$	11, 16, m=1-5	[8]
$CO_2CH_2CH_3$	10	[6]
$NHCOCH_{3-m}F_m$	11, m=0-3	[123], [124]
$CH=CH_2$	17	[97]
$OSi(CH_3)_2C(CH_3)_3$	11	[97]
$O_2(CH_2)_9CH_3$	11	[122]
$OCH_2CF_2CF_3$	11	[6]

The laborious synthesis of functionalised thiols leads to an increasing interest in tailoring the properties of SAMs by surface modification reactions on the pre-established monolayer. These efforts are discussed in the following section.

1.3.5. Surface Reactions of SAMs

The alkanethiolate SAMs employed for surface reactions contain a reactive tail group as a site for attachment of various compounds to the underlaying gold. The tail groups that are usually applied are -OH, -COOH, and -NH_2. These functionalities are also frequently incorporated in various polymers where attachment of species on the surface is desired. The commercial availability of thiols with long alkane chains terminated with -OH and -COOH groups renders these two moieties good candidates for surface modification of SAMs.

Amine-terminated SAMs are also useful in surface modification reactions due to their reactivity with a variety of functional groups. These systems have however been less studied due to the complications with oxidation and the zwitterionic nature of the mercaptoamine product in the synthesis of long-chained NH_2-terminated alkanethiols [112]. Therefore work of NH_2-terminated SAMs has focused on shorter-chained adsorbates such as cystamine and its disulphide [112]. Xiao used cystamine SAMs and reacted these with various succinimidylesters containing bifunctionality or photocrosslinkers [125]. Cystamine has also been exposed to modify surfaces with alkyldiisothiocyanates and further attachment of glucose oxidase [126]. A drawback of these studies is, however, that the short alkane chains in the cystamine are not able to establish a densely packed SAM on the gold surface due to limited Van der Waals interactions between the short alkane chains. The surface coverage has been reported to be as low as 35% [127].

Surface modifications of SAMs containing carboxylate end groups have been studied to a greater extent due to the formation of densely packed monolayers by easily accessible COOH-terminated alkanethiols. The carboxylate group can be transformed into its acid chloride by exposure to gaseous thionyl chloride ($SOCl_2$) and subsequent reaction with amines and alcohols to form amide and ester linkages, respectively [128][129]. The car-

boxyl group activated into its acid chloride has also been demonstrated by Kim et al. to react with a carboxylic acid-terminated thiol over a thioester linkage. The exposed carboxylic acid group was then regenerated into acid chloride with $SOCl_2$ (thionylchloride) in a subsequent step. The reiteration of this process resulted in the formation of a multilayer film that was additionally stabilized by employing a diacetylene-containing mercapto alkanoic acid which was polymerized by exposure to UV-light after each adsorption cycle [130]. Whitesides and coworkers used a COOH-terminated monolayer and treated this with trifluoroacetic acid resulting in a reactive SAM terminated in interchain carboxylic anhydride groups. Micro contact printing (μCP) techniques and exposure to poly(ethyleneimine) (PEI) with subsequent hydrolysis of unreacted anhydride groups resulted in patterned thin films of PEI covalently attached to the SAM by amide bonds [131]. The carboxyl groups could be activated with a succinimide ester in a similar way as the amine group and have been used for the covalent attachment of poly(L-lysine) susceptible to further derivatization [132]. The immobilization of glucose oxidase was recently demonstrated by Guiomar et. al. [133]. They used a mixed SAM of 1-mercapto-11-undecanoic acid and an unreactive hydrophobic short-chain alkanethiol (7-heptanethiol). The carboxylic groups were transformed into reactive succinimide derivatives and subsequently glucose oxidase was attached covalently to the SAM by amide linkages.

SAMs containing OH-terminated thiols on gold have also been used for many surface modification reactions and are shown in Figure 1.5. Bertilsson and Liedberg showed that 1-mercapto-16-hexadecanol readily reacts with trifluoroacetic anhydride in the gaseous phase to form the corresponding trifluoroacetate [134]. Pan et. al. later did the same reaction and found no difference between solvent- and vapor-phase derivatization [135]. The OH-terminated SAM also reacts with phosphorous oxychloride yielding a phosphate surface [117][134][136], chlorosulfonic acid ($ClSO_2OH$) to form a a sulphate surface [134], and octadecyltrichlorosilane ($CH_3(CH_2)_{17}SiCl$) to form a well ordered hydrophobic bilayer [98]. Löfås and Johnsson have reacted alcohol-terminated SAMs on gold with epichlorhydrin to produce an ethylene oxide surface allowing attachment of a dextran matrix to the gold film as part of a bio- sensor system [137]. Grunze and coworkers used OH and COOH-terminated SAMs in a laborious process when they used ultra high vacuum (UHV) techniques to condense a multilayer of phenyleneisocyanate onto the SAMs at low

temperature (130 K) followed by heating the samples slowly to room temperature which resulted in a bilayer in a carbamate and anhydride bonding, respectively [138].

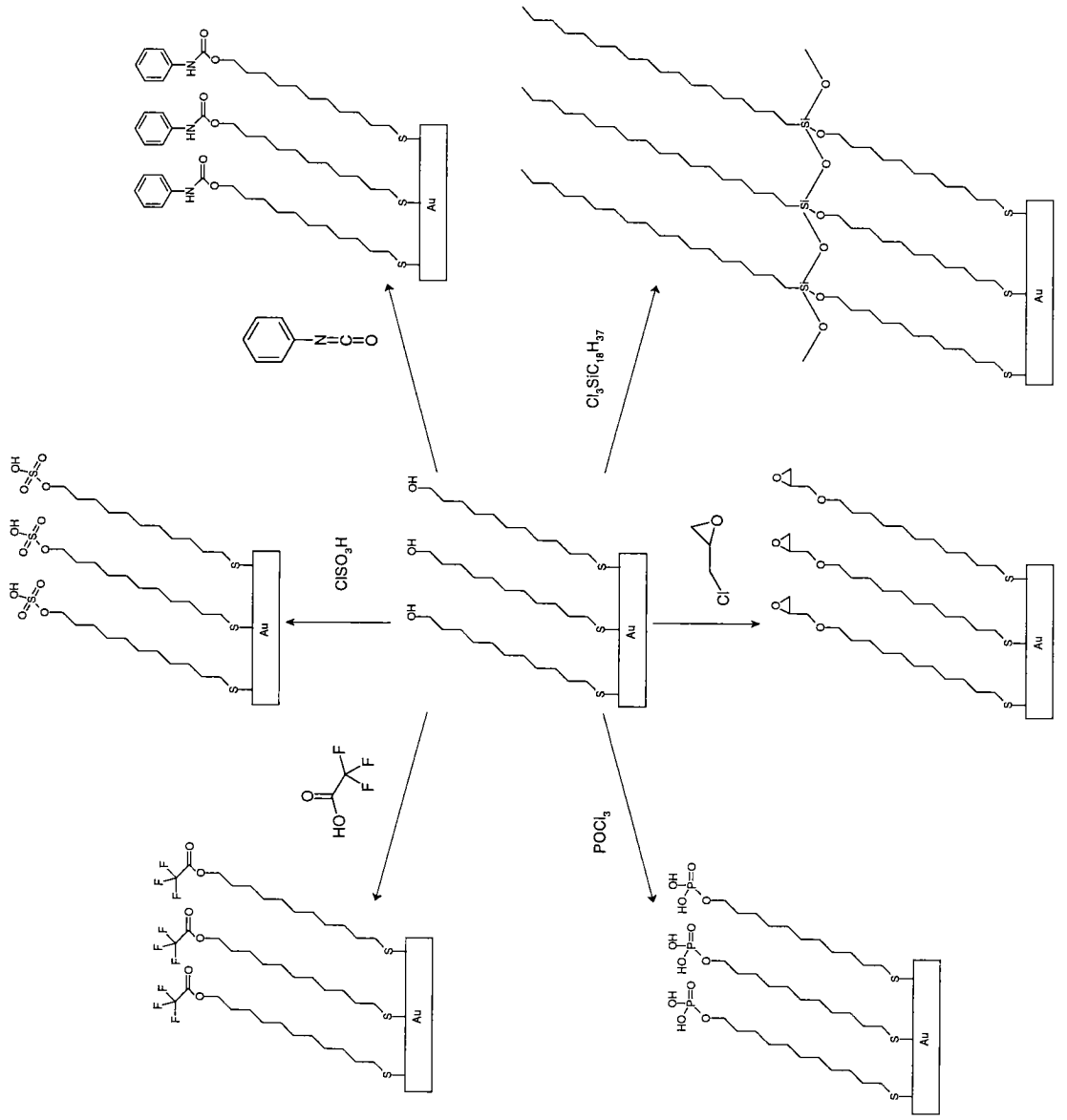

Figure 1.5. Overview of surface modification reactions of OH-terminated alkanethiols on Au(111). Details and references are described in the text.

1.4. Methods of Surface Characterisation

To obtain information about a thin film at a surface, there are a large number of different techniques available. Depending on the method used, different information will be received. Those techniques which have been used to characterise SAMs of alkanethiolates on gold over the last decade are listed in the table below and in the following, the most important analytical methods and tools used in this thesis for surface characterisation are described.

Table 1.2. Techniques used for characterisation of SAMs.

Property determined	Technique	References
Wettability	Contact angle measurements	[4],[12]
Composition	X-ray photoelectron spectroscopy (XPS)	[4], [139]
	Time of Flight secondary ion mass spectroscopy (ToF-SIMS)	[4], [139]
	Temperature programmed Desorption (TPD)	[139]
Structure and order	Infrared spectroscopy at grazing incidence reflection (GIR- IR)	[12], [140]
	Atomic force microscopy (AFM)	[139],[141]
	Low energy helium diffraction	[4]
	X-ray diffraction	[4]
	Electron diffraction	[4],[103]
	Surface raman scattering	[4], [139]
	Sum frequency generation spectroscopy (SFG)	[4],[139]
Thickness	Ellipsometry	[4],[142]
	Surface plasmon resonance spectroscopy	[4],[143]
Coverage	Quartz crystal microbalance (QCM)	[144]
	Surface acoustic wave device (SAWD)	[145]
	Electrochemical methods	[146]
Defects	Scanning probe microscopy (STM and AFM)	[139],[141]
	Wet etching	[147]

1.4.1. Contact Angle Measurements

When a drop of a liquid is placed onto a surface, the shape of the drop will be affected by the free energy of the surface and if the free surface energy difference between the surface and the liquid is high enough the liquid will wet the surface. When a liquid does not wet a surface completely, its tangent to the surface at the three-phase boundary forms an angle with the surface, in equilibrium defined as θ, the contact angle [4]. This is due to a boundary equlibrium between the three phases shown in Figure 1.6.

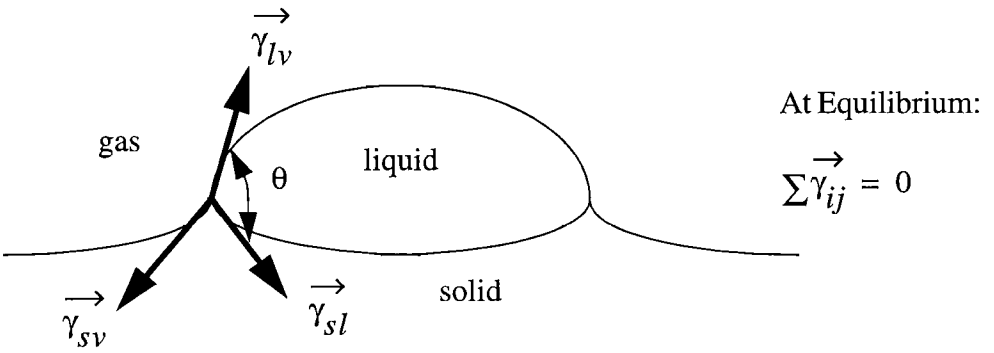

Figure 1.6. Schematic representation of the equilibrium Young's equation describing the contact angle θ.

where γ_{sv} is the solid vapour interfacial energy, γ_{sl} the solid liquid interfacial tension and γ_{lv} the liquid vapour interfacial tension. θ refers to the contact angle at equilibrium, hence the sum of the vectors are zero ($\sum\vec{\gamma}_{ij} = 0$). The interfacial energy (or interfacial tension) is defined as the free energy change upon expansion of the interfacial area between two phases by a unit area (see also thermodynamic work of adhesion, section 1.5.2. on page 58) [148]. The interfacial energy is often referred to the interfacial tension when one of the two phases is a liquid.

Usually, a perfectly rigid surface is assumed for simplicity and for the contact angle equilibrium, only the x -components are considered (see Figure 1.7.). The three-phase boundary and the contact angle, θ, can then be described by Young's equation [149]:

$$\gamma_{sv} = \gamma_{sl} + \gamma_{lv} \cos\theta \qquad (1.1.)$$

While γ_{sv} tends to spread the drop, γ_{sl} and γ_{lv} act in the opposite direction as can be seen in Figure 1.7. [150].

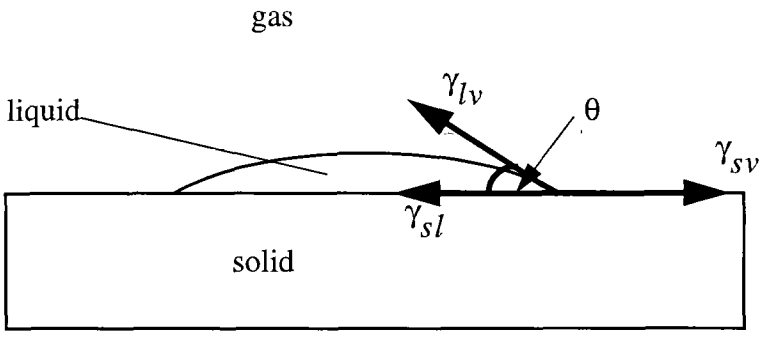

Figure 1.7. Schematic representation of the Young's equation describing the contact angle θ.

Young's equation is valid at best for perfectly homogeneous atomically flat surface and therefore supposes many simplifications. Normally the contact angle measured when a drop is put on a surface differs from the contact angle measured when a drop is withdrawn from a previously wetted surface although at equilibrium, the two must be equal. These two angles are defined as the advancing (θ_{adv}) and the receding contact angle (θ_{rec}). The difference between these two values are known as contact angle hysteresis [151][152][153]. Usually $\theta_{adv} > \theta_{rec}$. The contact angle hysteresis is caused by the roughness of the surface, heterogeneties of the surface, reorientation of surface molecules due to interactions between the surface and the liquid, and contaminations of either the surface or the liquid [4]. Values in the literature are usually referred to θ_{adv}.

For a rough surface, a metastable equilibrium is formed and the true contact angle (θ_{true}) can be defined by the observed contact angle and a roughness factor defined as the ratio between the true surface area and its geometrical area ($r \geq 1$) in the relationship:

$$\cos \theta = r \cos \theta_{true} \qquad (1.2.)$$

According to this equation the roughness of the surface leads to an increase of contact angles that are greater than 90°, and a decrease for those less than 90°. It has been found that roughening of a smooth surface results in an increase of the advancing contact angles, a decrease in the receding contact angles, and as a result an increase in the hysteresis [154][155].

For smooth surfaces with heterogeneous chemical composition, results of contact angle measurements can be interpreted in two ways. The first way is to interpret the results by the Cassie Equation [156]:

$$\cos\theta = \Xi_1 \cos\theta_1 + \Xi_2 \cos\theta_2 \tag{1.3.}$$

where θ is the contact angle of a liquid on the heterogeneous surface composed of a fraction Ξ_1 of one type of chemical groups and Ξ_2 of the second chemical groups (where $\Xi_1 + \Xi_2 = 1$), and θ_1 and θ_2 are the contact angles of this liquid on the pure homogeneous surfaces of 1 and 2, respectively. The Cassie equation is derived from the Young-Dupré equation:

$$\gamma_L (1 + \cos\theta) = W \tag{1.4.}$$

where γ_L is the surface energy of the liquid and W the work of cohesion of the liquid with the surface. Thus for two homogeneous surfaces we may write

$$\gamma_L(1 + \cos\theta_1) = W_1 \tag{1.5.}$$

$$\gamma_L(1 + \cos\theta_2) = W_2 \tag{1.6.}$$

while for a heterogeneous surface made up of patches of the surfaces 1 and 2 we have

$$\gamma_L (1 + \cos\theta) = W = \Xi_1 W_1 + \Xi_2 W_2 \tag{1.7.}$$

where Ξ_1 and Ξ_2 are the fractional areas of the patches. When equations 5-7 are combined we obtain the Cassie equation (1.3.). In this case it is assumed that the surface is composed of well separated domains of either type 1 or 2, so that the mean cohesion energy, *W*, is given by equation 1.7. However if the chemical heterogeneity is not formed by well separated domains but approaching molecular dimensions ("molecular mixing"), the theories of van der Waals and electrostatic forces [157] imply that the polarizability, surface charges or the dipole moments of the surfaces should be averaged rather than the cohesion energy. The polarizability or dipole moment of a system composed of different molecular or atomic moieties is simply the average (arithmetic mean) of the polarizability or dipole moments of each component. It is this average value that must be used in the equations for calculating the van der Waals interaction energies. If these quantities (i.e. polarization, surface charge, dipole moment, etc.) are denoted by w_1, w_2, w_L for the two homogeneous surfaces and the liquid, respectively, we obtain

$$\gamma_L (1 + \cos \theta_1) = W_1 \propto \{w_1 w_L\}^{1/2} \tag{1.8.}$$

$$\gamma_L (1 + \cos \theta_2) = W_2 \propto \{w_2 w_L\}^{1/2} \tag{1.9.}$$

and for the heterogeneous surface

$$\gamma_L (1 + \cos \theta) = W \propto [(\Xi_1 w_1 + \Xi_2 w_2) w_L]^{1/2} \tag{1.10.}$$

When equations 1.8.-1.10. are combined the same way as equations 1.5.-1.7. above we get the new relation:

$$(1 + \cos \theta)^2 = \Xi_1 (1 + \cos \theta_1)^2 + \Xi_2 (1 + \cos \theta_2)^2 \tag{1.11.}$$

known as the Israelachvili-Gee equation, which is suggested to replace the Cassie equation whenever the size of domains approaches molecular dimensions[158].

The Israelachvili-Gee equation is also a simplification of the reality since it completely neglects the interactions among surface functional groups. It is reasonable to assume that

the dipole moments of a surface group will depend on the dipole moments of its neighbours, and that the long-range dipole-dipole interactions will influence the functional groups at the surface[4].

The nature of equations (1.3.) and (1.11.) shows us, when we compare them with the same values of θ_1, θ_2, Ξ_1 and Ξ_2, that the Cassie equation (1.3.) will always predict a larger contact angle than that obtained from equation (1.11.) and that as moving from "molecular mixing" (molecular sized domains) to larger patches should result in progressive increase in the contact angle hysteresis [159][160][161].

The differences of the Cassie and the Israelachvili-Gee equations can tell interesting features of heterogeneous surfaces by simple contact angle measurements. When the sizes of the functional surface groups are similar (which is the case for hydroxyl groups -OH and methyl groups -CH_3, which are used in this thesis), one can assume that the surface fractions Ξ_1, and Ξ_2 are similar to the concentrations of the elements on the surface (they are occupying a similar area of the surface). By determining the surface concentration of a binary system with a different technique (e. g. XPS, see chapter 2.2.2.) and comparison of this result with the ones obtained from the contact angle measurements, one can get information on the size of the heterogeneties on the surface. If the result from the alternative technique is close to the value obtained from the Israelachvili-Gee equation, the system is rather "molecular mixed". If the result is close to the value from the Cassie equation one can assume that the surface functional groups are well-separated into domains or patches. This comparison is useful for the investigation of SAMs where the difference in molecular length of the two components is too small to be provide contrast in AFM (atomic force microscopy). The domain size of the two surface functional groups might be measured by lateral force microscopy (LFM), however, the resolution of the LFM technique is limited (5-10 nm) and no information on the domain sizes below the resolution of LFM will be obtained [162][163]. At these dimensions the comparison of the Cassie and the Israelachvili-Gee equation can give useful information on a chemically heterogeneous surface.

1.4.2. X-Ray Photoelectron Spectroscopy (XPS)

X-ray photoelectron spectroscopy (XPS), also called electron spectroscopy for chemical analysis (ESCA), is a highly sensitive technique for analysing chemical compositions at surfaces. The principle is based on the photoelectric effect first proposed by Albert Einstein in 1905, where photons cause the emission of electrons and the binding energy can be determined from the equation [12][139][143][165][166][167]:

$$E_b = h\upsilon_0 - E_k - \phi \qquad (1.12.)$$

where E_b is the binding energy of the electron before the photo ionisation, $h\upsilon_0$ the energy of the excited photon, E_k the kinetic energy of the emitted photoelectron, and ϕ the work function of the material which accounts for the amount of energy that must be provided to surmount the potential barrier at the surface. The emission process is shown in Figure 1.8. The number and the kinetic energy of the emitted photoelectrons are observed and the binding energy is derived from the above equation. Due to the unique set of binding energies for each element, XPS can be used to identify and determine the concentration of the elements in the surface.

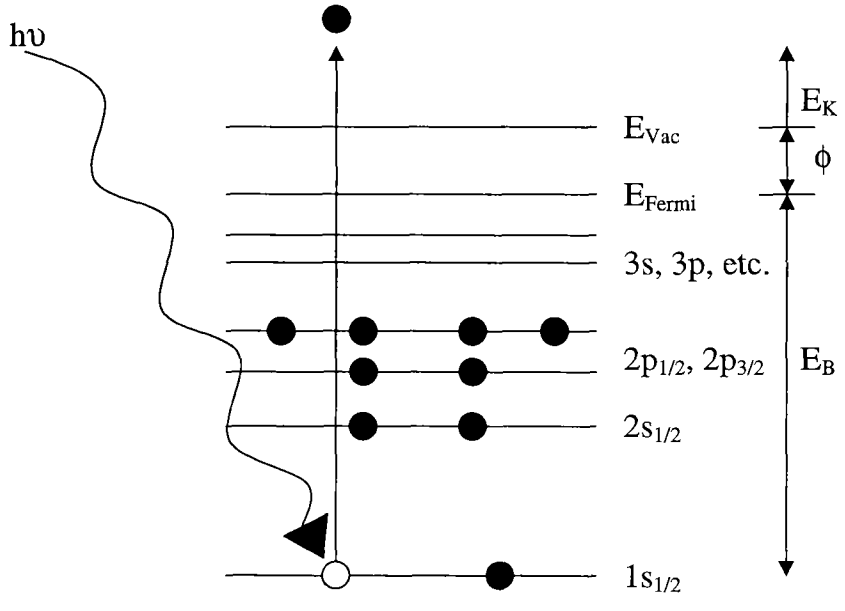

Figure 1.8. Schematic representation of the X-ray photoelectron emission process.

The energy of the incident photon determines whether valence or core electrons are emitted. For low photon energies < 100 eV, valence electrons are emitted and the technique is called Ultraviolet photonelectronspectroscopy (UPS). For photon energies > 100 eV (XPS), core electrons are emitted and no overlapping of the peaks of adjacent atoms occurs, resulting in better resolution than for UPS [167]. XPS was first described by Kay Siegbahn in 1967 [165]. In 1981 he was awarded the Nobel prize for his discovery [168].

XPS measurements are carried out under UHV (ultrahigh vacuum) conditions (~10^{-9} mbar) to prevent collisions of the emitted electrons before they are analyzed. The UHV also protects the X-ray anode from damage by oxidation and sputtering [167]. The appreciable desired photon energy is usually obtained by magnesium K (1253.6 eV) or aluminium K (1486.6 eV) X-ray radiation. The X-ray source produces not only the characteristic X-ray radiation but also some minor components at higher photon energies. These minor lines are characteristic for the particular X-ray source employed and can cause small satellite peaks. Software is usually installed to withdraw satellite peaks from the spectra by a filter function.

The photoelectrons emitted can only escape short distances in the material due to inelastic collisions with other electrons. This gives a unprecedented high surface sensitivity of the electrons emitted. 95% of the electrons detected come form the outermost 10 nm of the material [169]. The distance that a photoelectron can escape is dependent on its kinetic energy and referred as its inelastic mean free path [170]. The photoelectrons leaving the sample are detected in the vacuum chamber by an electron spectrometer and their kinetic energy is determined. The analyser accepts only those electrons having an energy within the range scanned for. This range is referred to as the pass energy and is fixed to maintain a constant energy resolution. The detection of different energies is accomplished by applying a variable electrostatic field before the photoelectrons enter the analyser [167].

The various binding energies of the core photoelectrons of a detected element corresponds to the different atomic orbitals of that element. The detailed position of the binding energy depends on the chemical environment or the chemical state of the core ionized atom, re-

spectively. These differences are called the chemical shift and are a result of a small change in electron density upon bond formation. If the electron density is lowered due to the bond formation, the binding energy of the core electrons is increased. The chemical shift is typically in the order of a few eV but can be up to 10 eV. It can be used to derive information about the oxidation state and the chemical neighbours of an element although the chemical shift is low compared to the resolution of the detector [139][171].

When a photoelectron is emitted there is a probability that an adjacent electron will be excited to a state a few eV above its ground state. The kinetic energy, E_k, of the analysed photoelectron is lowered and reflects the energy difference between the ground state and the excited state. In the spectrum the detected energy appears as a satellite a few eV higher in binding energy and with an intensity of up to 10% of the main peak. This additional peak is referred to as a "shake-up" satellite and occurs frequently in compounds containing aromatic moieties or C=O group due to $\pi \rightarrow \pi^*$ transitions [139][172].

Additionally to the qualitative analysis of the surface, XPS also allows to perform a quantitative analysis of the chemical composition of the surface. All elements except hydrogen and helium can be detected; the latter elements only comprise valence electrons. On a homogeneous surface, the peak intensity detected for an element A can be expressed as [173]:

$$I_A = N_A \cdot \sigma_A^e(h\upsilon) \cdot L_A(\gamma) \cdot \lambda_M(E_k) \cdot B \qquad (1.13.)$$

where
- I_A : measured XPS intensity of atom A [cps· eV]
- N_A : atomic density of atom A [atoms/volume unit]
- $\sigma_A^e(h\upsilon)$: cross section for electron e of atom A at photon energy $h\upsilon$
- $L_A(\gamma)$: angular asymmetry factor
- γ : angle between the X-ray beam and the e^- beam to the spectrometer
- $\lambda_M(E_k)$: mean free path length at E_k in the matrix M [Å]
- E_k : kinetic energy [eV]
- B : instrumental constant including (among others):

- the transmission function, T = f (E_A)
- detector efficiency
- flux of the characteristic X-ray line

From equation (1.13.), assuming that $L_A(\gamma)$ is the same for all atoms and $\lambda_M(E_k)$ is independent of $h\upsilon$, the atomic concentration of X_A can be derived as

$$X_A = \frac{(I_A)/(I_A^\infty)}{\sum_{i=A,B} (I_i)/(I_i^\infty)} \qquad (1.14.)$$

where I_A^∞ is the intensity from pure A and may be considered as a sensitivity factor, and $\sum_{i=A,B} (I_i)/(I_i^\infty)$ is the sum of all constituents of the solid.

When electric insulators are exposed to X-ray irradiation, the samples may be positively charged due to loss of the emitted electrons. Sample charging usually leads to a signal shift to lower kinetic and higher binding energy of the detected photoelectrons. This can be considered by calibration with photoelectrons of known binding energy. Adventitious carbon present as a contamination on all surfaces may be used as a reference but is still an inaccurate method due to variation of the values for the C(1s) signal in a contamination. When a known element is present in the thin layer to be analysed, e. g. the gold substrate in the case of self-assembled thiols, the shift of this element can be used as an internal standard to compensate for charging. Sample charging can be overcome to some extent by an electron flood gun. However an exact compensation of the surface charge is difficult [12][171][174].

The attenuation of the photoelectrons allows a depth profiling of the surface. The signal I_0, from any depth d is exponential attenuated and its value I at the surface is given by

$$I = I_0 \, e^{-d/(\lambda \cos\alpha)} \qquad (1.15.)$$

where α is the angle between the detected photoelectrons and the surface (take-off angle), and λ the attenuation length, which varies with E_k. The take-off angle α can be varied by

simply tilting the sample. In angle resolved XPS (AR-XPS) a sample is measured at different angles and a depth profile of the sample can be obtained. This is demonstrated in Figure 1.9. where the effective thickness of the layer detected by the analyser is varied by the take-off angle.

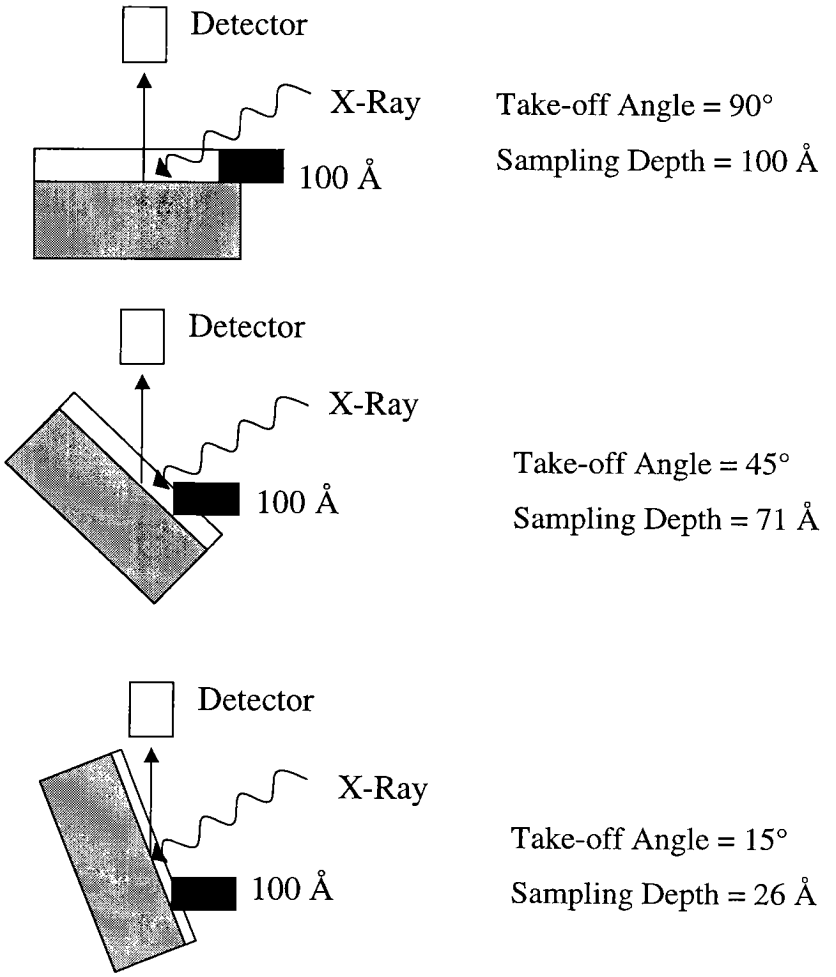

Figure 1.9. Demonstration of the angle-resolved XPS measurement (AR-XPS) where a depth profile of the sample can be obtained. The escape length of the photoelectrons is constantly assumed to be 3λ=100 Å (black marker in the figure) whereas the effective sampling depth is lowered with the grazing angle and marked as the white layer in the sample.

The escape length of the photoelectrons depends on instrumental factors. In this work it is constantly assumed as 10 nm and equal to 3λ for a take-off angle of 90°. Due to the

grazing angle the effective layer thickness detected by the analyser is lowered at low angles and hence the surface sensitivity is increased. Measurements are usually not carried out at lower angles than 10 ° since the design of the XPS-machine interferes with the spectra obtained [175].

1.4.3. Infrared Spectroscopy at Grazing Incidence Reflection (GIR)

Infrared spectroscopy (IR) has been used for characterisation of chemical species at surfaces since the 1950's [176]. With technical improvement such as Fourier-transformation (FTIR) and development of new components the capacity of the IR-technique has increased and today it is, in comparison to other characterisation techniques, a cheap and versatile instrument to obtain chemical information from surfaces and thin films.

The basic principle of IR is based on the change of molecular vibration energy. It can be described by the absorption of an infrared light quanta in a molecule and the excitation of the molecule from its ground-level to a higher vibrational energy level. This procedure is only possible when the change of energy is the same as the energy of the incoming IR quanta. If the transition occurs from a level higher than the ground level it is referred to as an overtone [139][177].

In contrast to the ubiquitous transmission infrared spectroscopy where the light beam is transmitted through a thin sample, the information obtained from a planar substrate relies on the reflection of the light beam. In a conventional transmission experiment it is the electric field of the incident IR wave that induces the absorptions, whereas in the reflecting experiment the incident IR wave combines with the reflected wave of approximately equal strength, producing a standing wave. It is this wave that induces the IR absorption of the species present at the surface. There are several different experimental set-ups for this type of IR-spectroscopy such as attenuated total reflection (ATR) [139], diffuse reflection (DRIFT) [139], and infrared spectroscopy at grazing incidence reflection (GIR) [12][26][41][139][178]. The last method is sometimes also alluded to as RAIR or RAIRS (reflection absorption spectroscopy), ERIRS (external reflection infrared spectroscopy), IRAS or IRRAS (infrared reflection absorption spectroscopy) although GIR is a more ap-

propriate description of the experimental conditions [12]. Of the mentioned methods, GIR is the most convenient one for the study of thin organic films on metal surfaces and is hence described below.

The incident IR-beam is reflected from the surface at a high angle, ϕ, close to 90° to the surface normal in a GIR-experiment (grazing angle). This is required to obtain a total reflection but also to acquire a maximum in the resultant electrical field which increases to almost 88° but falls rapidly to zero at 90° itself [12][179][180]. If the angle gets close to 90° it will also lead to practical problems such as a very large area of the reflected IR-beam leading to an intensity reduction in the detected light due to limited detector area, and hence the space requirement may become larger than the sample area [181]. In practice, optimum incidence angles are found at around 80° [181][182].

When the incident IR-beam is reflected at a surface, the incidence plane will be defined by the electric vector of the incident IR-beam and the surface normal, z (Figure 1.10.).

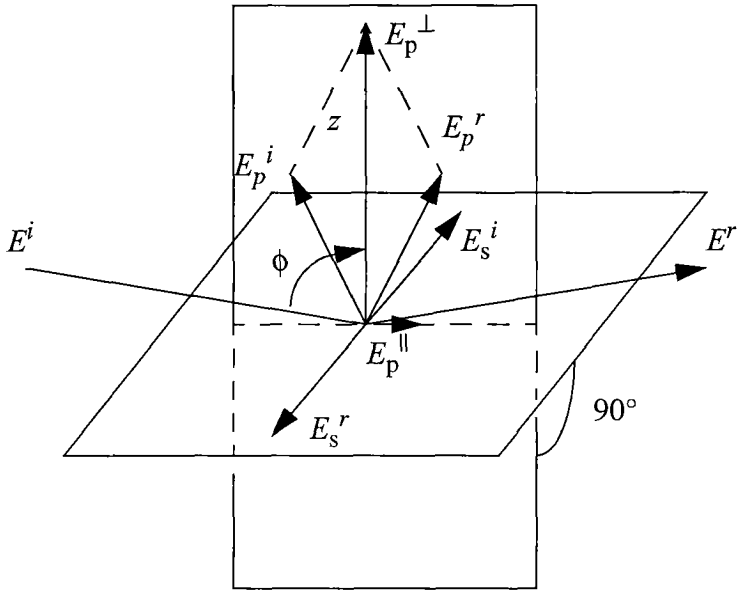

Figure 1.10. Reflection of an IR-beam at a surface with total reflection where:

E^i : Electrical field of the incident beam

E^r : Electrical field of the reflected beam

$E_p^{\parallel}$: Resulting electric field component in the incident plane and parallel to the surface

$E_p^{\perp}$: Resulting electric field component in the incident plane and normal to the surface.

E_p^i : Parallel electric field component of the incident beam

E_p^r : Parallel electric field component of the reflected beam

E_s^i : Electric field component of the incident beam normal to the incident plane

E_s^r : Electric field component of the reflected beam normal to the incident plane

ϕ : Incidence angle

z : Surface normal

The electric field at the surface is the vector sum of the incident, refracted and reflected electric field components. Since most of the incident intensity is reflected on a gold surface, the refractive wave contribution can be neglected [179]. For convenience, the electric field vector at the surface can be resolved into a component E_s, the electric field component normal to the incident plane, a component $E_p^{\parallel}$, the electric field component in the incident plane and parallel to the surface, and $E_p^{\perp}$, the electric field component in the incident plane and normal to the surface. The resulting fields can be described by:

$$E_s = E_s^i[\sin\theta + r_s \sin(\theta + \delta_s)] \quad (1.16.)$$

$$E_p^{\parallel} = E_p^i \cos\theta[\sin\theta - r_p \sin(\theta + \delta_p)] \quad (1.17.)$$

$$E_p^{\perp} = E_p^i \sin\theta[\sin\theta + r_p \sin(\theta + \delta_p)] \quad (1.18.)$$

where θ is an arbitrary phase and r_s and r_p the corresponding reflection coefficients respectively. δ_s and δ_p describe the corresponding phase change upon reflection for the plane normal and parallel to the incident plane, respectively. Since δ_s is close to -180° [180] and $r_s \approx 1$ for all ϕ, it can be derived from equation (1.16.) above that the -180° phase change leads to a destructive interference, i. e. $E_s \approx 0$. Hence, there will be no interaction of the component E_s with surface dipoles leading to a detectable IR-signal.

Opposite to δ_s, δ_p strongly depends on ϕ and changes sharply to -180° at ϕ=90°, where r_p=1 [12][180], also leading to a destructive interference. However at incident angles, ϕ, up to 85°, δ_p is below 90° which can lead to constructive interference. For the field components parallel ($E_p^{\parallel}$) and normal ($E_p^{\perp}$) to the surface, their values will depend on the incident angle, ϕ. Whereas $E_p^{\parallel}$ is small for all ϕ (cosϕ becomes zero at 90°), $E_p^{\perp}$ will increase with increasing ϕ to almost 90° but fall rapidly to zero at 90° itself. Thus, it can be concluded that the electric field normal to the surface is the only field that is significant at grazing incidence angles, (high ϕ) [12][178][180][183].

This unique feature of the grazing-angle experiment leads to the possibility not only to obtain information on the chemical structure of a molecule but also allows the calculation of its orientation with respect to an external reference system since molecules with transition dipoles oriented parallel to the surface will not be detected in an GIR-experiment. This is usually referred to as the "surface selection rule" shown in Figure 1.11. [4][12][125][181].

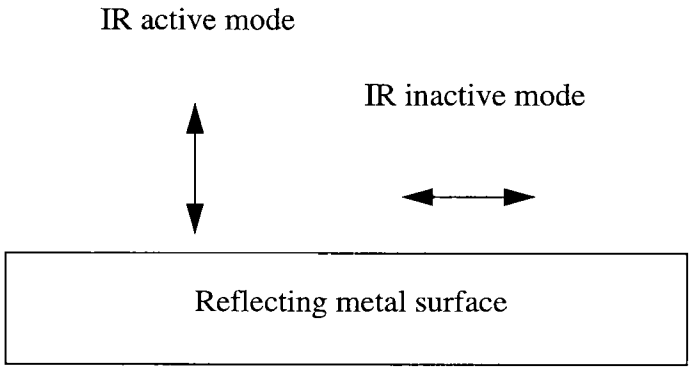

Figure 1.11. The surface selection rule for an GIR-experiment where the transition dipole moment perpendicular to the surface is IR-active whereas that parallel to the surface is inactive.

The absorption bands of an adsorbate observed in a GIR-experiment can differ from the bands observed in an ordinary transmission experiment. The shifts can arise from interactions such as π-bonds between the substrate and the adsorbate. The shift may also depend on the coverage due to interactions between molecules in the adsorbed layer as well as changes in the interactions between the adsorbate and the substrate itself. The integrated

intensity and the line width for a vibration of an adsorbate may also change with the coverage. These artefacts may cause problems to interpret vibration bands in an GIR-experiment [12].

To increase the signal-to-noise ratio, 500 scans are often employed for the analysis of a sample. It is often accurate enough to use a 4 cm^{-1} resolution although higher resolution and increased signal-to-noise ratio may be required to obtain information such as molecular packing and orientation [4]. The sensitivity is typically 1/1000 of a CO monolayer [179][184].

Practical problems are caused by atmospherical distortions such as contaminations with water, CO_2 or experimental parameters changing over time (e. g. ice formation on the detector). Such problems are reduced to some extent by carrying out the measurement in a vacuum chamber or by using a fresh background sample prior to measurement.

It can be concluded that infrared spectroscopy at grazing incidence reflection (GIR) is a useful technique to obtain information on the chemical structure as well as orientation of a self-assembled monolayer.

1.4.4. Ellipsometry

Ellipsometry is an optical technique for the determination of optical constants of a material or the thickness of a thin homogenous film. It is based on an analysis of the change in polarization state of incident light after reflection from a surface. Its principal setup for the instrument used in this thesis is shown in Figure 1.12. [12][26][41][178][185].

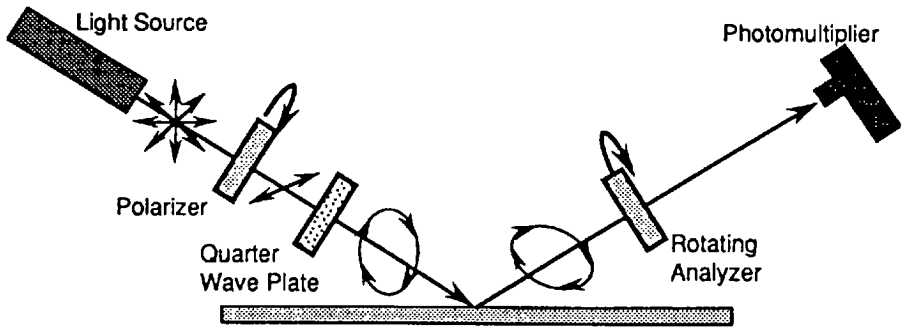

Figure 1.12. Depiction of the photometric ellipsometer used in this work. The ψ and Δ values described below are measured with the quarter wave plate, QWP, in place for ψ and both with and without the QWP for Δ [185].

When a plane-polarized light interacts with a surface at an angle, φ, it is reflected and can be decomposed into a component parallel (p-component) and perpendicular (s-component) to the plane of incidence. Due to the reflection, the amplitude ratio and phase of one polarization component relative to the other change. The resultant light of the combined p- and s-polarized reflected light beams will be elliptically polarized. The amount of ellipticity induced will depend on various things including the optical properties of the substrate as well as thickness and optical properties of an overlying film. The reflected components can be described as:

$$r_p = \frac{E_{rp}}{E_{0p}} = \left(\frac{|E_{rp}|}{|E_{0p}|}\right) \cdot e^{i(\delta_{0p} - \delta_{rp})} = \frac{|E_{rp}|}{|E_{0p}|} \cdot e^{i\delta_p} \qquad (1.19.)$$

$$r_s = \frac{E_{rs}}{E_{0s}} = \left(\frac{|E_{rs}|}{|E_{0s}|}\right) \cdot e^{i(\delta_{0s} - \delta_{rs})} = \frac{|E_{rs}|}{|E_{0s}|} \cdot e^{i\delta_s} \qquad (1.20.)$$

where E_{0p}, E_{0s} : Components of incident light parallel and perpendicular to the plane of incidence, respectively.

E_{rp}, E_{rs} : Components of reflected light parallel and perpendicular to the plane of incidence, respectively.

r_p, r_s : Complex reflection coefficients of the parallel and perpendicular components, respectively.

$\delta_{0p} - \delta_{rp}$: Phase difference of the parallel component that occurs upon reflection ($\delta_{0p} - \delta_{rp} = \delta_p$).

$\delta_{0s} - \delta_{rs}$: Phase difference of the perpendicular component that occurs upon reflection ($\delta_{0s} - \delta_{rs} = \delta_s$).

The reflecting components (1.19. and 1.20.) are combined to a complex reflection ratio between the reflection coefficients of the p- and s-polarized light (r_p and r_s) which is given by

$$\rho = \tan\psi e^{i\Delta} = \frac{r_p}{r_s} \qquad (1.21.)$$

with $\tan\psi$ the amplitude ratio of the p- and s- component of the incident electric field after interaction with the surface($|r_p|/|r_s|$), and Δ the differential phase change of the p- and s- components of the incident field after reflection($\Delta = \delta_p - \delta_s$). The two parameters ψ and Δ are called the ellipsometry angles. They are both obtained from one single ellipsometry measurement. In the instrument shown in Figure 1.12., the light intensity is measured as a function of position of the polarizer (photometric instrument) and two Fourier coefficients that are dependent on ψ and Δ are obtained. From the calculated values of ψ and Δ the complex reflection ratio, ρ, is finally derived [185][186].

The complex reflective index $\tilde{n}$ of the material is described as

$$\tilde{n} = n - ik \qquad (1.22.)$$

where n is the real part of the refractive index and k is the extinction coefficient or the imaginary part of the refractive index, respectively (k is 0 for a transparent medium, e. g. air). Since the change in polarisation state of the reflected light is caused by the material on which it has been reflected from, ρ can be used to the derive the complex refraction index of the material. In this work the refractive indices of the substrates have been derived in this way in a measurement prior to adsorption of the SAMs.

When the refraction indices of the substrate, the adsorbed film and the medium (air) are known together with the reflection angle and the wavelength of the light, the complex reflection ratio, ρ, can be used to calculate the thickness of the film, *d*, by a fitting procedure [12].

Ellipsometry is very sensitive and substances adsorbed from the atmosphere affect the results. The roughness of the surface may also cause a systematic error of the values obtained. On the other hand it is a non-destructive technique and in combination with the short time required for the measurement it is a versatile instrument for analysis of thicknesses of thin films [186].

1.5. Adhesion

Adhesion may be considered as the tendency of different materials to stick together when they are brought to an intimate interfacial contact. This is usually achieved by the use of an adhesive and this has been defined as "a material which when applied to the surfaces of materials can join them together and resist separation" [187]. To fulfil these requirements an adhesive must do two things [1][188]:

1. It must wet the surface (giving a low contact angle) since an intimate contact between the molecules of the adhesive and the atoms and molecules in the surface is required.

2. The adhesive must then harden to a cohesively strong solid to be able to carry a load over the joint.

All adhesives used up-to-date either contain polymers or polymers in the final state. The inner strength of attractive forces between atoms and molecules of the adhesive are referred to as cohesive forces. These forces can be higher than the adhesive forces. Upon testing of the strength of adhesives, a failure in the adhesive system will finally result. A failure which occurs between one of the substrates and the adhesive is referred to as ad-

hesive fracture. A failure within the adhesive is called a cohesive failure. A failure within one of the substrates is of course also possible although this fracture is of less interest in adhesion studies. The different types of fractures are displayed in Figure 1.13.

Figure 1.13. Schematic representation of a an adhesive fracture (left), cohesive fracture (middle) and a fracture within one of the materials joined together with an adhesive (right). The black part in the figure represents the adhesive.

1.5.1. Theories of Adhesion

There are several theories suggested to explain phenomena observed in connection with adhesion and the most important are briefly described below [1][187][188][189][190].

Physical adsorption theory [1][187][190]

The physical adsorption theory is a widely applicable theory and proposes that, when sufficiently intimate molecular contact is achieved at the interface, the materials will adhere because of the interatomic and intermolecular forces that are established between the atoms and the molecules in the surfaces of the adhesive and substrate. The forces accounting for the physical adsorption theory involves van der Waals forces. Stronger forces at the interface, such as covalent, ionic or hydrogen bonds, are described under the chemical bonding theory.

Van der Waals attractions at an interface require attractions between permanent dipoles or induced dipoles. In a molecule of the type A-B, where A and B are different elements with different electronegativity, the molecule will have a permanent dipole moment. Adjacent molecules with a dipole moment will have an attractive force to the A-B molecule. The orientational effect is sometimes mentioned as Keesom-forces.

A dipole situated close to a non-polar molecule will induce a dipole in the latter (Debye-interaction). The induced dipole moment will depend on the polarizability of the non-polar molecule and the electric field which is given by the surrounding dipoles and external electric fields. In two non-polar molecules instantaneous dipoles will be formed due to the fluctuating distribution of electrons. These instantaneous dipoles will lead to attractive forces between molecules and are often referred to as London dispersive forces.

The free energy U of all these interactions between two molecules are inversely proportional to the 6th power of the distance of separation, r, as given by the Lennard-Jones potential between molecules [148][157][191][192]:

$$U = -\frac{A}{r^6} + \frac{B}{r^{12}} \tag{1.23.}$$

where A is the attractive constant and B the repulsive constant, which are related to eachother. The force F between the two molecules is given by $F = -(dU)/(dr)$, that is,

$$F = -\frac{6A}{r^7} + \frac{12B}{r^{13}} \tag{1.24.}$$

This means that the attractive forces fall rapidly with distance and are only effective at distances less than a few diameters of the molecules. If the molecules are to close to each other, the repulsive factor will dominate. Hence, there is a distance r_0 where the net force is zero and the free energy U is at minimum. For two macroscopic plates the interactions are different. The free energy is inversely proportional to the square of the separation distance and the attractive force diminishes with the inverse cube of distance between the plates [157].

Of the three forces mentioned above (van der Waals forces, induced and permanent dipoles), the attractions between permanent dipoles are the strongest ones and are usually of a magnitude around 4 kJ/mol, although they have been reported to be as high as 20 kJ/mol [187]. Huntsberger [193][194] and others [195][196] have calculated the attractive forces between two planar bulk phases due solely to dispersion forces derived from the knowledge of the surface free energies. They showed that at a separation of one nanome-

tre, the attractive force would result in a joint strength of around 100 MPa, which is considerably higher than the experimental strength of most adhesive joints. The divergence between theoretical and experimental results is due to differences in the theoretical and practical contact area, most likely arising through contaminants at the surface, air-filled voids or other defects. Despite the disparity between the theoretical and experimental results the calculation reveals that, in theory, strong adhesive joints can be made up of only van der Waals forces at the surface.

Chemical bonding theory [1][187][188][189]
The chemical bonding theory involves strong forces between adhesive and substrate such as covalent, ionic, or hydrogen bonds. Evidences of covalent bonding over the interface between an adhesive and substrate have been found with infrared spectroscopy [197][198] as well as other techniques [199].

It is expected that covalent and ionic bonds should form stronger bonds than hydrogen bonds. Covalent and ionic bonds have been reported to form bonds with energies in the range of 60-700 kJ/mol and 600-1100 kJ/mol, respectively, while bond energies of hydrogen bonds are reported up to 40 kJ/mol [200][201][202].

A supplement to the chemical bonding theory is the acid-base interaction theory relying on Lewis acid-base interactions at an interface resulting in an acid-base complex [190][202]. The acid-base interactions encompass both covalent and noncovalent (ionic and hydrogen bonds) interactions and have been reported to be as strong as ionic bonds [187].

It is obvious that the chemical bonding theory accounts for some (theoretically) very strong interactions at an interface. Klein et al. [203] found infrared evidence of covalent primary bonds between a polyurethane adhesive and epoxy-based primers, and such interfacial interactions gave the highest joint strengths. However, the chemical bonding theory has also limitations. The biggest problem related in forming a chemical bond at the interface is the short distance of a few Ångströms that is necessary for the two reactants

to form a chemical bond over the interface. Contaminations will significantly influence the possibility to form chemical bonds.

Diffusion theory [1][187][189][190]

When at least one of the substrates consist of a polymer, polymer molecules in contact may interdiffuse so that the initial boundary is eventually removed. This requires that the macromolecules, or chain segments of the polymers (adhesive and substrate) possess sufficient mobility (temperature must be above glass transition temperature, T_g) and are at least partially compatible. Here, where polymer phases contact rigid flat substrates, this theory is of limited usefulness.

Electrostatic theory [1][187][188][190]

The electrostatic theory relies on differences in the electronic band structures of substrate and adhesive. Upon contact, electrons will be transferred from one phase to the other, forming an electrical double layer, which gives a force of attraction. As most polymers are insulators, it seems difficult to apply this theory to adhesives [1].

Mechanical Interlocking [1][187][188][190]

When a rough surface with cavities is brought into contact with an adhesive, the adhesive may interlock prior to hardening. The mechanical interlocking of the hardened adhesive contributes to the adhesion mechanism in this theory. Problems with this theory involve uncertainties in the pretreatment of the surface to obtain the appropriate topography needed for the interlocking [187]. This theory, which is of great importance in practise, is to a great extent excluded in this thesis due to the use of flat substrates.

Weak boundary layer [1][188][190]

The weak boundary layer theory proposes that clean surfaces can give strong bonds to adhesives but contaminants such as rust, oils or greases create a layer which is cohesively weak. The weak boundary layer will thus reduce the adhesion unless the adhesive dissolves the contaminants as in the case of some acrylic adhesives [1]. Since adhesion is always influenced by the cleanness of the substrates this is a theory applicable to all adhesive problems.

1.5.2. Methods of Adhesion Measurements

The thermodynamic work of adhesion, W_A, between two different media, 1 and 2, is defined as the work required to separate a unit area of two phases in contact, as shown in Figure 1.14. (upper left part). For two identical media (1 = 2) it is referred to as the work of cohesion (upper right part in Figure 1.14.) [157]. The surface energy is the free energy change γ when the surface of a medium is increased by a unit area. Now the process of creating unit area of surface is equivalent to separating two half-unit areas from contact (Figure 1.14., upper right part), so that we may write $\gamma_1 = \frac{1}{2} W_{11}$.

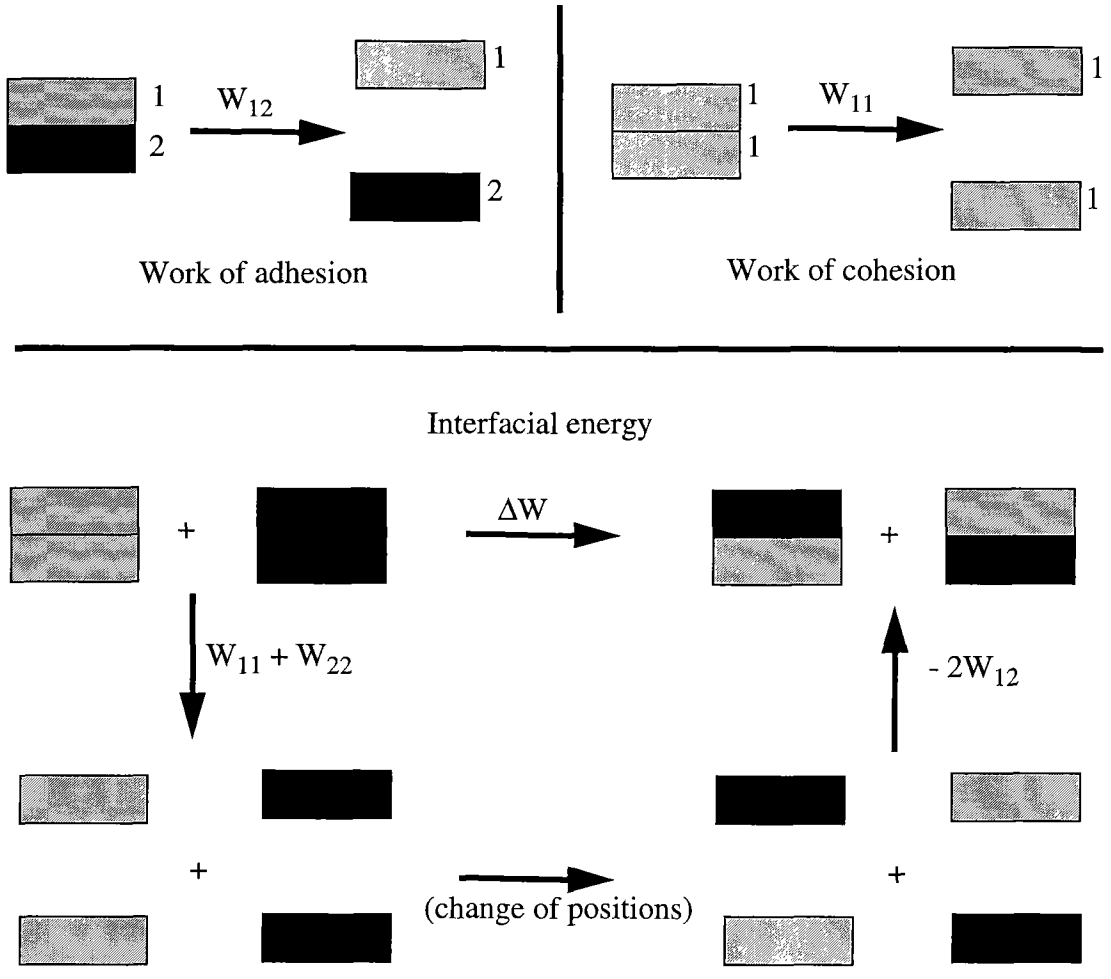

Figure 1.14. Definition of various energy terms associated with the adhesion and area changes of surfaces [148].

When two medium are in contact, the free energy change in expanding their interfacial area by unit area is known as their interfacial energy or interfacial tension γ_{12}. The energetics associated with this process is shown in Figure 1.14. (lower part) [148]. The total free energy change is therefore:

$$\gamma_{12} = \frac{1}{2} \Delta W = \frac{1}{2} W_{11} + \frac{1}{2} W_{12} - W_{12} = \gamma_1 + \gamma_2 - W_{12} \qquad (1.23.)$$

which is often referred to as the Dupré equation [204]. For the adhesion between a solid (1) and a liquid (2) with air as the surrounding medium, we can rewrite the Dupré equation ($\gamma_1 = \gamma_{sv}$, $\gamma_2 = \gamma_{lv}$ and $\gamma_{12} = \gamma_{sl}$) as:

$$W_A = \gamma_{sv} + \gamma_{lv} - \gamma_{sl} \qquad (1.24.)$$

and when combining this equation with the Young's equation (1.1.) we obtain the Young-Dupré equation:

$$W_A = \gamma_{lv} (1 + \cos \theta) \qquad (1.25.)$$

which gives useful information of the interaction of a liquid with a surface. Of course, adhesives usually are not liquids but, at least, a simple contact angle measurement can be used as a first approach to estimate the characteristics of a surface.

Mechanical testing of adhesive joints are a widely used technique to obtain practical information about adhesion forces. There are several different test methods available to provide information about adhesive joints. Some of these are shown in Figure 1.15. where the lap-shear test provides information about shear stresses in an adhesive joint. The blister test can be used to obtain data about the adhesive fracture energy. Here a blister is formed by injection of a compressed fluid or gas through a hole in the sample. subsequently the energy release rate and the load at which the debonding process propagates are monitored [205][206]. The released energy measured by the blister test includes both the thermodynamic work of adhesion and the viscoelastic deformation of the adhesion, which

usually corresponds to more than 50% of the measured energy. It has been suggested that the study of the maximum local bending moment provides a more accurate description of the intrinsic adhesive fracture energy [206].

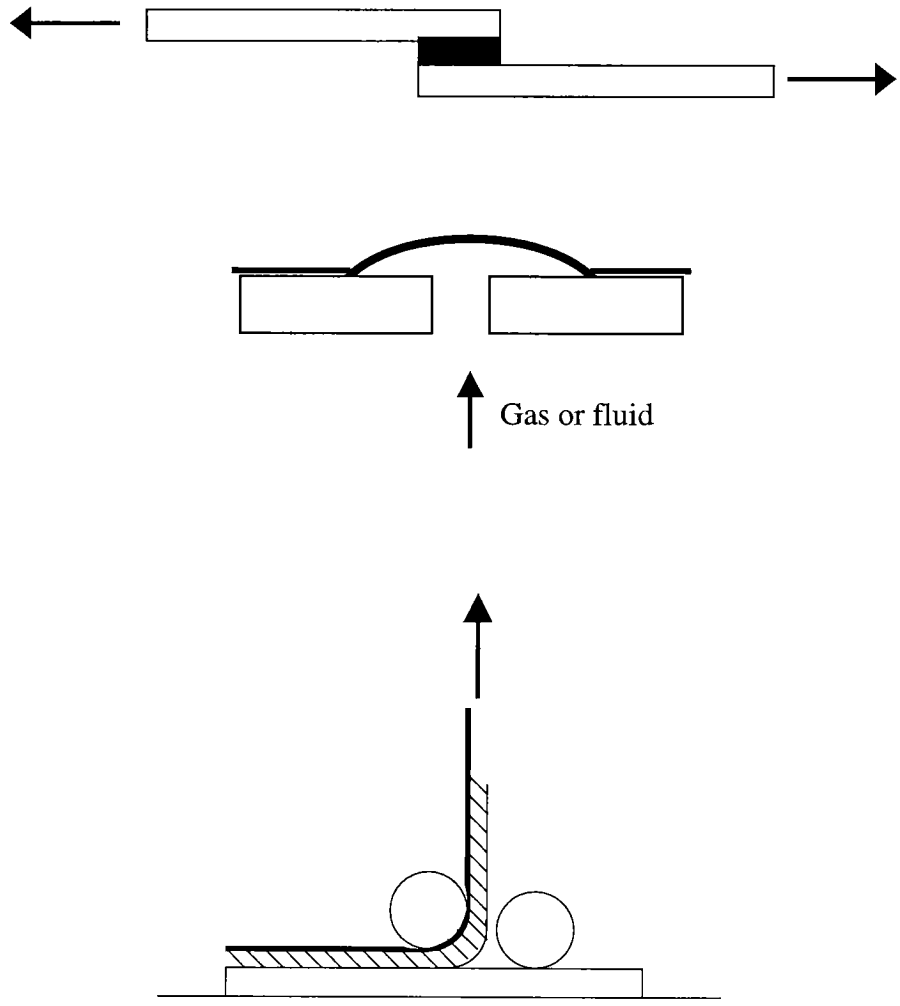

Figure 1.15. Schematic representation of some test methods for adhesion. From above: Lap-shear test, blister test, and the peel-test, which has been used in this thesis.

The 90° peel-test used in this thesis (Figure 1.15.) involves peel or cleavage forces in a fracture. The test is accomplished by establishing a constant radius of curvature after a initial failure and by monitoring the load required to promote peeling. A graph displaying the force as a function of the peel distance is obtained. Two different types of load behaviour are usually noted [205]:

A: After an initial force peak, which is usually neglected, a fairly constant peel force is obtained while the delamination propagates until a complete separation.

B: For other adhesives stick-slip behaviour is observed, where the load builds up to a critical value at which the sample "unzips" and during which the load drops to a very low value. This process is then repeated several times until separation of the substrates are obtained. The peel force is considered as the as the average value of the slick-slip process.

The results obtained are heavily influenced by the adhesive used, the modulus of the substrate and the material that is peeled, the thickness of the peeled material, the peel rate as well as the thickness of the adhesive layer. An advantage of the peel test is that a continuous record of the fluctuating peel strength can be obtained as well as information on the scattering of the measured values in a single joint [1].

1.6. Goals of this Thesis

The underlaying phenomena of adhesion are not yet fully understood despite of the numerous suggested theories, of which some are described in section 1.5.1. on page 54. In this context there are several issues that are interesting to gain deeper insight, such as the influence on adhesion of the amount of functional groups present at the interface and available for chemical bonding with the adhesive. Of course, the nature of the functional groups at the surface will also play an important role in this context. Such questions will be addressed in model systems.

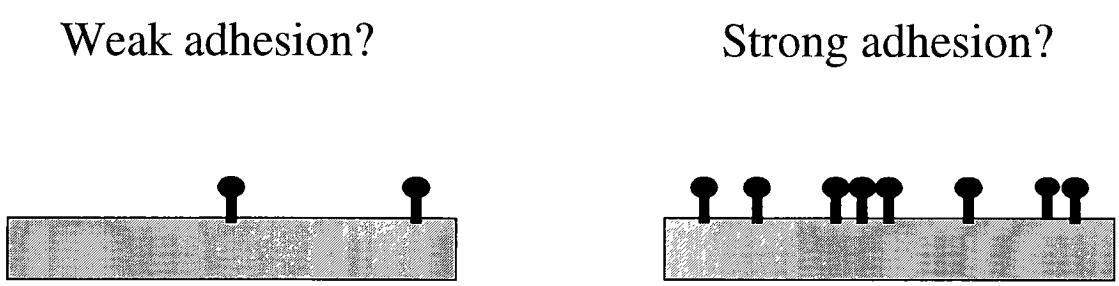

Figure 1.16. One of the goals of this thesis is to investigate the influence on adhesion of different functional groups as well as their concentration.

In order to study such issues, self-assembled monolayers (SAMs) are used to create a promising, well-defined surface. The surface concentration of functional groups can be varied by use of two alkanethiols with different endgroups. We note, however, that it is not completely evident from the literature if the components separate into domains or if the components are randomly mixed.

The self-assembly technique allows to make surfaces with a vast variety of functional end groups. In order to obtain well-ordered monolayers it is necessary to use long-chained alkanethiols containing at least 8 CH_2-groups. Only few commercially available alkanethiols terminating in other groups than methyl exist with these chain lengths. The synthesis of long-chain alkanethiols with functional endgroups is usually a very laborious process. Another problem with the synthesis of tailored alkanethiols is the purity of the product. A little fraction of a contaminant in the synthesized thiols will influence the order and the packing density of the SAM and contaminants might be incorporated in the monolayer.

An alternative to the demanding synthesis of tailored alkanethiols is to perform derivatisation on a pre-established and well-ordered monolayer. Such reactions must however be carried out under mild conditions in order not to affect the adsorbed monolayer. Some attempts have been made in this direction and are described in section 1.3.5. on page 32. All of these attempts have indeed resulted in a successful derivatization of the underlaying monolayer but the flexibility to perform surface reactions are limited and sparsely de-

scribed in the literature. There is therefore a general interest in finding a versatile and straight-forward method to modify self-assembled monolayers of commercially available substances, which allows chemical anchoring of a variety of compounds to the monolayers. A specific tailoring of such SAMs would also be useful for addressing questions raised in the context of adhesion.

The remainder of this thesis is organised as follows: in chapter 2, the characterisation of the gold substrate is described together with the formation of mixed self-assembled monolayers. The order within such mixed SAMs is also discussed. Chapter 3 deals with the modification of hydroxyl-terminated SAMs and their reaction with 1,4-phenylene diisocyanate (PDI). Kinetic aspects of the reaction are discussed together with a characterisation of the resulting isocyanate-bearing monolayers. A quantitative study of the derivatization of mixed SAMs is also included together with a discussion of the stability of derivatised thin layers. The possibilities to functionalise the isocyanate-modified monolayers with a wide variety of substances are considered in chapter 4.

In chapter 5 the tailored self-assembled monolayers are applied as substrates for adhesion studies regarding the influence of amount and functionality upon adhesion for different adhesive systems. Finally, the conclusions drawn from the work in this thesis are summarized in chapter 6 and the details of the experimental procedures are given in chapter 7.

2. Adsorption of Self-Assembled Monolayers (SAMs)

The production of self-assembled monolayers (SAMs) are today a convenient and well-established technique to produce thin layers with little effort and good reproducibility. Such layers, composed of molecules with 10 or more carbon atoms per alkyl chain, are highly ordered and densely packed [3][4]. Besides the methyl-terminated 1-alkanethiols, ω-substituted 1-alkanethiols of the formula $HS(CH_2)_nX$, where X is, e.g., a halogen atom or a hydroxyl, amino, carboxylic acid, ester, or nitrile group, have also been employed as well as mixed monolayers of 1-alkanethiols with different terminal groups [6][97]. The functional end groups thus introduced change the surface's wetting properties and chemical reactivity [207][208][209]. In this chapter, the wetting properties and the surface composition of mixed monolayers made of 1-dodecanethiol (DDT) and 1-mercapto-11-undecanol (MUD) are discussed together with the characterisation of the underlaying gold substrate.

2.1. Characterisation of the Gold Substrate

The gold substrates used in this thesis have been thoroughly characterised and described in earlier studies at the institute of polymers [12][26][41][178][210]. The substrates were prepared by evaporating ca. 2000 Å of gold with a deposition rate of ca. 15 Å/s and at a pressure of ca. 10^{-5} mbar onto silicon (100) wafers cut into rectangles of dimensions 18×40 mm, which had previously been covered with 60 Å of chromium as an adhesion promoter. The obtained gold surfaces consist of crystallites predominantly presenting the (111) face [12][186]. This can be explained by thermodynamic reasons since the (111) face is exhibiting the lowest surface area and thereby has the lowest surface energy [107]. The distance between two gold atoms for this face has been determined as 2.88 Å [12][107].

The evaporated gold surfaces are highly reflective which makes them convenient for characterisation with GIR and ellipsometry. However at a resolution higher than that for the human eye (approximately 50 μm [108]), the gold surfaces are not perfectly flat. Obser-

vations with AFM and SEM show flat grains of a diameter of 300-6000 Å. Between the grains there are valleys, which are sometimes deeper than 100 Å [12]. The roughness of the surface within a grain is significantly lower. Profilometry investigations have shown an average roughness (R_a) of 5-15 Å over a grain [178]. This is in agreement with R_a of 20-25 Å determined by AFM [12]. Since these roughnesses are of the same dimension as the thickness of SAMs investigated in this thesis, it is for AFM-characterisation necessary to have a smoother gold surface to be able to detect variations in the SAM.

The Si-wafers used for the evaporation have a much smoother surface (R_a< 5 Å) than the gold surface obtained after evaporation. STM investigations also show that the surface roughness increases with the thickness of the gold film [26]. On the other hand, the refractive indices, which are important for ellipsometry measurements, are influenced by the underlaying silicon layers and the adhesion primer for thin gold films [26]. Stable values for the refractive indices of gold which are consistent with those found in the literature [211] are only obtained for films with a thickness of 2000 Å or higher. For gold film with a thickness of 2000 Å the refractive indices for films determined in this work had values of n between 0.1529 and 0.1622. The extinction coefficients, k, used had values between -3.2956 and -3.5528. these values are in agreement with literature values [178]. Earlier investigations have shown that k is the crucial part for obtaining consistent thicknesses and low deviations in ellipsometric measurements [41].

The conflicting interests of obtaining low surface roughness and consistent values of the refractive indices can be solved by the production of an ultralarge atomically flat template-stripped gold surfaces, where a gold film is evaporated on mica, glued onto a Si-wafer and removed from the mica in contact with the gold layer first deposited [212]. These atomically flat gold surfaces exhibit a surface roughness of less than 3 Å over a distance of 25 μm. However the manufacture of these surfaces is very laborious and since the thiols employed for the mixed SAMs in this thesis have the same molecular length, also a roughness of 3 Å would influence the results. To obtain information of interest from a scanning microscopy technique of mixed SAMs of the compositions used here, a lateral resolution higher than available today from the lateral force microscopy (LFM) would be required [162]. For these reasons the work in this thesis emphasizes the ellipsometer technique.

Thus the parameters of the gold surface have been optimized for ellipsometry analysis and gold films of 2000 Å have been employed.

The gold surfaces obtained from evaporation are of high free energy [97] and should therefore be wetted by water. However upon exposure to the atmosphere they are covered by a few Å of contaminants [97]. This leads to an advancing contact angle of water of 50 to 70° depending on how quickly the measurement is performed after evaporation. A prolonged exposure to atmosphere results in a contact angle of ~80 °. This is in good agreement with literature values [87] although these are highly affected by other chemicals used in the laboratory and possibly reconstruction of the surface.

Ellipsometry investigations show that the contaminating layer is below 5 Å. These measurements are however of limited reliability since the refractive indices that are determined prior to the thickness measurement are also influenced by adsorbed contaminants. The exposure time to air is significant for the refractive indices obtained. They increase with time due to an increasing amount of adsorbed contaminants [178]. The interaction forces between the contaminant layer and the surface are, however, weak and a contaminating layer is expelled from the surface upon immersion in a solvent [178]. All samples used for ellipsometry in this thesis have been determined with refractive indices within ten minutes after evaporation and then immediately immersed in the adsorption solution.

Survey spectra of XPS measurements of gold substrates show that the surface is indeed contaminated by hydrocarbon as well as oxygen species (Figure 2.1.). Hydrocarbons are identified by the peak around 285 eV and oxygen is found at 532 eV. All other peaks derived from the gold surface and the two strongest gold peaks at 84 and 87 eV are reproduced in Figure 2.2. A quantitative study of the high resolution spectra is included in Table 2.1.. In a similar XPS-study, Bain *et al.* found the layer of contaminants to be around 6 Å [97].

Closer examination of the contaminated carbon species at gold surfaces in this study and a comparison with well defined SAMs of octadecanthiol (ODT) in a different study [178] have shown that the contamination layers have a thickness of a few Å and are in accor-

dance with results from ellipsometry measurements described above and the XPS results in Table 2.1..

.

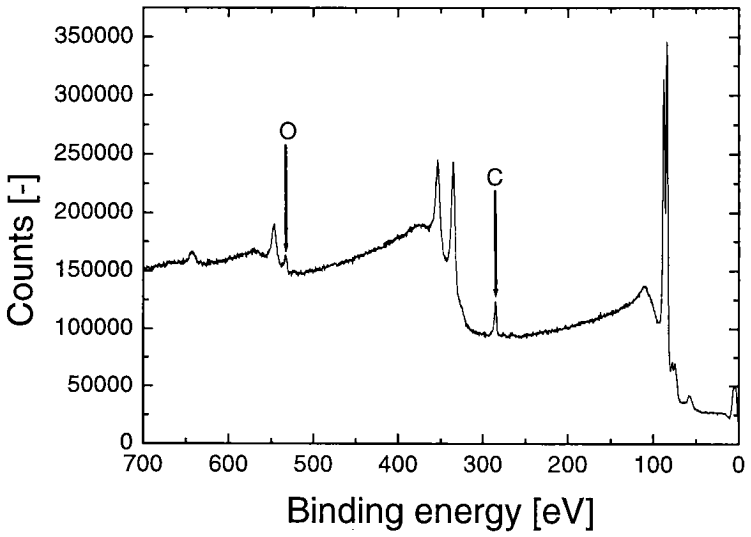

Figure 2.1. XPS-survey spectra of a gold wafer. The wafer is immediately contaminated with carbon and oxygen species seen as the peaks at 285 and 532 eV, respectively. All other peaks are originating from the gold surface.

Table 2.1. Atomic composition of elements determined by high resolution XPS at an take-off angle of 15° for a gold substrate and a gold substrate covered with a MUD-monolayer.

Element	Gold-substrate	MUD-monolayer
O	3.0	9.2
C	65.4	67.3
S	-	1.5
Au	31.6	22.0
Total	100.0	100.0

The Au ($4f_{7/2}$) and ($4f_{5/2}$) levels in high resolution spectra appear at 84.0-84.2 eV and 87.6-87.8 eV, respectively (Figure 2.2.). The deviations from the reference values (84.0 and 87.6, respectively) are due to charging of the samples or experimental artefacts. Such deviations are, however, in accordance with earlier studies [178] and literature values [167][173]. For all samples used in this thesis the Au($4f_{7/2}$) peak has been used as a internal standard for XPS studies, i.e., each sample has been calibrated to a Au($4f_{7/2}$) binding energy of 84.0 eV.

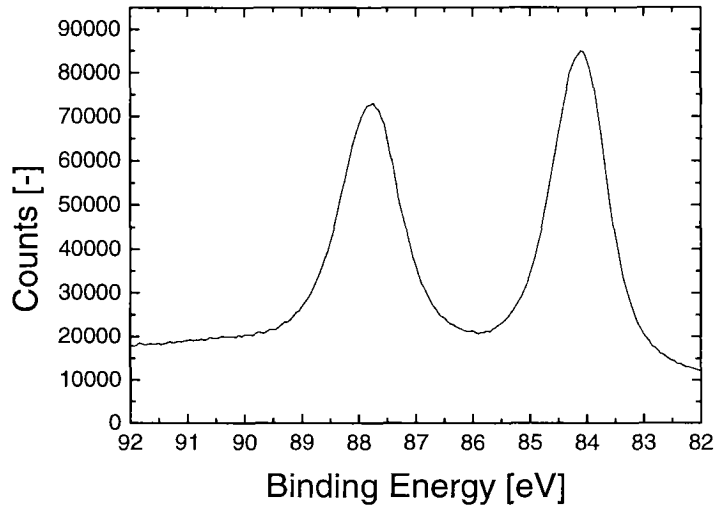

Figure 2.2. High resolution XPS spectra of the Au (4f) region.

2.2. Characterisation of Mixed Self-Assembled Monolayers

For the preparation of mixed monolayers, alkanethiols employed were 1-dodecanethiol (DDT) and 1-mercapto-11-undecanol (MUD). Monolayers of DDT, of MUD, and mixed monolayers of these molecules on gold have already been described [6]. Accordingly, gold samples were immersed in ethanol solutions of the thiols for 16 h (reported to be sufficient to establish equilibrium [97]) at a total concentration of 1 mM.

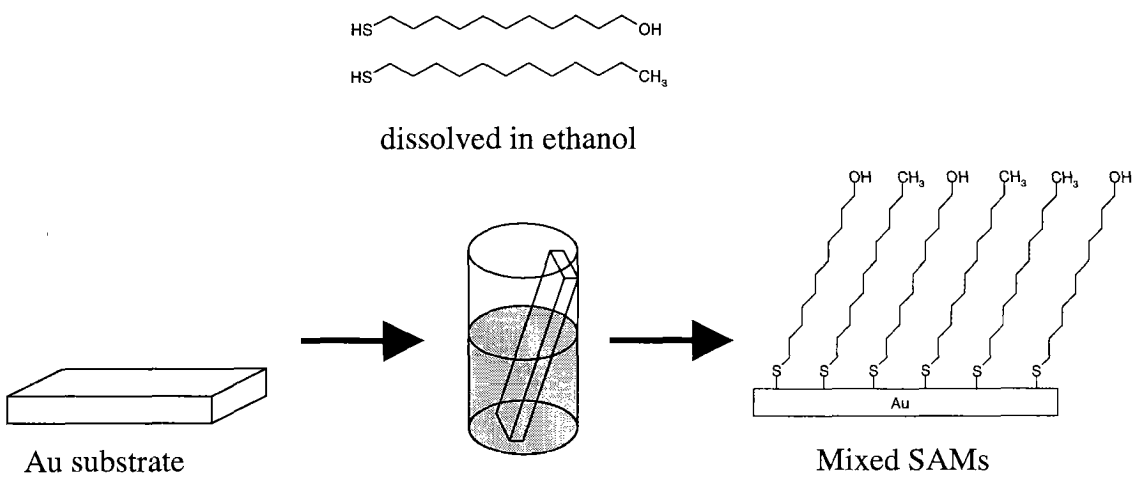

Figure 2.3. Schematic representation of the production of mixed self-assembled monolayers.

2.2.1. Results from Contact Angle Measurements

The advancing contact angles of water on the pure DDT and MUD monolayers were found to be 115 and 13°, respectively. Hexadecane (HD) is a nonpolar liquid and therefore of low surface energy. Thus the advancing contact angles of HD are lower and were found to be 48 and 5° for the DDT and the MUD layers, respectively. The advancing contact angles of the mixed layers are all between the values of the pure monolayers and are shown in Table 2.2.. Contact angles below 15° are difficult to measure and are often referred to as <15°. For consistency in the determination of surface concentration by contact angle measurements below, a numerical value is given in Table 2.2. also for angles below 15°. The obtained contact angles do not vary linearly with the fraction of MUD in the solution y_{MUD}, which is an indication of a different surface fraction of MUD (Ξ_{MUD}) from the solution it was immersed in.

Table 2.2. Advancing contact angles of water and hexadecane, $\theta_a(H_2O)$ and $\theta_a(HD)$, on monolayers of DDT and MUD and mixed monolayers composed of DDT and MUD with different fractions of MUD in the solution y_{MUD}. The standard deviations of the specified values are within ±2°.

y_{MUD}	$\theta_a(H_2O)$	$\theta_a(HD)$
0.0	115	45
0.1	109	42
0.2	103	39
0.3	100	37
0.4	92	35
0.5	86	34
0.6	74	28
0.7	59	21
0.8	42	11
0.9	34	7
1.0	13	3

The $\theta_a(H_2O)$ have also been used to estimate the relative surface fraction, Ξ_{MUD} with the help of the Cassie equation [156]

$$\cos\theta = \Xi_{MUD}\cos\theta_{MUD} + (1-\Xi_{MUD})\cos\theta_{DDT} \qquad (1.3.)$$

and the Israelachvili and Gee equation[158]

$$(1+\cos\theta)^2 = \Xi_{MUD}(1+\cos\theta_{MUD})^2 + (1-\Xi_{MUD})(1+\cos\theta_{DDT})^2 \qquad (1.11.)$$

where θ is the advancing contact angle on the mixed monolayers and θ_{MUD} and θ_{DDT} are the advancing contact angles on the pure MUD and DDT monolayers, respectively. Both of these semi empirical equations are considered to yield similarly good correlations [6];

Israelachvili and Gee have suggested Eq. 1.11. as an alternative to Eq 1.3. "whenever the size of chemically heterogeneous patches approaches molecular or atomic dimensions" [158]. The mixed SAMs should fit this description for surfaces with randomly distributed molecules, while Eq. 1.3. is thought to be more accurate for the description of surfaces with distinct patches or phase-separated islands. It is worth to note that estimations from the two equations will always give a lower Ξ_{MUD} for the Israelachvili and Gee relation. This is a result of the two equations (see chapter 1, section 1.4.1. Contact Angle Measurements).

The result of the estimations for mixed monolayers of DDT and MUD are shown in Figure 2.4. For $y_{MUD} < 0.7$, Ξ_{MUD} is significantly lower than y_{MUD}. This originates from the solvent the thiols were dissolved in. The nonpolar DDT-molecule dislikes the polar ethanol solvent and is more likely to attach to the gold surface. Laibinis et al. performed a similar study where the adsorption was made from both isooctane and ethanol solution [6]. For the nonpolar solvent isooctane the opposite was observed and the polar MUD-molecule were present at the gold substrate to a much higher fraction than to the concentration in solution. Laibinis' adsorption from isooctane has been recalculated and the results are shown in Figure 2.5. Due to the different results depending on the choice of solvent it is likely to be possible to obtain the same surface ratio of the two thiols as in the solution, if an appropriate solvent is chosen. Ulman et al. have shown results pointing in this direction when they used tetrahydrofuran as solvent for the production of mixed SAMs from MUD and DDT [213]. This issue was however not followed closer in this work. For a probable desire to keep the surface composition of MUD low in the application for adhesion measurements described in chapter 5, ethanol was the only solvent for the production of mixed SAMs used in this study due to its versatility to obtain low Ξ_{MUD} in mixed SAMs.

Further it is obvious from Figure 2.4. that something changes for the system studied here when y_{MUD} is increased above 0.7 in the adsorbing solution. For $y_{MUD}>0.8$, $\Xi_{MUD} \approx y_{MUD}$, in accordance with Laibinis' adsorption experiments from ethanol. For SAMs adsorbed from isooctane, no change of this kind was observed (Figure 2.5.).

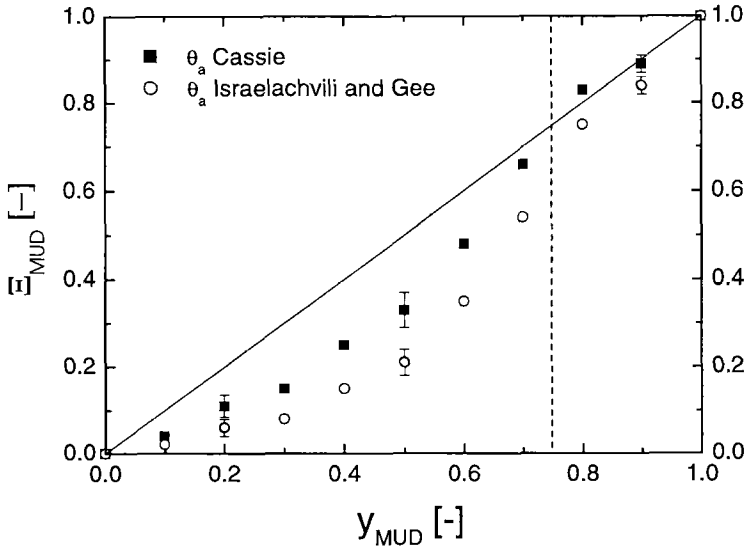

Figure 2.4. Surface fraction of MUD, Ξ_{MUD}, in mixed monolayers with DDT as a function of the corresponding fraction of MUD in solution, y_{MUD}, calculated from contact angle measurements with water using Cassie's equation and the equation of Israelachvili and Gee. The indicated straight line represents the situation for $\Xi_{MUD} = y_{MUD}$.

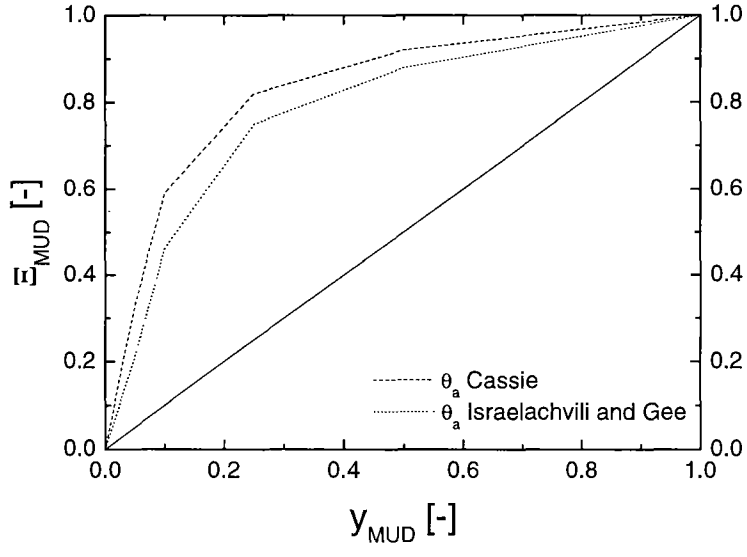

Figure 2.5. Surface fraction of MUD, Ξ_{MUD}, in mixed monolayers with DDT as a function of y_{MUD} adsorbed from isooctane. Results recalculated from reference [6].

2.2.2. Results from XPS Measurements

XPS gives valuable information about the composition of the mixed monolayers. The atomic compositions of pure SAMs from DDT and MUD are included in Table 2.3.. All the mixed SAMs had atomic compositions in between these two extremes. The atomic composition of oxygen in these mixed SAMs can be used for a determination of the amount of oxygen in the samples as described below.

Table 2.3. Atomic composition of elements determined by high resolution XPS for pure DDT and MUD-monolayers.

Element	DDT	MUD
O	0.0	9.2
C	74.4	67.3
S	2.1	1.5
Au	23.5	22.0
Total	100.0	100.0

As described in chapter 1, the self-assembly is due to the affinity of sulphur to gold. Sulphur is in fact detected by XPS, and the S(2p) high resolution XPS spectra of a MUD monolayer is dominated by a broad, asymmetric, non-resolved signal with a maximum at around 162 eV and a shoulder at ca. 163.5 eV, representing the $2p_{3/2}$ at the maximum and the $2p_{1/2}$ peak at the shoulder (Figure 2.6.).

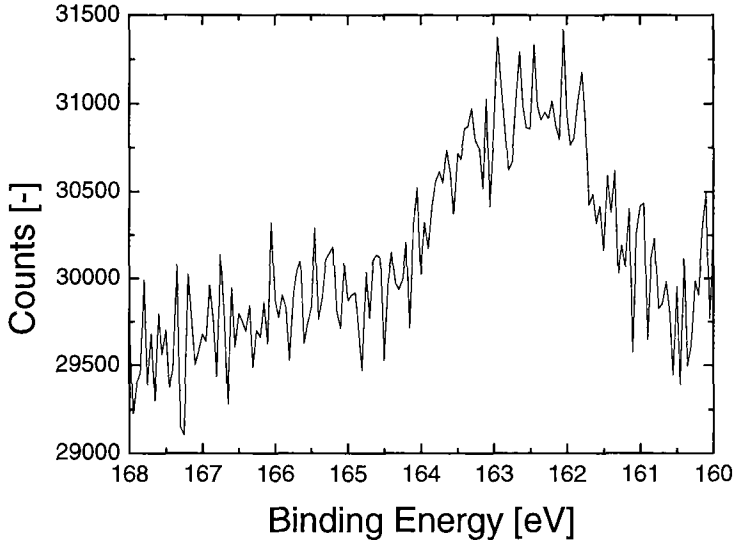

Figure 2.6. High resolution XPS spectra of the S(2p) peak of a 1-mercapto-11-undecanol (MUD) monolayer.

The amount of oxygen detected in each sample will depend on the amount of MUD in the SAM and this was used to determine the compositions of the mixed SAMs in the following way. For each sample, the intensity of the photoelectron signal of oxygen was compared to the intensity of the SAM composed solely of MUD. To avoid variations in the experimental setup (e.g. distances between X-ray gun, sample and detector) all samples were normalized to the intensity of the Au($4f_{7/2}$) peak in the same sample as an internal standard. Typical XPS spectra of the O(1s) regions are shown in Figure 2.7., where the intensity of the oxygen signal increases with the fraction of MUD in the solution. The dashed line shows the position of the peak maximum in the spectrum from the pure hydroxyl-terminated monolayer. A slight shift to higher binding energy is observed as Ξ_{MUD} decreases. This shift is not a consequence of charging between the samples since the position of the Au ($4f_{7/2}$) was constant within ±0.2 eV prior to calibration described in section 2.1

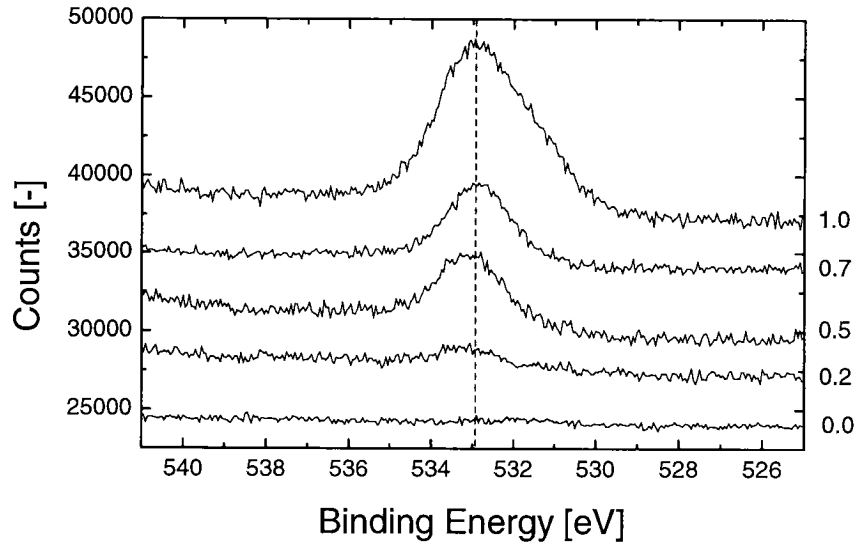

Figure 2.7. O(1s) peak in the XPS spectra of mixed SAMs. The values on the right hand side correspond to the fraction of MUD in the solution, y_{MUD}. The dashed line indicates the peak position of the pure MUD-monolayer (y_{MUD}=1.0).

The surface fractions Ξ_{MUD} derived from the intensity of the O(1s) peak after internal calibration to the Au($4f_{7/2}$) peak are shown in Figure 2.8. as a function of the fraction in solution, y_{MUD}. The determined numerical values for Ξ_{MUD} are also shown in Table 4 on page 81. For $y_{MUD} < 0.7$, Ξ_{MUD} is significantly lower than y_{MUD} in accordance with the results from contact angle measurements. Also for $y_{MUD} > 0.8$, $\Xi_{MUD} \approx y_{MUD}$, which was observed in section 2.2.1. as well. This could be due to the increased coverage of the surface with hydroxyl groups, which may render the surface more polar and suitable to hydrogen bonding, especially when Ξ_{MUD} becomes above 0.5. At this surface fraction of MUD the distance between the individual hydroxyl groups is decreased to numbers where hydrogen bonding can occur and may favor the adsorption of MUD.

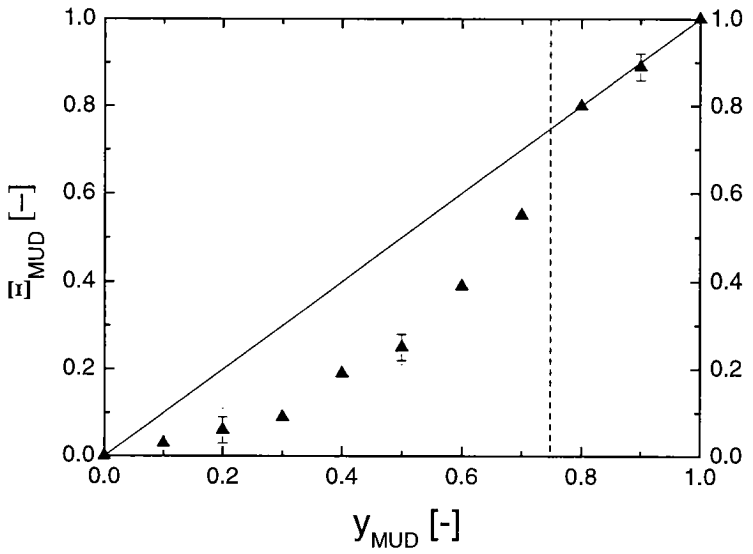

Figure 2.8. Surface fraction of 1-mercapto-11-undecanol (MUD), Ξ_{MUD}, in mixed monolayers with 1-dodecanethiol (DDT) as a function of the corresponding fraction of MUD in the adsorbing solution, y_{MUD}, determined by XPS according to the description in the text. The indicated full line represents the situation for $\Xi_{MUD}= y_{MUD}$, and the dashed line indicates a possible phase boundary between mixed and phase-segregated systems.

The C(1s) peak in the XPS spectra reveals variations for different y_{MUD}. With increasing y_{MUD} a tail or shoulder is observed on the high energy side of the carbon-peak. This shoulder can be resolved to an additional peak which arises from the carbon atom adjacent to the hydroxyl group (the C-O atom) [167][172]. The peak-maximum is found at around 286.6 eV. The dashed line shows the position of the peak maximum in the spectrum from the pure DDT monolayer (y_{MUD}=0.0). A slight shift to higher binding energy is observed as y_{MUD} increases as a consequence of a higher contribution of the C-O shoulder. Resolving the asymmetric C(1s) peak into a C-C peak at 285.0 eV and a C-O peak at 286.6 is valuable for obtaining information of the composition of the mixed SAMs. Fitting without constraints delivers an increasing C-O contribution with increasing y_{MUD}. Comparison of the C-O fraction to that for the pure MUD-monolayer will deliver an estimation on the surface concentration, Ξ_{MUD}, in the same way as for the O(1s)-peak described above. No

internal standard like the Au($4f_{7/2}$) peak is necessary in this case since the obtained values are already compared to the total carbon peak they are generated from.The quantification of Ξ_{MUD} with this technique gives results in good agreement to those shown in Figure 2.8., indicating that sample-to-sample variations do not significantly influence the calculated compositions.

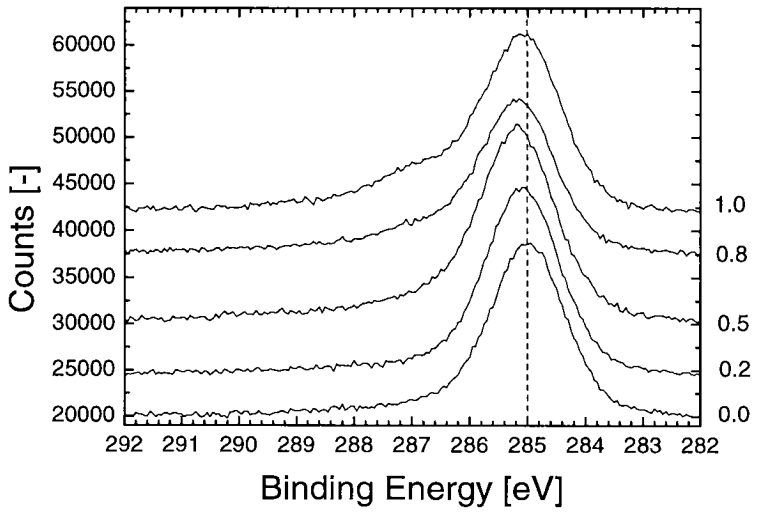

Figure 2.9. C(1s) peak in the XPS spectra of mixed SAMs. The values on the right side correspond to the fraction of MUD in the solution, y_{MUD}. The dashed line indicates the peak position of the pure DDT- monolayer (y_{MUD}=0.0).

The shift of the main peak of the binding energy increases with increasing hydroxyl concentration and is determined to be about 0.3 eV higher for y_{MUD}=1.0 than for y_{MUD}=0.0. The shift of the peak maxima to a higher binding energy arises from a higher contribution of the C-O shoulder which increases with the concentration of MUD (y_{MUD}) in the adsorbate solution.

2.2.3. The Mixed SAMs

A comparison of the contact angle- and the XPS-technique applied to quantify Ξ_{MUD} is shown in Figure 2.10. It is obvious that the values obtained from XPS lie between the results derived from the Cassie and the Israelachvili-Gee equations.

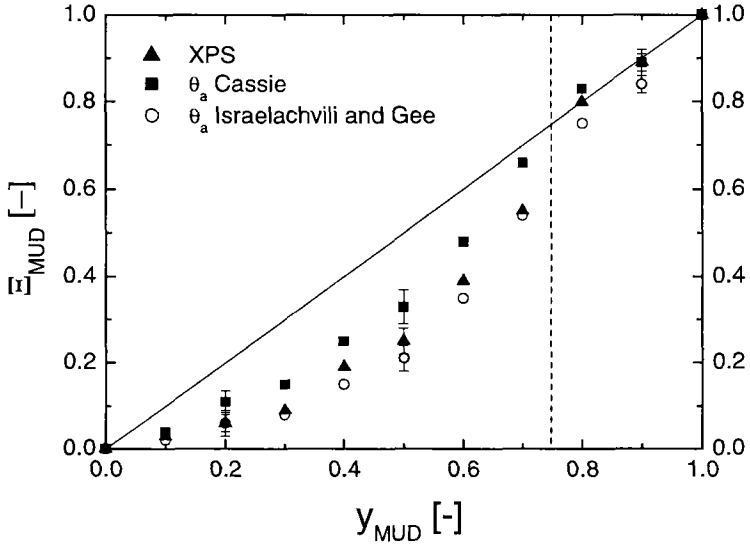

Figure 2.10. Surface fraction of 1-mercapto-11-undecanol (MUD), Ξ_{MUD}, in mixed monolayers with 1-dodecanethiol as a function of the corresponding fraction of MUD in the adsorbing solution, y_{MUD}, determined by XPS (triangles) and calculated from contact angle measurements with water using Cassie's equation (squares) and the equation of Israelachvili and Gee (open circles). The indicated full line represents the situation for $\Xi_{MUD} = y_{MUD}$, and the dashed line indicates a possible phase boundary between mixed and phase-segregated systems.

The low Ξ_{MUD} values for $y_{MUD} < 0.7$ and the shift to $\Xi_{MUD} \approx y_{MUD}$ for $y_{MUD} > 0.8$ is confirmed from both techniques. This can be explained by hydrogen bonding between adjacent hydroxyl groups of adsorbed MUD molecules when Ξ_{MUD} becomes large (above 0.5). In solution, the possibilities for MUD to form hydrogen bonds are always good (with ethanol and other MUD-molecules). For $y_{MUD} > 0.8$ there are also good possibilities for

MUD to form hydrogen bonds with neighboring MUD-molecules adsorbed on the surface as well as the solvent (ethanol from "above the surface"). Compared to the solution, the difference in possibilities to form hydrogen bonds at the surface are small and $\Xi_{MUD} \approx y_{MUD}$. However, at low y_{MUD} (<0.7) there are few possibilities for MUD to form hydrogen bonds at the surface (only with ethanol from "above the surface"). Thus, hydrogen bond formation is favored in solution and $\Xi_{MUD} < y_{MUD}$.

Comparison of the XPS results with the two equations from contact angle measurements suggest that for low Ξ_{MUD} the adsorption follows the Israelachvili and Gee equation and at higher Ξ_{MUD} the XPS results better fit to the Cassie equation. This can be interpreted as follows: at low concentrations the mixed SAMs are randomly mixed and that when the surface gets polar enough to allow hydrogen bonding between a substantial amount of MUD molecules, a phase separation takes place. The suggested phase separation upon domination of one component over the other was also observed in a system of 1-mercapto-11-undecanoic acid and 7-heptanethiol studied by Evans and coworkers [133]. They found that for fractions of below 0.2 of either component the system was better described by the Cassie equation. In the rest of the cases the surface fractions determined by XPS were better described by the Israelachvili and Gee equation.

In conclusion it can be said that for the system studied here it is hard to say whether the Cassie or the Israelachvili and Gee equation better describes the system for $y_{MUD} < 0.2$. For $0.2 \leq y_{MUD} \leq 0.7$ the surfaces of the mixed SAMs are better described by the Israelachvili and Gee equation suggesting that the monolayers are randomly mixed. Finally for $y_{MUD} > 0.7$ the system is separated into domains or patches according to the better fit to the Cassie equation. In the following chapters all values for Ξ_{MUD} are referred to those determined by XPS (Table 4 on page 81).

Table 2.4. Surface fraction of 1-mercapto-11-undecanol (MUD), Ξ_{MUD}, in mixed monolayers with 1-dodecanethiol (DDT) determined by XPS for different fractions of MUD in the adsorbing solution, y_{MUD}. Typical estimated error is shown in Figure 2.8.

y_{MUD}	Ξ_{MUD}
0.00	0.00
0.10	0.03
0.20	0.06
0.30	0.09
0.40	0.19
0.50	0.25
0.60	0.39
0.70	0.55
0.80	0.81
0.90	0.89
1.00	1.00

3. Reactions of SAMs with Phenylenediisocyanate

In the following, a versatile method to introduce isocyanate groups on self-assembled monolayers (SAMs) and mixed monolayers containing 1-mercapto-11-undecanol, MUD is described. Isocyanate groups are well known to react readily under mild conditions with an extraordinarily broad variety of functional groups [214] and, accordingly, we have performed model reactions with some substances, i.e., alcohols, amines, and water. These model reactions are described in chapter 4.

The transformation of SAMs consisting of MUD and mixed monolayers of MUD and dodecanethiol (DDT) into highly reactive isocyanate-bearing layers were performed by reaction of the hydroxyl groups in the monolayers and mixed layers with 1,4-phenylene diisocyanate (PDI). The reaction is schematically shown in Figure 3.1. PDI reacts with only one of its isocyanate groups, yielding a carbamate (urethane) group and a terminal isocyanate group susceptible for further reactions (see chapter 4).

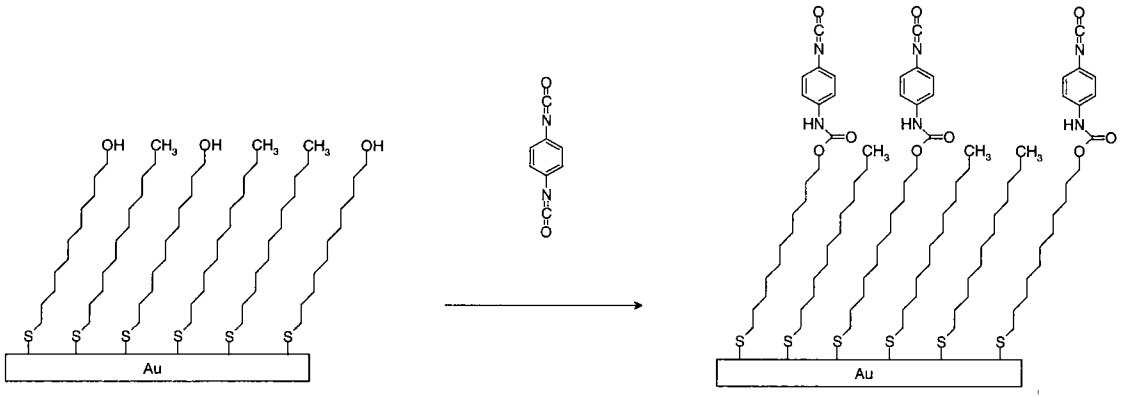

Figure 3.1. Schematic representation of the reaction of mixed SAMs with 1,4-phenylene diisocyanate (PDI) into reactive monolayers.

The reactions were carried out in 0.1 M solutions of 1,4-phenylene diisocyanate in water-free toluene at 40 °C for 2 h under an argon atmosphere for the quantitative study in section 3.2. For the kinetic study in section 3.1. the concentration, temperature and time were varied as described.

3.1. Basic Studies

In order to study the kinetics of the proposed reaction samples of MUD-monolayers were treated with 0.01 M PDI solutions in toluene at temperatures of 25, 40, 60, and 80 °C at different reaction times, varying from 1-18 h. The resulting layers were investigated with ellipsometry, reflection infrared (IR) spectroscopy at grazing incidence reflection and XPS. The results from determination by ellipsometry are shown in Figure 3.2.

For the proposed reaction an increase in the thickness of the monolayer can be estimated to approximately 10 Å using standard bond lengths and bond angles as well as van der Waals radii according to the literature [215][216][217]. The estimated value was used as a first assumption for the comparison of different reaction temperatures.

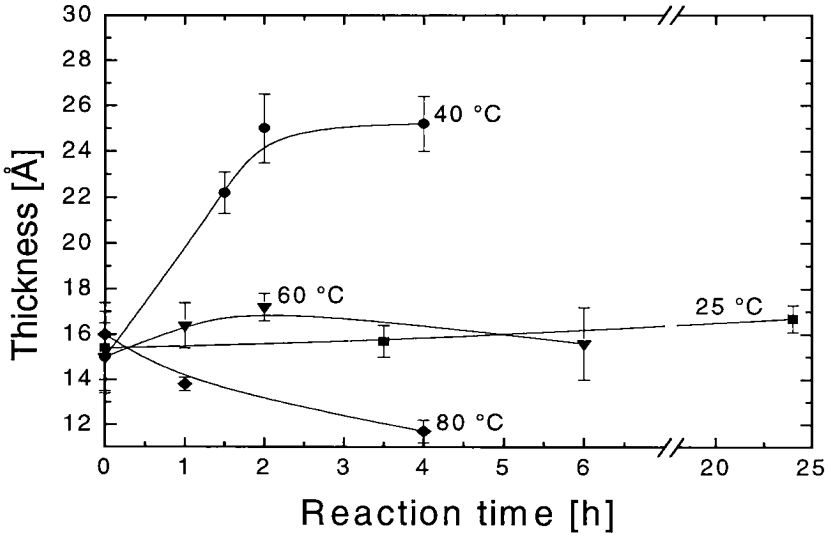

Figure 3.2. Thickness of MUD monolayers after reaction with PDI as a function of the reaction time at different temperatures. The reaction temperatures are shown at the right hand side and the indicated lines are guides to the eye.

For a reaction temperature of 25 °C the thickness slowly increases with the reaction time but has not changed significantly after a reaction time of 24 h. After a reaction time of 163 h the thickness was determined to 18.0 ± 1.4 Å which is significantly lower than expected

after a complete yield of the reaction. A temperature increase of 15° C to 40° C did indeed improve the reaction rate and already after 1.5 h the thickness reaches 22.2 ± 0.9 Å. Prolonged reaction time did not increase the thickness of the modified SAM after 2 h when a thickness of 25 ± 1.5 Å was obtained. At 60° C the thickness of the SAM first increases slightly but prolonged reaction time results in a decrease back to approximately the initial thickness. At 80 °C significantly lower thicknesses are observed, presumedly as a result of MUD desorption. This hypothesis is supported by the fact that after 4 h at 80 °C, the layer thickness [11.7 (±0.3) Å] was even below the value of pure MUD monolayers.

The IR-measurements delivered information about the proposed reaction at all temperatures, hence the vibration bands described in section 3.2. "Characterisation of the Reacted SAMs by GIR Measurement" on page 81 were found. However no quantitative information could be obtained from the comparison of the intensities of the vibration bands at the temperatures studied. This is descending from orientation effects upon desorption of the underlaying SAM resulting in a less ordered layer with random orientation.

XPS measurements were also performed on the SAMs after reaction at different temperatures. Upon reaction, nitrogen is introduced as a new element at the surface and the N(1s) spectra of the PDI-treated layers reveal a single peak at 400.3 eV. The ratio of oxygen and nitrogen at the modified surface can be used as an indication of the yield of the reaction. For a full reaction yield, 2 atoms each of nitrogen and oxygen from the PDI will be connected to the hydroxyl group in the monolayer. Hence a O/N ratio of 3 to 2 would be found on the fully modified surface. An increase of the reaction temperature from 25° to 40° C consequently decreases the O/N ratio from 5.95 to 3.12 (Table 1 on page 86) suggesting a higher reaction yield of the hydroxyl groups present at the surface for the higher temperature. A reaction time of 4 h at 80° C however results in a O/N ratio of 1.1. This is lower than what is expected for a complete reaction (O/N=1.5) and might be due to hydrolysis of the isocyanate or a desorption of the underlaying MUD monolayer resulting in holes in the monolayer. The holes that arise due to desorption might expose the gold surface to PDI molecules that adsorb and explain the obtained O/N ratio. The O/N ratio at 80° C in combination with the low thickness obtained from ellipsometry suggest to keep the reaction temperature as low as possible, where still a reasonable reaction rate can be maintained.

These results are in good agreement with earlier studies by Whitesides and coworkers who found that the SAMs desorb in a hydrocarbon solvent upon heating to 70° C [97]. To avoid these problems the reaction temperature was chosen as low as possible while still maintaining a feasible reaction rate. XPS and ellipsometry studies suggested 40° C as the optimum reaction temperature for further investigations.

Table 3.1. Atomic composition of elements determined by high resolution XPS for pure MUD-monolayers after reaction with PDI at 25 °C and 40° C for 1 h and a concentration of 0.01 M.

Element	pure MUD-layer	25° C	40° C	Estimated for complete reaction
O	9.2	9.0	9.7	19.1
C	67.3	65.8	66.8	67.7
N	-	1.5	3.1	12.7
S	1.5	1.2	1.6	0.5
Au	22.0	22.5	18.8	-
Total	100.0	100.0	100.0	100.0
O/N	-	5.95	3.12	1.50

The estimation for a complete reaction in Table 3.1. (as well as Table 3.2.) was calculated for a bilayer consisting of PDI as an overlayer and MUD as an underlayer. Attenuation of the underlayer was considered by using the method described in section 3.3.1. "Angle-Resolved XPS". Hence the gold substrate is not considered in the estimation.

As for all chemical reactions, the reaction rate does not only depend on the temperature at which the reaction is accomplished but also on the concentration of the reactants. To minimize desorption and degradation of the layers (see section see section 3.6. 'Stability of the Reacted SAMs" on page 103) during derivatization, experiments were conducted at various concentrations of PDI in solution. A tenfold increase of the PDI concentration (from 0.01 M to 0.1 M) was employed and resulted in a decrease of the O/N ratio from

3.12 to 1.58 suggesting a nearly complete yield (O/N=1.5) of the available hydroxyl groups (Table 2 on page 87). Thus the reaction rate is increased by an increase in PDI concentration and the reaction time can be minimized to avoid possible desorption of the derivatized monolayer. Also for reasons to retain the covalently attached and highly reactive isocyanate groups from hydrolysis the reaction time should be minimized (for more information see section 3.6. "Stability of the Reacted SAMs" on page 103). For the proposed derivatization reaction the best conditions were found at a temperature of 40 °C, a MUD concentration of 0.1 M, and a reaction time of 2 h.

Table 3.2. Atomic composition determined by high resolution XPS for MUD-monolayers after reaction with PDI at 40° C for 2 h and at concentrations of 0.01 and 0.1 M.

Element	pure MUD-layer	0.01 M	0.1 M	Estimated for complete reaction
O	9.2	9.7	10.5	19.1
C	67.3	66.8	67.5	67.7
N	-	3.1	6.6	12.7
S	1.5	1.6	1.6	0.5
Au	22.0	18.8	13.8	-
Total	100.0	100.0	100.0	100.0
O/N	-	3.12	1.58	1.50

3.2. GIR Measurements

The IR spectra in Figure 3.3. confirm the reaction proposed in Figure 3.1. (assignments of vibrations see Table 3 on page 88). In particular, signals of the carbamate (urethane) group formed by the reaction of hydroxyl with isocyanate groups appear at 1719, 1545, and 1236 cm^{-1} and of the non-reacted second isocyanate group at 2278 cm^{-1}. The signal at 1604 cm^{-1} is attributed to an aromatic C-C stretching vibration of the phenylene

moiety and the vibration at 1315 cm^{-1} to a C-N vibration of the aryl unit [218]. The C-H stretching vibrations of the methylene groups of the alkyl chain in the SAM arise at 2919 and 2852 cm^{-1}, in agreement with the literature [99].

Table 3.3. Infrared frequencies and vibrational assignments of mixed monolayers of DDT and MUD after reaction with phenylene diisocyanate

frequency (cm^{-1})	assignment	description
2965	ν_{as} (CH_3)	asymmetric C-H stretch
2919	ν_{as} (CH_2)	asymmetric C-H stretch
2878	ν_s (CH_3)	symmetric C-H stretch
2852	ν_s (CH_2)	symmetric C-H stretch
2278	ν (N=C=O)	isocyanate stretch
1719	ν_{as}(C=O)	amide I, asymmetric carbonyl stretch
1601	ν (C_{ar}-C_{ar})	aromatic carbon stretch
1548	ν (C-N)	amide II, C-N stretch (and N-H bending)
1514 (shoulder)	ν (C-C)	aromatic C-C stretch
1414	δ (CH_2)	methylene scissors deformation
1315	δ (N-C)	N-C deformation on the aryl side
1236	ν (C-N)	amide III, C-N stretch (and N-H bending)
1082	ν (C-O)	C-O stretch

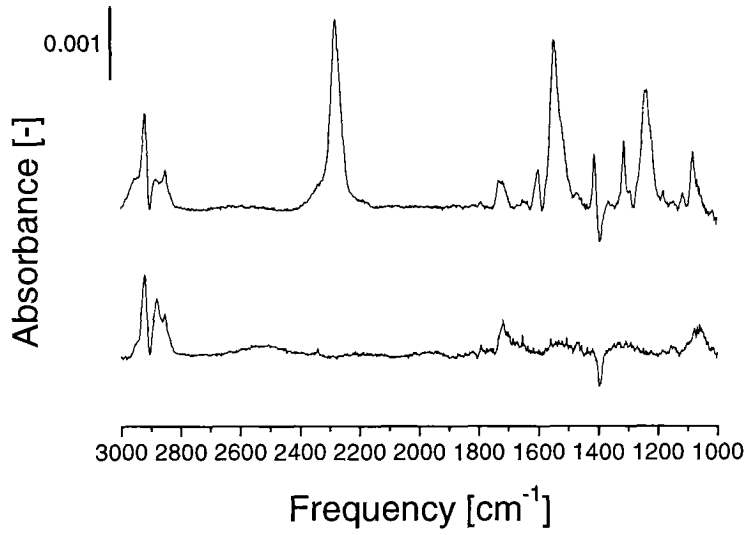

Figure 3.3. Infrared spectra at grazing incidence reflection of a 1-mercapto-11-undecanol monolayers before (lower spectrum) and after reaction (upper spectrum) with phenylene diisocyanate (PDI).

There is evidence (Figure 3.4.) from IR spectra with $\Xi_{MUD} \geq 0.2$ that the expected reaction was indeed successful for all samples. In particular, the presence of the strong isocyanate stretching vibration at 2278 cm^{-1} and the amide stretching vibrations at 1719 and 1548 cm^{-1} (amide I and amide II vibrations, respectively, see Figure 3.6.) allude to a conversion of only one of the two isocyanate groups of PDI. The signal intensities were too small to confirm unambiguously the presence of carbamate or isocyanate groups on the samples with Ξ_{MUD} of 0.06. In blank experiments with methyl-terminated surfaces ($\Xi_{MUD} = 0$), the signals of the isocyanate and carbamate group were absent. Importantly, however, the amide II vibration is strong after reaction of the hydroxyl groups with PDI while the amide I vibration, which represents the C=O vibration, is hardly visible.

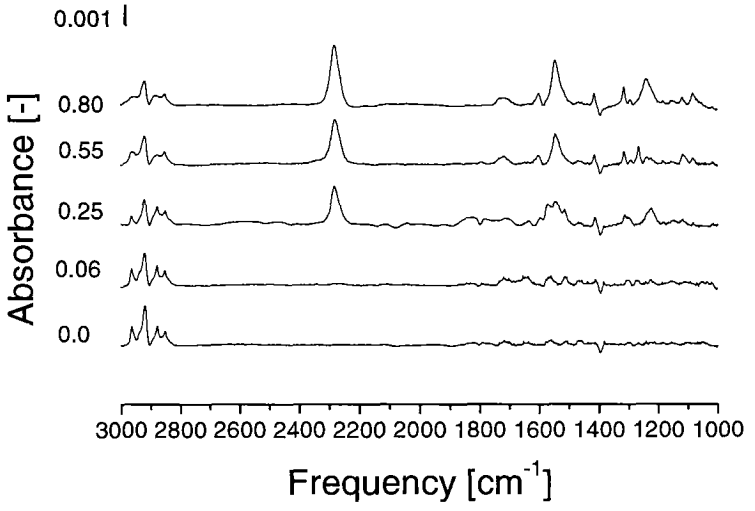

Figure 3.4. Infrared spectra at grazing incidence reflection of mixed monolayers of 1-mercapto-11-undecanol (MUD) and 1-dodecanethiol after reaction of MUD with phenylene diisocyanate. The numbers on the left edge of each spectrum refer to the surface fraction of MUD, Ξ_{MUD}.

For comparison, in the low-molecular-weight carbamates benzenecarbamic acid hexylester and benzene-1,4-bis(carbamic acid hexylester) the amide I and amide II vibrations of non-oriented molecules are characterized by a ratio of nearly 1 in isotropic spectra taken in KBr (Figure 3.5.). The different amide vibrations are schematically shown in Figure 3.6. The strong band found at 1699 cm^{-1} is the C=O stretch (amide I) which occurs at 1719 cm^{-1} in the SAM. The ratio of intensity between the amide I and amide II vibrations is around 1, whereas in the oriented SAM the intensity of the amide I vibration is very low or completely missing. Since the surface selection rule (see section 1.4.3. "Infrared Spectroscopy at Grazing Incidence Reflection (GIR)" on page 42) states that only vibrations perpendicular to the plane of the substrate are visible, it is obvious that the amide linkage is highly oriented with the C=O group lying in the surface plane. The relatively high intensity of the C-N vibration (amide II) indicates that this group is oriented perpendicular to the surface. The orientation in the reacted SAM is also confirmed by the high intensity of the amide III vibration, which has a lower intensity than the amide I vibration in the

isotropic reference (Figure 3.5.). The amide III vibration has a similar orientation of the transition dipole moment as the amide II vibration.

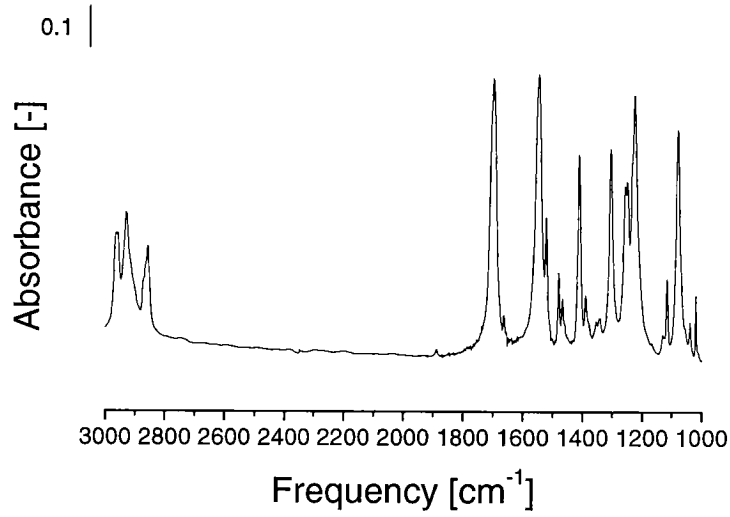

Figure 3.5. Infrared spectrum of benzene-1,4-bis(carbamic acid hexylester).

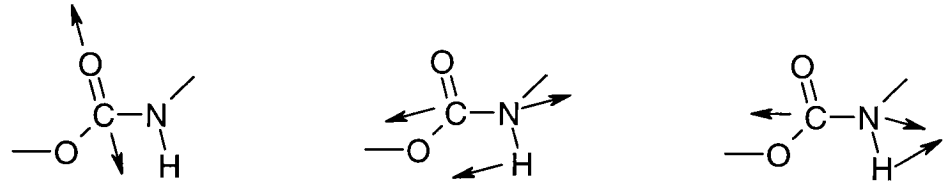

Amide I (~1700 cm^{-1}) Amide II (~1550 cm^{-1}) Amide III (~1250 cm^{-1})

Figure 3.6. Infrared vibration modes of amide I, amide II, amide III in carbamate, where the amide I vibration is almost perpendicular to the amide II and III vibrations.

Hence, the carbonyl group of the converted PDI moiety is directed at a low angle to the surface, in agreement with a more or less perpendicular orientation of the aromatic unit, which is in agreement with layer thickness measurements obtained with ellipsometry (section see section 3.4. 'Characterisation of the Reacted SAMs by Ellipsometry" on page 95).

3.3. XPS Measurements

The C(1s) X-ray photoelectron spectra after reaction with PDI are dominated by a broad, asymmetric signal at 284.8 eV, which arises at similar energy as the C(1s) peak in the MUD monolayer (285.1 eV, Figure 3.7.). The shoulder in the asymmetric signal at 284.8 eV consists of the carbon atoms attached to the hydroxyl group in the underlying MUD layers as well as of aromatic carbon atoms attached to nitrogen atoms of the carbamate and isocyanate groups. A symmetric peak occurs at 289.3 eV and represents the non-resolved carbon atoms of the carbamate and the isocyanate groups (Figure 3.7.).

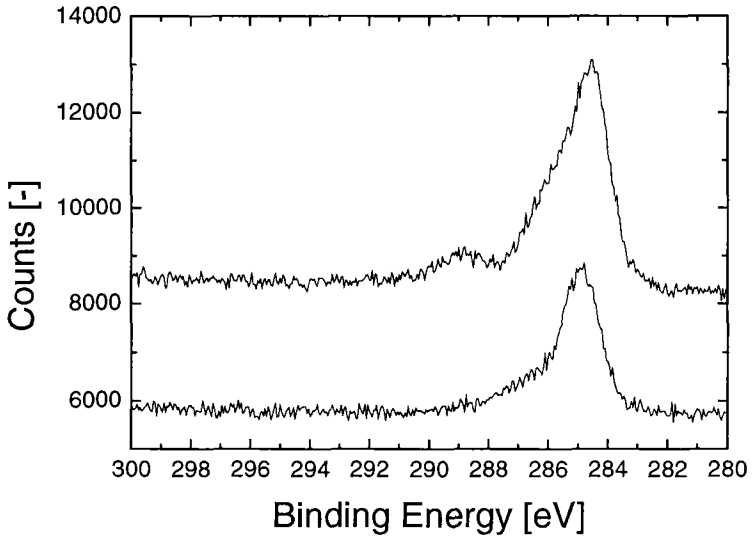

Figure 3.7. XPS of the C(1s) region of a 1-mercapto-11-undecanol (MUD) monolayer before (lower spectrum) and after (upper spectrum) conversion with PDI. The new peak at 289.3 eV is due to carbon atoms from the carbamate and the terminal isocyanate group. The shoulder around 286 eV originates in carbon atoms attached to oxygen atoms in the underlaying MUD as well as carbon atoms attached to nitrogen atoms formed by the reaction with PDI.

The suggested reaction introduces nitrogen to the monolayer and the N(1s) spectra of the PDI-treated layers reveal a single peak at 400.3 eV, i.e., the nitrogen atoms of the carbamate and the isocyanate groups are not resolved (Figure 3.8.).

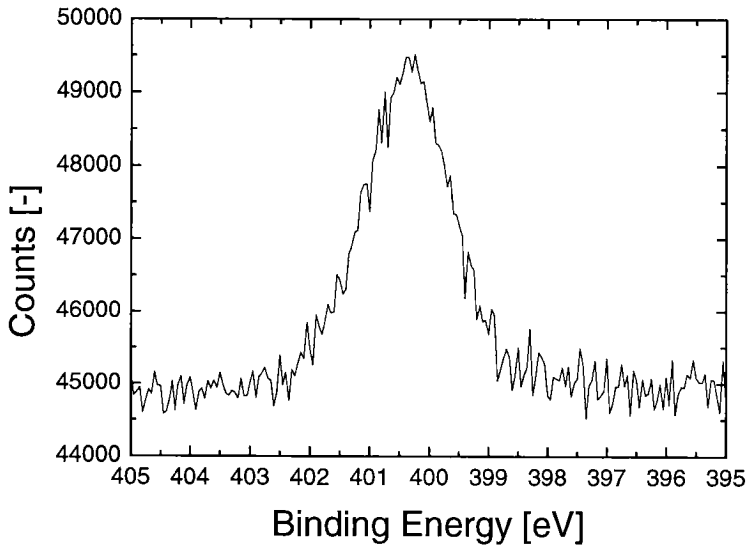

Figure 3.8. High resolution XPS spectrum of the N(1s) region of a 1-mercapto-11-undecanol (MUD) monolayer after reaction with PDI.

The O(1s) binding energies, which arise at 532.9 eV in the MUD monolayers, are transformed after reaction with PDI to a broad, non-resolved signal with a maximum at 532.3 and a shoulder at ca. 533.5 eV, representing the three different oxygen atoms in the carbamate and isocyanate group. For comparison, treatment of a DDT monolayer with PDI under the same reaction conditions did not deliver hints for adsorbed or reacted PDI molecules by IR spectroscopy, ellipsometry, or XPS.

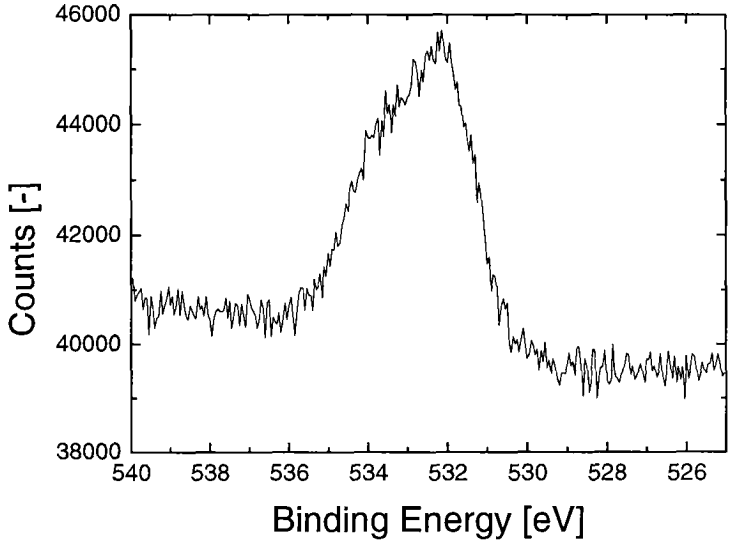

Figure 3.9. High resolution XPS spectra of the O(1s) region of a MUD-monolayer after reaction with PDI.

3.3.1. Angle-Resolved XPS

Angle resolved XPS (AR-XPS) was used to obtain information of the elemental composition in the derivatized SAM after reaction with PDI. Measurements were performed at take-off angles of 15°, 25°, 45° and 75° between the surface of the examined SAM and the detector. The higher angles allow detection of emitted photoelectrons that descend from deeper atom layers at the surface region. Thus the AR-XPS gives depth information of the atomic composition and can also be used for the determination of the thickness of an overlaying layer [219]. Figure 3.10. (upper part) shows the elemental compositions obtained from the measurements. Most significant is the increase of the gold fraction at higher take-off angles, confirming that the elements originating from the adsorbed monolayer and the proposed modification reaction are placed on top of the gold surface. All other element fractions decrease with the angle and oxygen is the element decreasing the most, thus proposing a higher surface presence than the other elements. To obtain information about the individual content between the other elements a subtraction of gold was performed and the results are shown in the lower part of Figure 3.10.

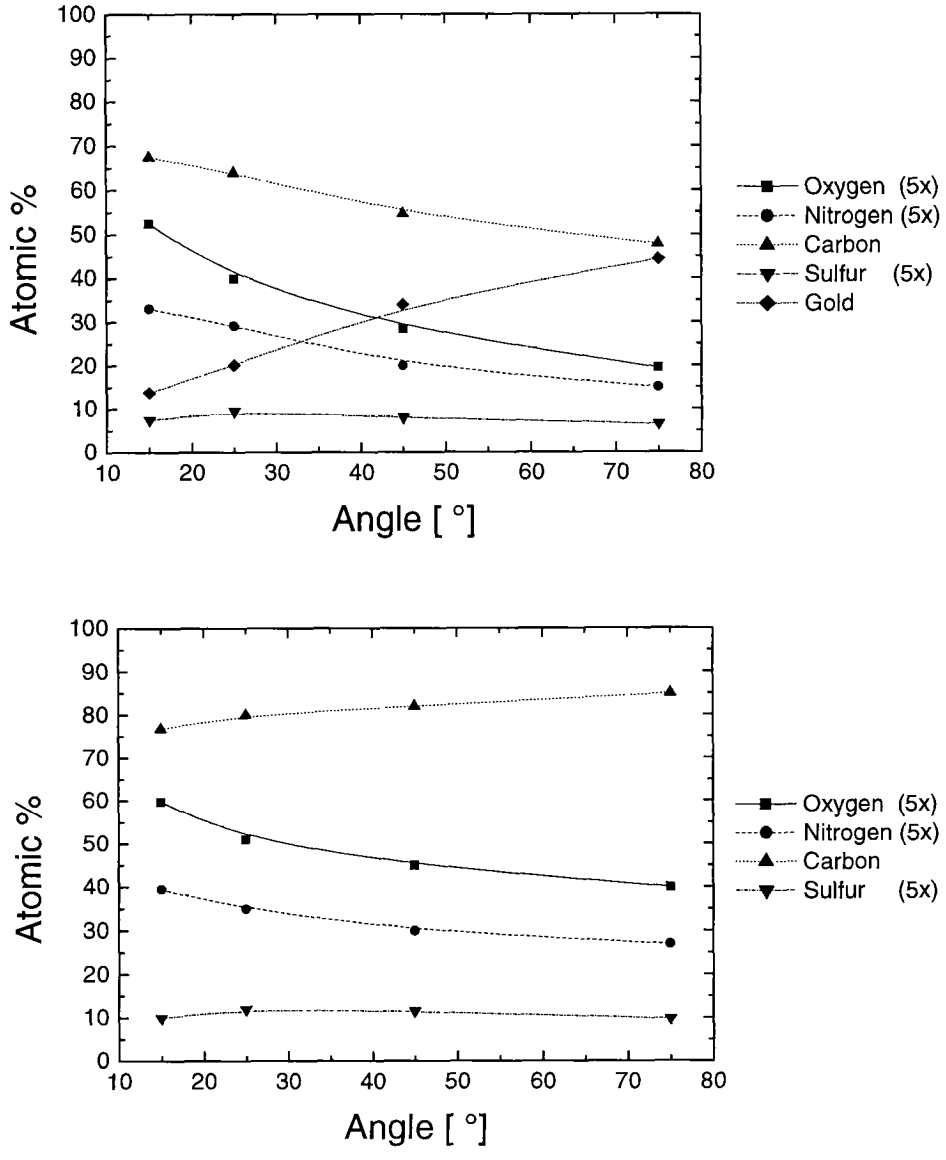

Figure 3.10. Elemental composition of the surface after reaction with PDI determined by angle resolved XPS (upper figure). In the lower figure gold is omitted for a better representation of the SAM. The elements O, N and S have been magnified for clarity. The indicated lines are guides to the eye.

From the lower figure it is obvious that oxygen and nitrogen fractions decrease with the take-off angle. This confirms that these elements are present to a high extent in the outermost surface layer, and decrease when the depth analysed increase. Carbon, which is

present at all levels of the modified monolayer, increases with the take-off angle due to the densely packed alkane chains in the underlaying preformed SAM. For the sulphur peak it is hard to obtain secure information due to the low signal-to-noise ratio of this element in the spectra. It seems however that the sulphur concentration increases when the take-off angle is changed from 15° to 25°. For the higher take-off angles the values obtained are constant within the experimental error of the XPS-instrument. An increase of the sulphur fraction is to expect if it is the head group in the established monolayer. This is suggested from our results and is in accordance with the well-established theory (see section 1.3. "Self-Assembled Monolayers (SAMs) of Thiols" on page 19).

Angle resolved XPS measurements were also used for the determination of the thickness of the overlayer using the method described by Andrade [219]. The thickness is obtained by comparing the ratio of intensity between an element from the overlayer I_B, and an element from the underlaying layer I_A, at different angles. The intensity of the elements are compared after correction for cross-section and transmission function (see section 1.4.2. "X-Ray Photoelectron Spectroscopy (XPS)" on page 37). The intensity ratio is given by

$$\frac{I_B}{I_A} = \frac{\lambda_B}{\lambda_A} \cdot (\exp((t_B/(\lambda_B \sin\alpha)) - 1)) \qquad (3.1.)$$

where λ_B : mean free path length of the overlayer B [Å]
λ_A : mean free path length of the underlayer A [Å]
t_B : thickness of the overlayer B [Å]
α : take-off angle [°]

The values for the mean free path length used in the model were 35.4 Å for the overlayer (carbon) and 39.8 Å for the underlayer (gold). The mean free path lengths were determined by using the formula λ (Å)= 9.0 +0.022(kinetic energy in eV) as suggested by Whitesides for photoelectrons in SAMs of alkanethiols on gold [220]. The results are shown in Figure 3.11. The model suggests a thickness of around 25 Å for the measurements at higher angles. The intensity ratio at 15 ° however suggests a significantly lower thickness (~16 Å) than for the other angles. This can be due to experimental artefacts at the low

grazing angle between the sample and the detector or to the relatively high fraction of other elements in the monolayer at the low angles, resulting in a low total fraction of carbon (Figure 3.10. lower part). The results should however be treated with caution since the model has limitations. The thickness obtained is considerably affected by the values for the mean free path lengths used. Other assumptions include surface homogeneity and that no damage of the sample occurs during the repeated exposure to X-ray radiation at the different angles [219].

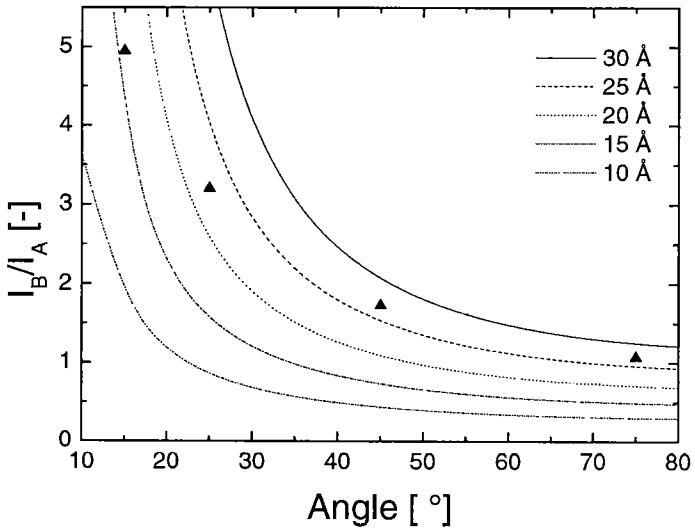

Figure 3.11. Thickness of a MUD-monolayer after reaction with PDI determined by angle resolved XPS after the method suggested by Andrade [219]. The lines correspond to theoretical intensity ratios calculated for a given thickness with the inelastic mean free paths mentioned in the text. The symbols correspond to the empirical results from the measurements.

3.3.2. Quantification of Mixed SAMs

The reaction of surface hydroxyl groups with PDI was also performed on mixed layers of DDT and MUD at Ξ_{MUD} of 0.06, 0.25, 0.55, and 0.8. Monitoring the systems with XPS confirmed reactions of PDI on all these mixed monolayers and the atomic compositions are included in Figure 3.12. Upon reaction with PDI, oxygen, nitrogen and carbon are anchored to the monolayer by the hydroxyl groups in the underlaying SAM. Thus an increase of Ξ_{MUD} will result in a proportional increase of these elements and an increase of oxygen and nitrogen is indeed visible in the lower part of the figure. It is more difficult to interpret the carbon content due to its high presence in a pure DDT monolayer (Ξ_{MUD}=0.0). An important indication of the suggested reaction is however the decrease of the relative fractions of gold and sulphur at the surface which is in accordance with an increasing thickness of the total layer.

The conversion of the hydroxyl groups was estimated by comparison of the integrated N(1s) and O(1s) signals after reaction [extent of reaction (p): $p=x/(2-2x)$ where x is the ratio of the normalized integrated N(1s)/O(1s) ratio; to elucidate the normalization factor which compensates the different cross sections of N(1s) and O(1s), an XPS of polyamide-66 was measured]. The conversion of the hydroxyl groups (cf. Figure 3.13.) was constant within experimental error for all Ξ_{MUD}, namely 83-103%. About 0.4% oxygen but no nitrogen was detected in blank experiments, where pure DDT monolayers (Ξ_{MUD}=0 in Figure 3.13.) were exposed to PDI; neither of these two elements could be detected on pure DDT monolayers prior to immersion in PDI solutions. We believe that the amount of oxygen is due to a contamination that also causes a decrease of 6° of the contact angle after immersion of DDT monolayers in PDI solutions. It is assumed that all samples are contaminated to the same extent, and 0.4% oxygen have been subtracted from all samples for the estimation of the reaction yield, therefore. If this correction is not applied, the conversion of hydroxyl groups is estimated to 79±10%, again for all samples.

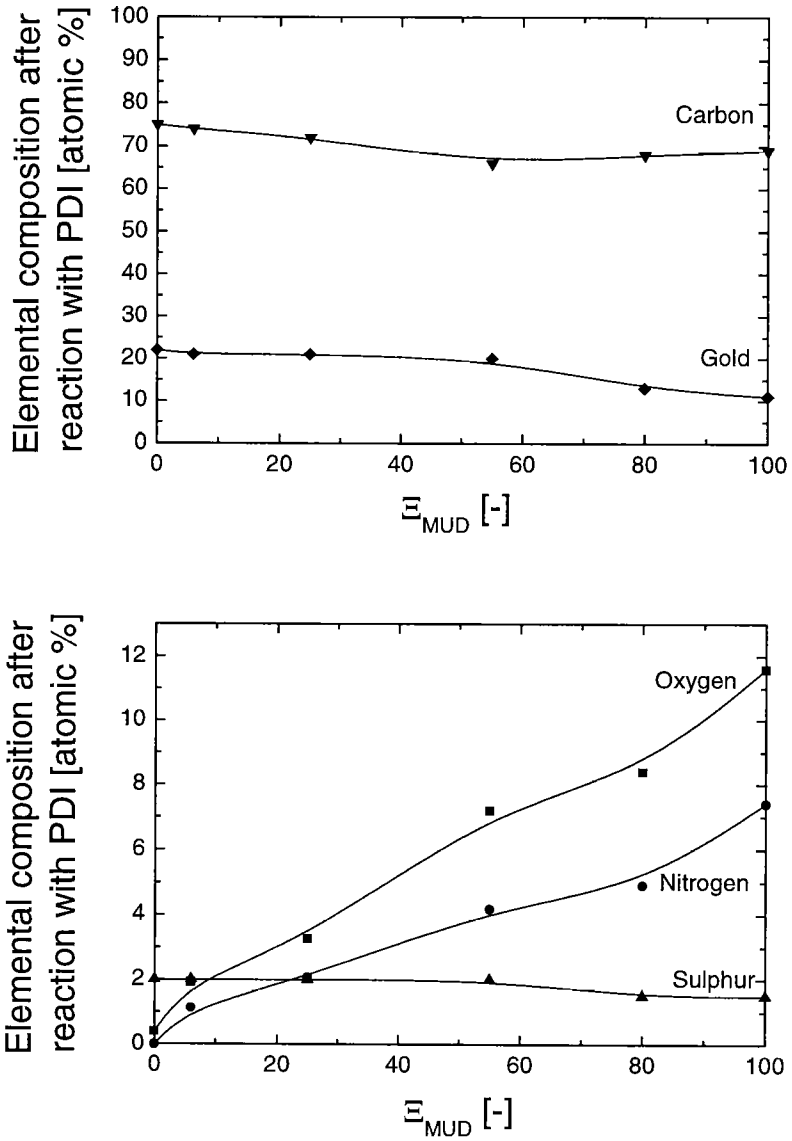

Figure 3.12. Atomic composition of carbon (triangle down), gold (diamond), oxygen (square), nitrogen (circle) and sulphur (triangles), determined by XPS, on mixed monolayers of 1-mercapto-11-undecanol (MUD) and 1-dodecanethiol after exposure to phenylene diisocyanate as a function of the surface fraction of MUD, Ξ_{MUD}. The indicated lines are guides to the eye.

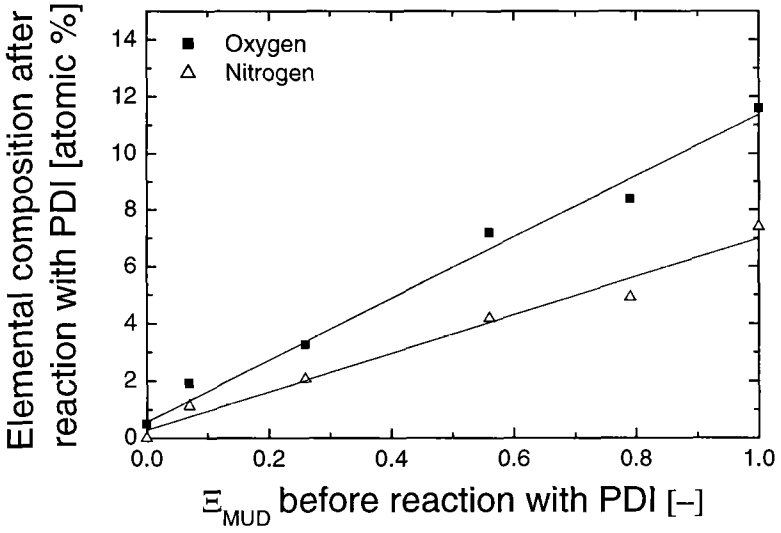

Figure 3.13. Atomic composition of oxygen (squares) and nitrogen (triangles), determined by XPS, on mixed monolayers of 1-mercapto-11-undecanol (MUD) and 1-dodecanethiol after exposure to phenylene diisocyanate as a function of the surface fraction of MUD, Ξ_{MUD}. The indicated lines represent linear regression fits.

The area available per molecule of an alkanethiol molecule on gold has been estimated as 21.4 $Å^2$ [103], and we estimate the space required for a phenyl ring oriented perpendicularly to the surface to be similar (22.1 $Å^2$ using standard bond lengths and van der Waals radii [215][216][217]). Of course, the phenyl groups demand more space if they are tilted, and hence a complete conversion of the surface hydroxyl groups at $\Xi_{MUD} = 1$ could be possible if the PDI molecules, attached to the surface via a carbamate group, were oriented with the aromatic moiety at an angle close to 90° with respect to the surface.

3.4. Ellipsometry

As expected, the layer thicknesses increase after reaction with PDI with increasing Ξ_{MUD} (Figure 3.7.). At maximum coverage with hydroxyl groups, the thickness increment amounts to ca. 9 Å, indicating reacted moieties which are oriented preferentially perpen-

dicularly to the surface; using standard bond lengths and bond angles [217] we estimate the increase in layer thickness to 9.3 Å for an orientation of the residual phenylene isocyanate unit of 90° to the surface and 8.7 Å for 70° orientation.

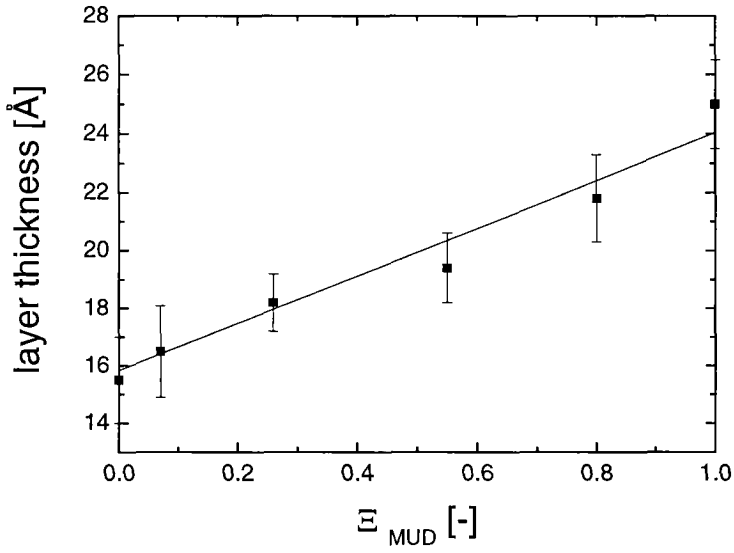

Figure 3.14. Average layer thickness, determined by ellipsometry, after reaction of 1-mercapto-11-undecanol (MUD) with phenylene diisocyanate as a function of the surface fraction of MUD, Ξ_{MUD}, in mixed monolayers with 1-dodecanethiol (DDT). The error bars refer to the standard deviation. The indicated line represents a linear regression fit.

3.5. Contact Angle Measurements

The advancing contact angles of water and hexadecane on the PDI-modified layers are presented in Table 4 on page 102, together with the values on pure monolayers of DDT and MUD after PDI treatment. The contact angles of water were measured rapidly, i.e. within 20 s after contact with water, since the isocyanate groups hydrolyse (see below). The values so obtained were reproducible and significantly above those on fully hydrolysed layers (see below). $\theta_a(H_2O)$ on pure DDT layers immersed in the PDI solutions decreased by 6° compared to freshly prepared layers, differences of these order of magnitude have also been reported previously and are believed to be caused by contamination adsorbed from the solvent [97] (see also above). The $\theta_a(H_2O)$ tend to increase upon

PDI treatment because hydroxyl groups are more hydrophilic than isocyanate groups. The $\theta_a(H_2O)$ at $\Xi_{MUD} > 0.25$ are markedly above those on completely hydrolysed layers (see section 4.3. "Reactions with Water" on page 113), indicating that the isocyanate groups are not fully hydrolysed under the conditions for the contact angle measurements. The difference of the $\theta_a(H_2O)$ before and after PDI treatment is the more pronounced the higher the hydroxyl fraction at the initial surface and reaches 52° at $\Xi_{MUD}=1$ (Figure 3.15.). Hexadecane cannot form hydrogen bonds with surface hydroxyl groups, and it appears that $\theta_a(HD)$ decreases with increasing specific surface energy of the organic layers which is expected to increase with increasing fraction of isocyanate groups [221][222].

Table 3.4. Advancing contact angles of water and hexadecane, $\theta_a(H_2O)$ and $\theta_a(HD)$, on monolayers of DDT and MUD and mixed monolayers composed of DDT and MUD with different surface fractions of MUD, Ξ_{MUD}, after exposure to 0.1 M PDI solutions for 2 h at 40 °C. The standard deviations of the specified values are within ±2°

Ξ_{MUD}	$\theta_a(H_2O)$ [°]	$\theta_a(HD)$ [°]
0	107	41
0.06	102	39
0.25	91	13
0.55	74	12
0.8	68	5
1	66	3

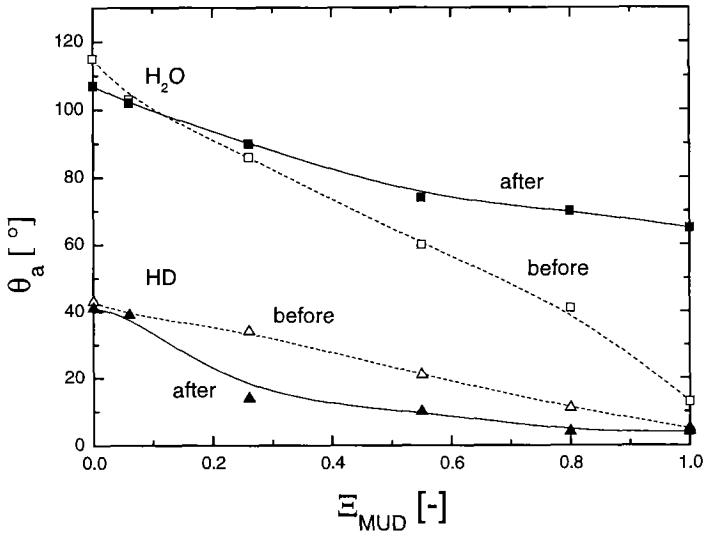

Figure 3.15. Advancing contact angles, θ_a, of water (squares) and hexadecane (circles) before (filled symbols) and after reaction (open symbols) of 1-mercapto-11-undecanol (MUD) with phenylene diisocyanate as a function of the surface fraction of MUD, Ξ_{MUD}, in mixed monolayers with 1-dodecanethiol. The indicated lines are guides to the eye.

3.6. Stability of the Reacted SAMs

Isocyanate groups react with water to carbamic acids, which, by decarboxylation, rapidly yield amine groups (Figure 3.16.). The stability of the terminal isocyanate group at Ξ_{MUD}=1 towards traces of water in solvents was investigated by IR spectroscopy and contact angle measurements. After conversation with PDI, samples were left in "dry" toluene for 24 h whereupon the original intensity of the NCO vibration in IR spectra decreased by 44% while the intensity of the other vibrations remained constant. In addition, a decrease in $\theta_a(H_2O)$ of 7° was observed on these samples, indicating hydrolysis of some of the isocyanate groups into amine groups.

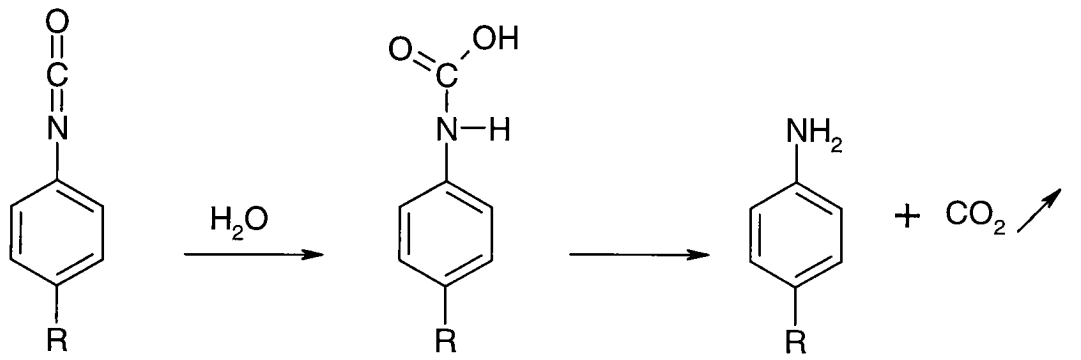

Figure 3.16. Decomposition of isocyanate into an amine and carbon dioxide.

NCO-terminated SAMs exposed to laboratory air will react with humidity in the air and related GIR spectra are shown in Figure 3.17. The exposure lead to a complete loss of the NCO vibrations after 20 h (and an increase of the intensity of CH_2 and CH_3 vibrations due to contaminations adsorbed from air). The contact angle of water increased to ~75°, similarly to values observed on pure gold samples left in air for a prolonged time.

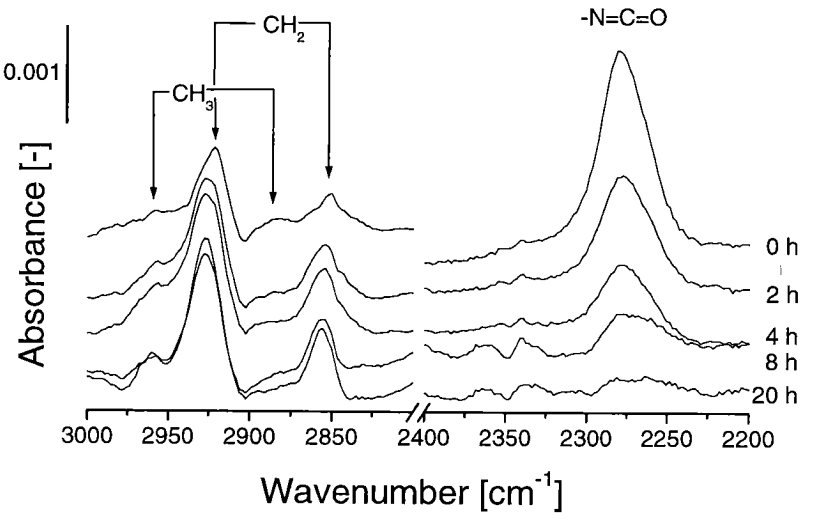

Figure 3.17. Infrared spectra at grazing incidence reflection of a NCO-terminated SAM (Ξ_{MUD}=1) exposed to laboratory air. The NCO vibration at 2278 cm^{-1} decreases with time and is completely lost after 20 h. The CH_2 and CH_3 vibrations increase gradually due to contamination from the air.

Thus the isocyanate-bearing monolayers are found to be more stable in a "water-free" solvent than in ambient air. However the decrease in IR intensity together with the decrease of the contact angle is a strong indication that hydrolysis occurs also in the solvent. Therefore it should be emphasized that further functionalisation of isocyanate-bearing SAMs should be accomplished immediately after PDI-modification and that the reaction time of the second functionalisation should be minimised to avoid hydrolysis.

3.7. Conclusions

IR investigations of the reacted MUD-SAMs and the mixed SAMs clearly show that the introduction of 1,4-phenylenediisocyanate is successful for all samples with $\Xi_{MUD} \geq 0.2$ with the formation of a carbamate group, while the other isocyanate group remains unaffected and reactive. XPS measurements lead to the conclusion that the surface hydroxyl groups have been converted to a high extent (93 (±10%)), independent of Ξ_{MUD}. The thickness of the monolayers increases upon introduction of PDI with numbers in accordance with the theoretically estimated values. Hence, the conversion of surface hydroxyl groups with PDI is more or less complete.

The phenylene diisocyanate molecules are anchored to the hydroxyl groups in the SAM over a well oriented carbamate linkage as suggested by orientation studies by GIR. The carbonyl group of the conversed PDI moiety is directed at a low angle to the surface, in agreement with a more or less perpendicular orientation of the aromatic unit. The angle between the aromatic unit and the surface normal is by ellipsometry estimated to be within 0-20 °. The high conversion of the reaction with PDI as determined by XPS is only possible (for high Ξ_{MUD}) when the aromatic ring is oriented at a low angle to the surface normal. Thus, all three methods are in good agreement of a highly oriented isocyanate-bearing layer.

The conversion of surface hydroxyl groups with PDI should offer a versatile and straightforward method to modify surfaces and to facilitate further reactions with additional compounds. These reactions are the described in the following chapter.

4. Reactions of Phenylenediisocyanate-modified SAMs

Self-assembled monolayers and mixed monolayers containing 1-mercapto-11-undecanol, MUD, can, as described in chapter 3, be transformed into highly reactive isocyanate-bearing layers by reaction with 1,4-phenylene diisocyanate (PDI). Since PDI reacts with only one of its isocyanate groups, yielding a carbamate (urethane) group, there will be a terminal isocyanate group susceptible for further reactions. Isocyanate groups are well known to react readily under mild conditions with an extraordinarily broad variety of functional groups [214] and, accordingly, we have performed model reactions with some substances, i.e., alcohols, amines, and water, as described in the following.

In order to convert the isocyanate-terminated monolayers, the corresponding samples were placed into neat methanol, 1-hexanol, or 3-dimethyl-1-butanol for 2 h at 25 °C, if not otherwise indicated in the text. For the reaction of isocyanate-terminated monolayers with 1,2-diaminoethane or diethylamine, the substrates were exposed to 0.1 M solutions of the amines dissolved in water-free toluene for (typically) 2 h at 25 °C. Reactions of isocyanate-terminated monolayers with water were carried out in neat water for 5 minutes at room temperature. All modified monolayers were washed with toluene and dichloromethane and then dried under a stream of argon.

4.1. Reactions with Alcohols

The reaction of hydroxyl groups with isocyanate groups proceeds also when the isocyanate groups are anchored to the monolayer. Isocyanate-modified surfaces prepared from MUD monolayers were brought in contact with neat methanol, hexanol, and 3,3-dimethylbutanol at 25 °C. The reactions follow the scheme as shown in Figure 4.1. All employed alcohols react with the terminal isocyanate group yielding a second carbamate (urethane) group on the alkyl chain and ending in one or three methyl groups.

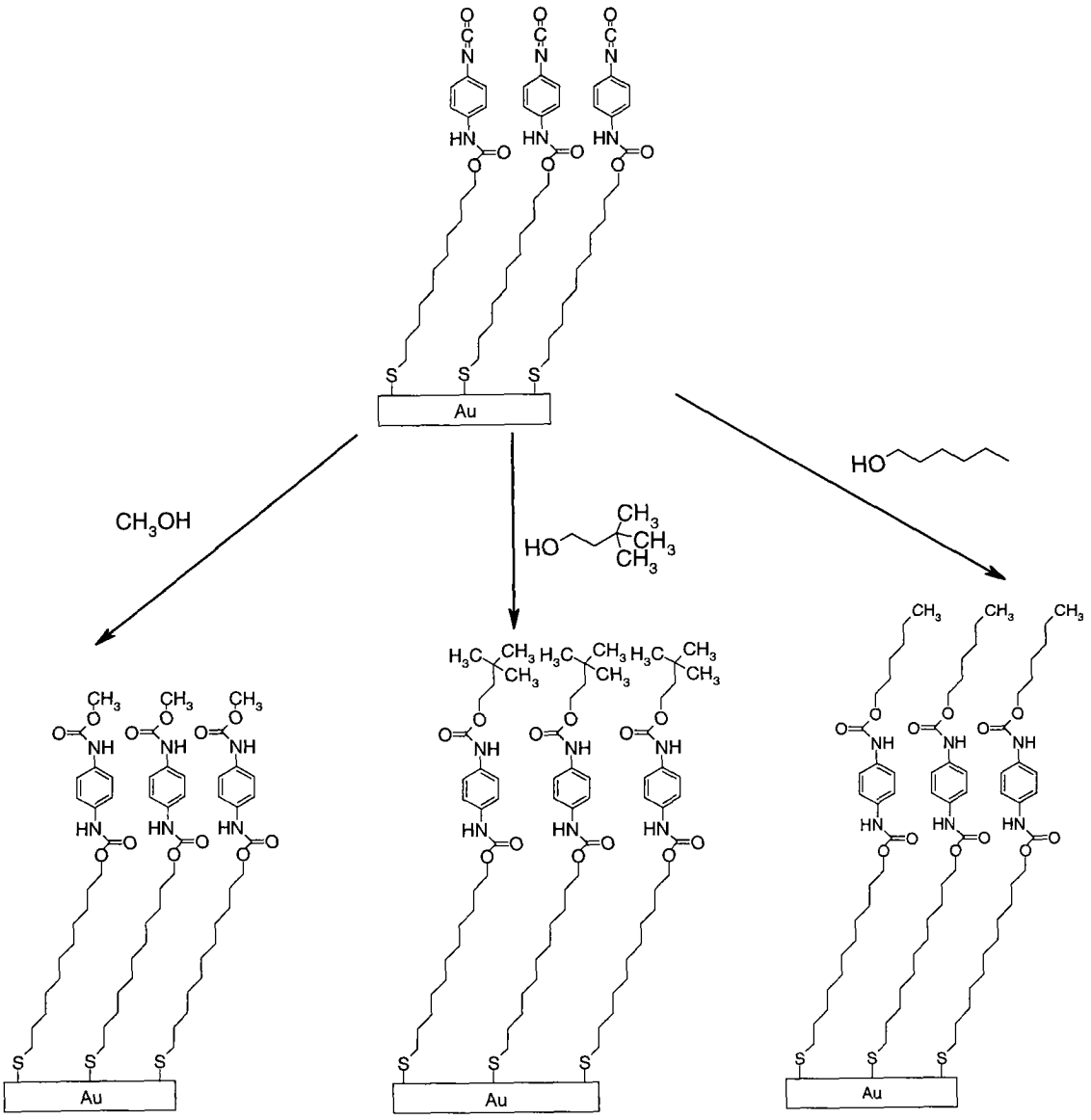

Figure 4.1. Overview of reactions performed on phenylene diisocyanate-modified SAMs with alcohols, such as methanol, 3,3-dimethylbutanol and hexanol.

Comparison of the IR spectra for the different alcohols suggest a higher reaction rate for methanol, the smallest alcohol employed. After a reaction time of 2 h with methanol the isocyanate vibration at 2278 cm^{-1} disappeared totally, whereas the samples with hexanol and 3,3-dimethylbutanol still exhibited isocyanate signals in their IR spectra. After 5 h, the vibration of the isocyanate groups at 2278 cm^{-1} disappeared completely in the cases of methanol and hexanol, suggesting a complete conversion of the isocyanate groups,

while a small signal was still visible in the case of 3,3-dimethylbutanol (Figure 4.2.). We assume that the bulky end groups of 3,3-dimethylbutanol either prevent a complete reaction or markedly decrease the reaction rate. Since reactions of 5 h duration with these systems are already long (cf. the hydrolysis of the isocyanate groups in toluene, see section 3.6. "Stability of the Reacted SAMs" on page 99), longer exposure is not promising. The signals of the newly attached alcohols (C-H stretching vibrations of methyl groups) arise at around 2965 cm^{-1}. The relatively high fraction of methyl groups in dimethylbutanol is reflected in a particularly high intensity ratio of the CH_3- and the CH_2-vibrations in IR spectra (Figure 4.2.C. and especially Figure 4.3.C.).

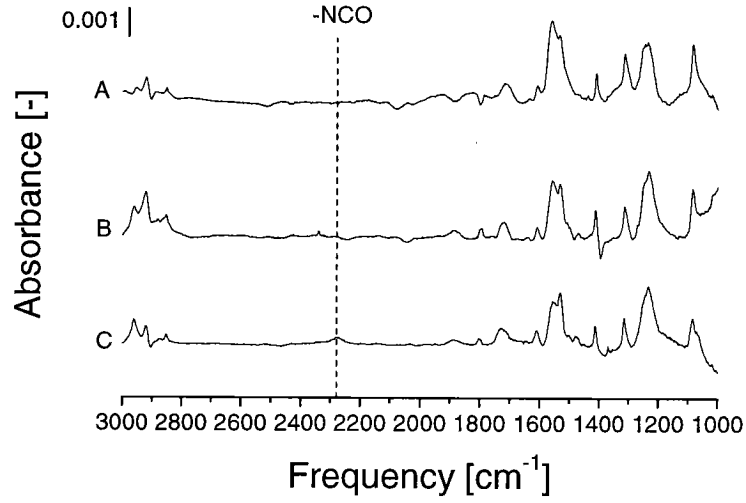

Figure 4.2. Infrared reflection absorption spectra of 1-mercapto-11-undecanol monolayers after conversion with phenylene diisocyanate followed by reaction with A) methanol, B) hexanol and C) 3,3-dimethylbutanol.

The order of a monolayer has a relation to frequency and the width of the asymmetric CH_2 vibration in IR-spectra as described by Nuzzo and coworkers when they studied temperature programmed desorption (TPD) of a SAM [78]. This technique has later been extended for the study of the order of mixed monolayers [198]. The asymmetric CH_2 vibration which normally appears at 2919 cm^{-1} suggests that the chains are fully extended and reside in a crystal-like environment. If there were significant numbers of gauche defects in

the overlayer, or if the layer was not densely packed, then the position of this band would shift to higher frequency, while the width would broaden. After reaction with methanol and hexanol, the asymmetric CH_2 vibration is still found at 2919 cm^{-1} (see Figure 4.3. A and B) suggesting no change in the underlaying MUD-layer. This is also an indication of a well ordered overlayer of the upper alkyl chain after modification with hexanol. For the 3,3-dimethylbutanol-modified SAM the asymmetric CH_2 vibration is slightly shifted and found at 2924 cm^{-1}. This is an indication of more gauche conformations in the alkyl chains. These gauche defects can descend from a disordered overlayer or from an increasing disorder in the MUD-layer due to sterical hindrance introduced by the bulky side groups in 3,3-dimethylbutanol. A comparison of the alcohol-modified SAMs with the isocyanate-terminated SAM prior to reaction (not shown) give, however, for none of the alcohols an indication of a less ordered layer regarding the width of the asymmetric methylene vibration. These are all of similar size. A possible explanation of these data is that the peak shift of 3,3-dimethylbutanol in Figure 4.3.C. descends from a disordered overlayer and that the underlaying MUD-layer remains ordered.

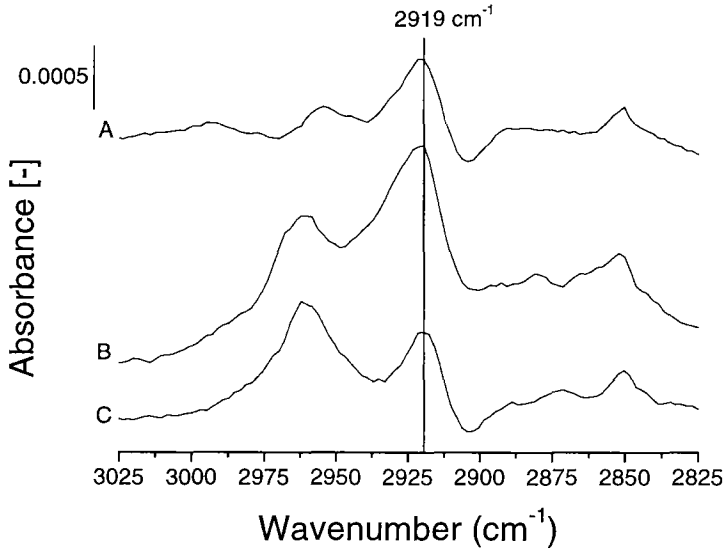

Figure 4.3. Infrared reflection absorption spectra of the CH_2 and CH_3 region for 1-mercapto-11-undecanol monolayers after conversion with phenylene diisocyanate followed by reaction with A) methanol, B) hexanol and C) 3,3-dimethylbutanol. The indicated line represents the peak position of a crystalline-like CH_2 vibration (2919 cm^{-1}).

XPS data show the expected increase in O/N ratios upon reaction of the isocyanate groups with alcohols (Table 4.1.). O/N ratios increase for all alcohols employed upon modification and are significantly higher than 1.58 obtained for the NCO-terminated monolayer. The theoretical O/N ratio after the modification is 2.0 and calculation of the reaction yield are basically possible. Related estimations are, however, difficult due to the relatively large error of the reaction yield of PDI with MUD (ca. 10%). The obvious decrease of the gold fractions after the modification reactions are an indication of an increased layer thickness.

Table 4.1. Atomic composition determined by high resolution XPS for MUD-monolayers after reaction with PDI and modification with alcohols.

Element	Methanol	3,3-Dimethyl-butanol	Hexanol	pure PDI-layer	pure MUD-layer
O	14.4	10.5	12.6	10.5	9.2
C	65.5	69.8	68.9	67.5	67.3
N	7.8	5.2	6.9	6.6	-
S	1.2	1.7	1.0	1.6	1.5
Au	11.3	12.8	10.6	13.8	22.0
Total	100.0	100.0	100.0	100.0	100.0
O/N	1.84	2.04	1.82	1.58	-

The increased layer thickness proposed by the XPS measurements could not be verified by ellipsometry in the case of methanol and 3,3-dimethylbutanol. The thicknesses obtained were within the standard deviation of the values for the isocyanate-terminated layers, which is reasonable in the case of methanol where only a single methoxy group is added on the isocyanate bearing layer. For the hexanol modification, however, an increase of the layer thickness with increasing Ξ_{MUD} was observed (Figure 4.4.). The thickness increases similarly to the trend observed in Figure 3.14. on page 97, to a final increment of ca. 9 Å at $\Xi_{MUD} = 1$. Such values are expected for extended hexyl chains.

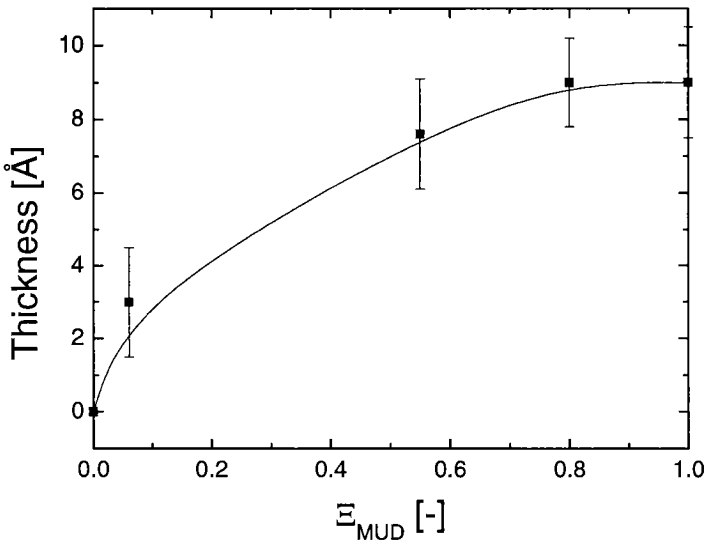

Figure 4.4. Relative increase in layer thickness, determined by ellipsometry, after reaction of hexanol with isocyanate-bearing monolayers as a function of the surface fraction of MUD, Ξ_{MUD}, in mixed monolayers with 1-dodecanethiol (DDT). The error bars refer to the standard deviation obtained by repeated experiments and the indicated line is a guide to the eye.

The $\theta_a(H_2O)$ on the layers exposed to hexanol on samples prepared at $\Xi_{MUD} = 1$ are 90°, indicating a surface layer of rather disordered alkyl groups [224][225][226][227][228][229][230]. On the methanol-exposed layers, $\theta_a(H_2O)$ is significantly lower (60° at $\Xi_{MUD} = 1$), possibly because the carbamate groups are not covered completely by the short methyl groups; the wetting properties are markedly influenced by the carbamate groups. In the case of dimethylbutanol, the contact angle was 81°, between those of the methanol- and hexanol-treated layers. One might therefore conclude that the dimethylbutyl groups also do not cover the carbamate groups at the surface.

Contact angle measurements were also performed on mixed SAMs after reaction with PDI and modification with hexanol. The results are shown in Figure 4.5. It is obvious that for high Ξ_{MUD} the contact angle increases to values above those for the isocyanate-terminated layer, because the layer of anchored hexanol buries the polar carbamate linkage as

suggested by the ellipsometric data presented. The minimum contact angle for the hexanol-functionalised layer is found at Ξ_{MUD}=0.55 where the upper layer is rather disordered, exhibiting methylene groups at the interface as well as not covering the polar carbamate linkage resulting in the lower contact angles. Similar results have been found in a study of mixed SAMs containing long- and short-chained thiols terminating in methyl groups. For mixed surface compositions, the contact angles found were significantly lower than on pure SAMs due to disordered layers exposing methylene groups at the surface [231].

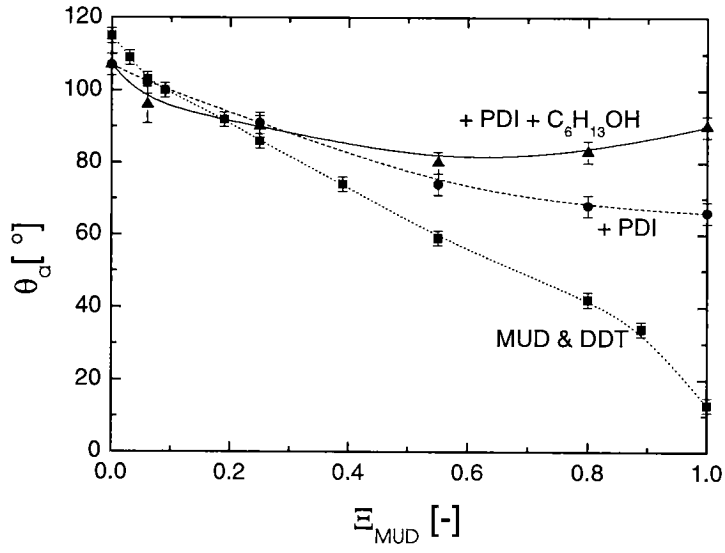

Figure 4.5. Contact angle measurements for mixed SAMs of MUD and DDT (squares), after reaction with PDI (circles) and modification with hexanol (triangles). All data are presented as a function of the surface fraction of MUD in the underlaying monolayer. The indicated lines are guides to the eye.

4.2. Reactions with Amines

There has been a growing interest to immobilize proteins onto surfaces over the last 10 years [108]. One of the most evident functional groups in a protein for its anchoring onto a surface is a terminal amine group or a secondary amine group from the peptide linkage in the protein. As model substances for these, amines were investigated regarding possi-

bilities to functionalise the isocyanate-terminated monolayer. The amines employed were 1,2-diaminoethane (ethylenediamine, $H_2NCH_2CH_2NH_2$) as a primary diamine and diethylamine ($HN(CH_2CH_3)_2$) as a secondary amine. Due to their difference in chemical structure in the ω-position a successful anchoring would result in a hydrophilic amine-terminated layer in the case of ethylenediamine and a rather hydrophobic layer ending in methyl groups for diethylamine. Both molecules react with the terminal isocyanate group yielding a urea linkage as shown in Figure 4.6.

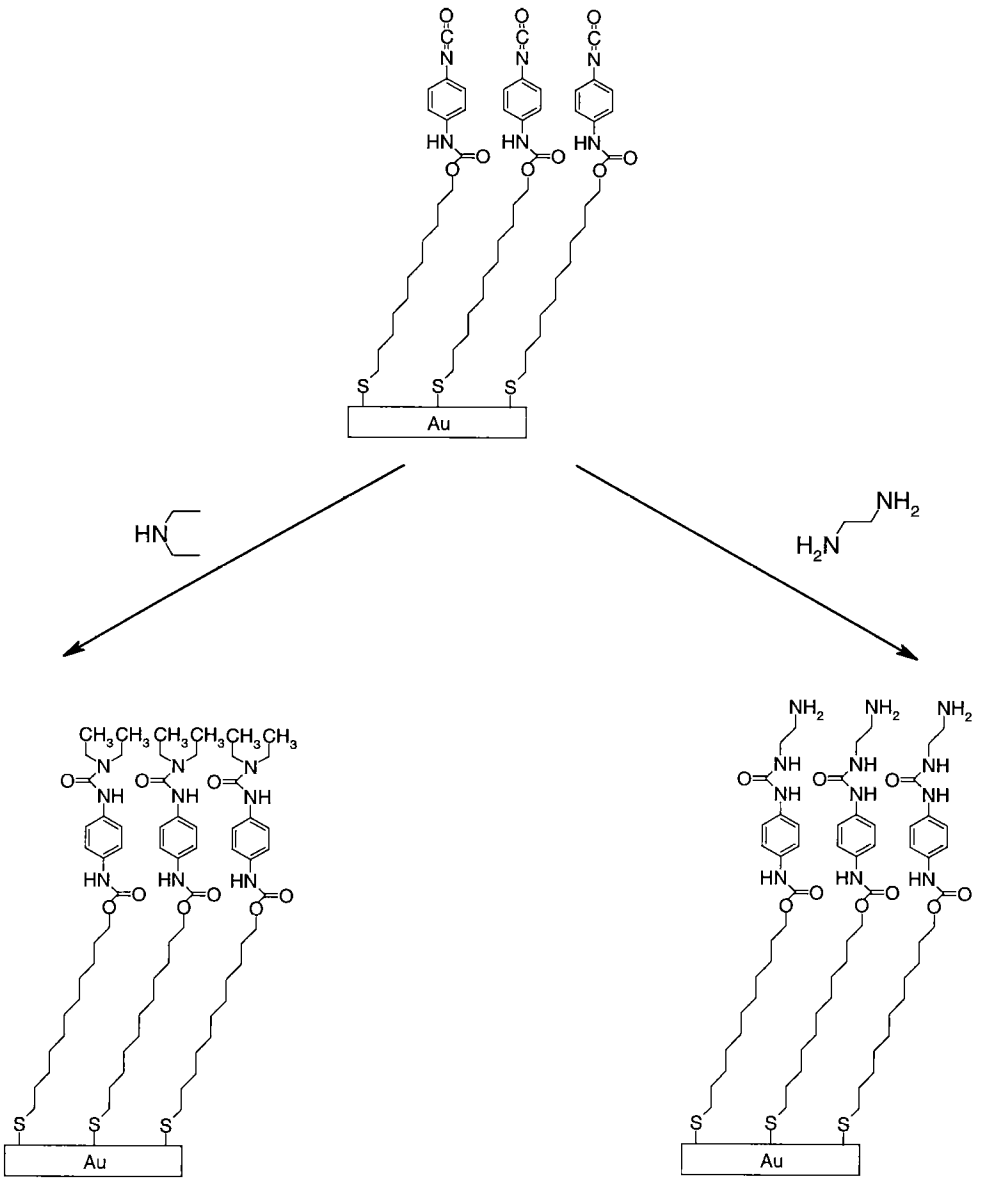

Figure 4.6. Schematic representation of reactions of phenylene diisocyanate-modified SAMs with amines yielding a urea linkage.

Complete conversion of the surface isocyanate groups (Ξ_{MUD}=1) with diethylamine (0.1 M in toluene) was obtained at 25 °C after 2 h, as indicated by IR spectra (Figure 3.3.A.). As in the cases of the reactions with the alcohols, new C-H vibrations of the methyl groups appear at 2965 cm^{-1} while the isocyanate signal at 2278 cm^{-1} vanishes. The C=O vibrations of the urea groups formed become visible at 1660 cm^{-1}. In XPS a decrease of the O/N ratio from 1.5 to 0.98 was observed (Table 4.2.) in accordance with the expected value of 1 after full conversion. The layer thickness of 27.0 (±1.0) Å does not differ significantly from that before the reaction (25.0 (±1.5) Å) since the added unit is relatively short. As expected, the ethyl groups are too short to render the surface as hydrophobic as in the case of the hexanol-treated samples, and the $\theta_a(H_2O)$ on the diethylamine-modified layer of 75° is comparable with that after the reaction with methanol.

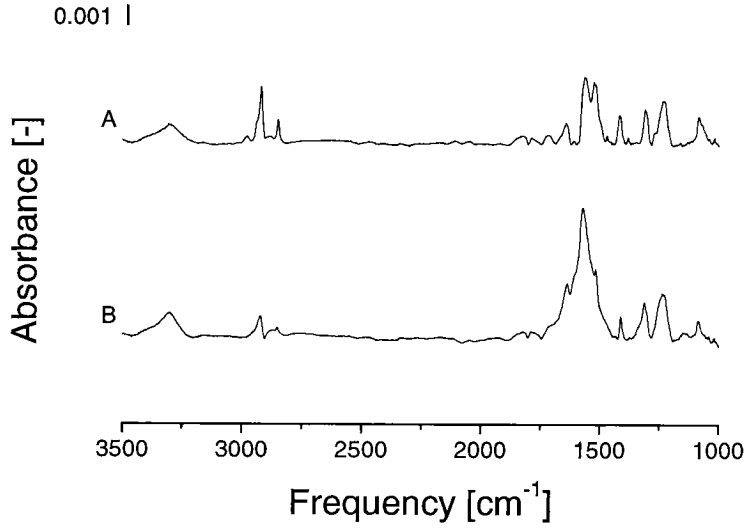

Figure 4.7. Infrared reflection absorption spectra of 1-mercapto-11-undecanol monolayers after conversion with phenylene diisocyanate followed by reaction with A) diethylamine, B) ethylenediamine.

1,2-Diaminoethane (ethylenediamine, $H_2NCH_2CH_2NH_2$) was also reacted with surfaces modified with PDI at Ξ_{MUD} = 1. The reaction conditions were identical to those of the transformations with diethylamine. In principle, 1,2-diaminoethane can react with one or both amine groups. The IR peak of the isocyanate group at 2278 cm^{-1} essentially disappears after a reaction time of 2 h, instead the urea vibration at 1660 cm^{-1} arises. The signal

intensity in the region of the N-H vibration at 3296 cm^{-1} (Figure 3.3. B) is higher than those of the methylene vibrations, in contrast to the diethylamine-exposed samples, probably because of terminal amines that did not react with isocyanate groups. The O/N ratio after reaction with 1,2-diaminoethane (Table 4.2.) confirms an increase of the nitrogen fraction at the surface. The obtained value is fairly close to the theoretical value of 0.75. The decrease of the gold fraction compared to that before the modification is an indication of an increase in layer thickness at the surface which could be confirmed by ellipsometry, where an increase from 25.0 (±1.5) to 30.5 (±1.3) Å was found. The $\theta_a(H_2O)$ of 41° is clearly below the values of the above reported reactions with alcohols and diethylamine but close to those on NH_2-terminated SAMs [232] and to the amine-terminated layers prepared by hydrolysis of isocyanates (see section 4.3. "Reactions with Water" on page 117), indicating that indeed the surface is significantly covered with amine groups.

Table 4.2. Atomic composition determined by high resolution XPS for MUD-monolayers after reaction with PDI and modification with amines.

Element	Diethyl-amine	Ethylene-diamine	Pure PDI-layer	Pure MUD-layer
O	10.6	11.2	10.5	9.2
C	68.4	63.5	67.5	67.3
N	10.8	12.2	6.6	-
S	0.9	0.8	1.6	1.5
Au	9.3	12.3	13.8	22.0
Total	100.0	100.0	100.0	100.0
O/N	0.98	0.92	1.58	-

4.3. Reactions with Water

The hydrolysis of isocyanates has already been described in chapter 3 (see section 3.6. "Stability of the Reacted SAMs" on page 99) where isocyanate groups react with water to carbamic acids, which, by decarboxylation, rapidly yield amine groups. A schematic representation of the reaction is shown in Figure 4.8., whereas the details of the mechanism of the hydrolysis are found in Figure 3.16.

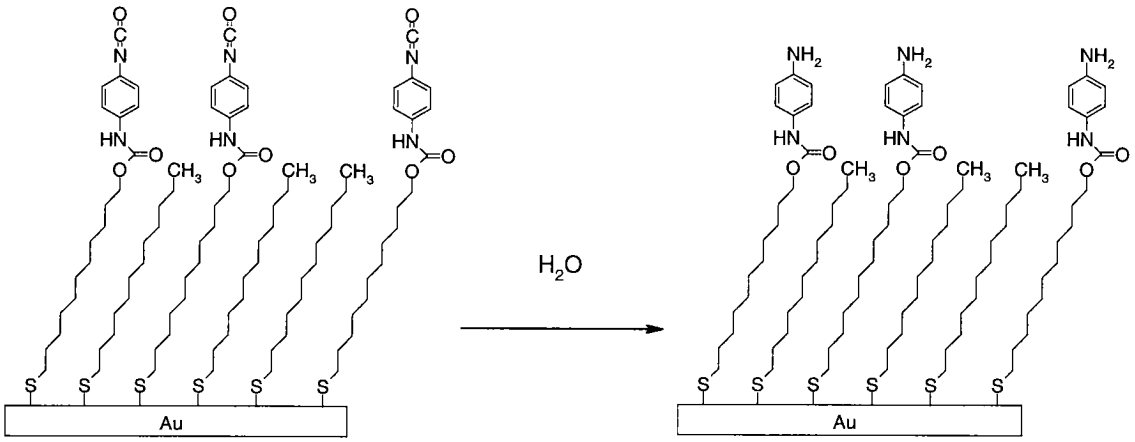

Figure 4.8. Schematic representation of reactions of phenylene diisocyanate-modified SAMs with water as described below.

Surfaces prepared by reaction of PDI with MUD monolayers or mixed monolayers of DDT and MUD were also contacted with neat water at room temperature. In IR-spectra, the NCO vibration disappears completely after 5 minutes, indicating a complete transformation of the isocyanates into amines (see Figure 4.9.). The intensity in the region of amine stretching vibrations increases at 3296 cm^{-1}, in agreement with the surmised reaction (the signal of the N-H deformation vibration overlaps with the amide I vibration). The increased intensity of the aromatic C-C stretch vibration at 1514 cm^{-1}, which is also observed for the modification with diethylamine (Figure 3.3.A.), could be due to orientational changes of the phenyl ring although it should be mentioned that the shoulder at 1514 cm^{-1} in the isocyanate layer prior to modification (See Figure 3.3. on page 85) also has been found to be of high intensity in some samples.

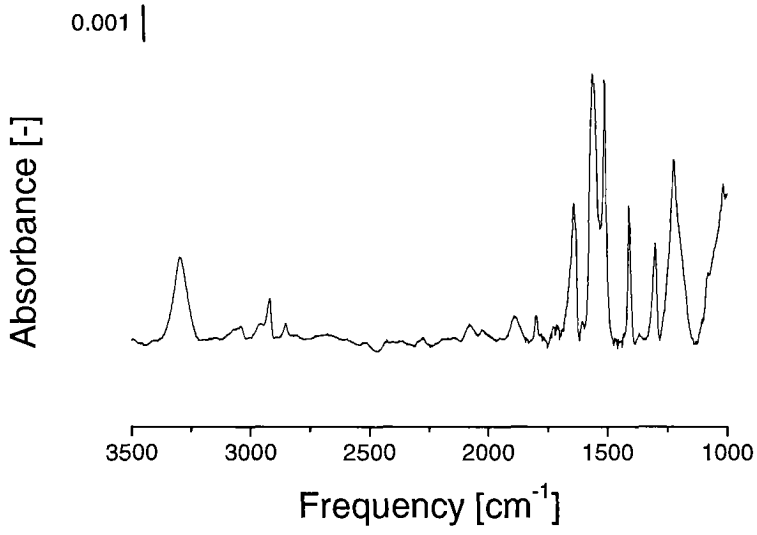

Figure 4.9. Infrared reflection absorption spectra of 1-mercapto-11-undecanol monolayers after conversion with phenylene diisocyanate followed by reaction with neat water.

The O/N ratio obtained from XPS decreases from 1.56 to 1.20, a relative increase of nitrogen atoms that is expected upon hydrolysis of isocyanate to amine groups. A theoretical O/N ratio of 1 is expected for a complete reaction. This difference in ratios could be explained by a possible contamination of water on the surface, which has previously been suggested for polar SAMs [213].

The advancing contact angles of water decrease with increasing content of MUD originally present at the surface (Table 4.3.), in proportion to the increased surface coverage with amine groups. The $\theta_a(H_2O)$ of 39° on the hydrolysed surfaces prepared from MUD monolayers corresponds to the value of the 1,2-diaminoethane-treated surfaces mentioned above (see section 4.2. "Reactions with Amines" on page 113) and literature values of other surfaces terminated with a dense layer of amino groups [232]. DDT monolayers, which were also subjected to the same procedure for comparison, did not show any difference in the contact angle upon water treatment.

Table 4.3. Advancing contact angles of water, $\theta_a(H_2O)$, after reaction of isocyanate groups with water. The isocyanate-containing surfaces were prepared from PDI and monolayers of MUD and mixed monolayers composed of DDT and MUD with different surface fractions of MUD, Γ_{MUD}. MUD surfaces ($\Xi_{MUD}=0$) have also been considered for comparison. The standard deviations of the specified values are within ±2°.

Ξ_{MUD}	$\theta_a(H_2O)$ [°]
0	107
0.06	100
0.25	75
0.55	56
0.8	50
1	39

The hydrolysis results in significantly lower contact angles for the monolayers at high Ξ_{MUD} as seen in Figure 4.10. It can therefore be concluded that the hydrolysis of the isocyanate groups which might occur at the surface due to the water droplet used for the measurement itself is of less importance. This was also suggested in IR-measurements where the loss of the intensity of the NCO vibration was negligible after contact angle measurement.

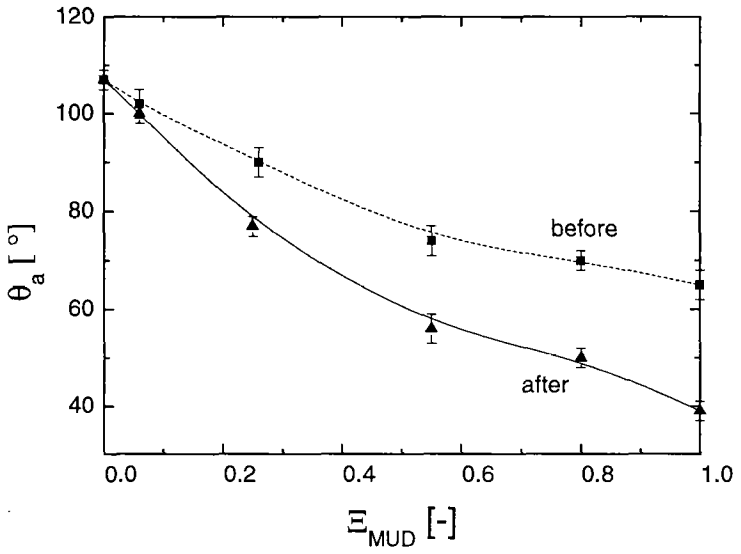

Figure 4.10. Advancing contact angles, θ_a, of water before (squares) and after hydrolysis (triangles) with water of SAMs reacted with phenylene diisocyanate as a function of the surface fraction of MUD, Ξ_{MUD}, in mixed monolayers with 1-dodecanethiol. The indicated lines are guides to the eye.

4.4. Conclusions

The PDI-activated SAMs react at mild conditions with alcohols, amines, and water, as evidenced by XPS, IR reflection spectroscopy at grazing incidence, contact angle measurements, and layer thickness measurements by ellipsometry. The results from GIR imply high extents of reaction of the isocyanate groups under the reaction conditions applied here for all substances (water, methanol, hexanol, diethylamine, and 1,2-diaminoethane) except for 3,3-dimethylbutanol, where the vibration of the isocyanate groups at 2278 cm^{-1} was still visible after a reaction time of 5 h. This is possibly due to a slow rate or insufficient space for the reaction (steric hindrance of the bulky side groups).

XPS measurements were undertaken of the modified surface to determine the composition of elements in the outermost surface layer. The O/N ratios are, as seen in Table 4.4., in fairly good agreement with theoretical values suggesting a high yield of the reactions.

Table 4.4. O/N ratios of SAMs obtained by XPS after derivatisation with PDI and after functionalisation of PDI-terminated SAMs with different model substances.

reactant	O/N ratio	
	XPS	theoretical
PDI	1.56	1.5
MeOH	1.84	2
$H_3C(CH_2)_5OH$	1.82	2
$HO(CH_2)_3(CH_3)_3$	2.04	2
$HN(CH_2CH_3)_2$	0.98	1
$H_2N(CH_2)_2NH_2$	0.92	0.75
H_2O	1.20	1

Data from ellipsometry and contact angle measurements of the modified layers give results in good agreement with expectations and literature values for contact angles where available [232]. It can thus be concluded that the conversion of self-assembled monolayers with PDI to isocyanate-covered layers offers a versatile and straightforward method to bind a variety of compounds to SAMs by use of commercially available substances.

5. Adhesion Studies

Adhesion of materials involves interactions within the "interphase" between two distinct materials. There are several theories described in the literature dealing with the fundamental understanding of adhesion [1][187][188][189][190]. However, none of the theories can explain observed adhesion phenomena in general and with great detail. The basic mechanism of adhesion is still unresolved [188]. In order to study the influence of different functional groups on adhesion, self-assembled monolayers on gold substrates were used. By studying the strength of adhesive joints as a function of surface concentrations of different functional groups, we expect to obtain information on the influence of strong chemical interactions between substrate and adhesive on adhesion (Figure 5.1.).

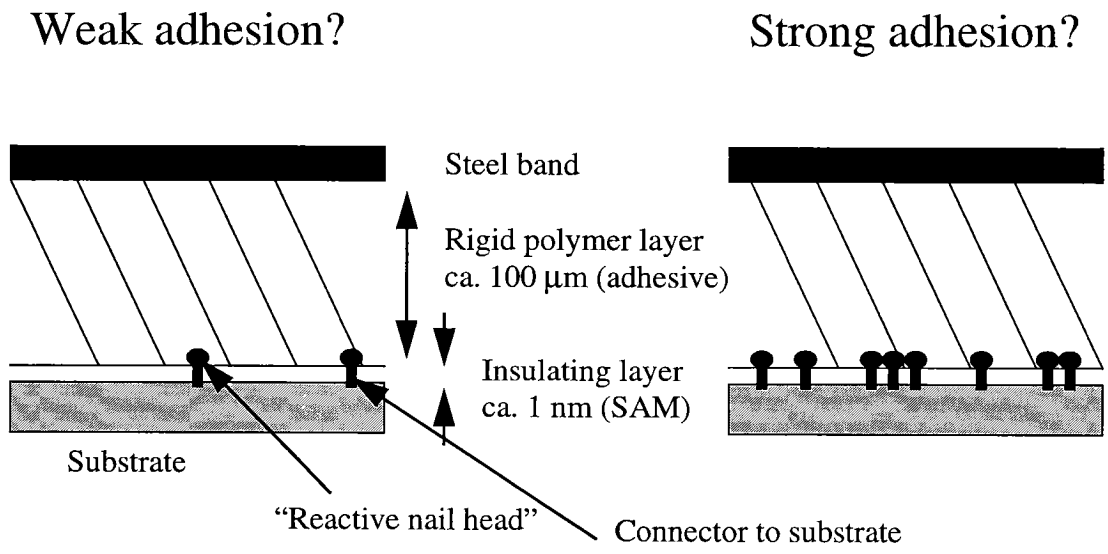

Figure 5.1. Schematic representation of the samples used for adhesion studies.

Methyl-terminated alkanethiol SAMs give high contact angles with water, as shown in chapter 2., and the related surfaces are therefore of low surface free energy. Materials with low surface free energy such as polyolefins and polytetrafluoroethylene (PTFE, "Teflon") are hard to join with adhesives because those usually do not wet the surface and because no reactions occur. Contact angles of water are reported in the literature to be 94 and 97° for polyolefins such as polypropylene and polyethylene, respectively [233]. Since methyl-terminated SAMs also have poor wetting properties (contact angle

of 115° for pure CH_3-terminated SAMs, see Table 2 on page 67) we use them as model surfaces with poor adhesion properties. By introducing functional groups in the monolayer without loss in order we expect to obtain a surface with well-known surface characteristics. Functional end groups were introduced to the SAMs by adsorption of 1-dodecanethiol (DDT) and 1-mercapto-11-undecanol (MUD) dissolved in ethanol, yielding mixed monolayers terminating in CH_3 and OH. Mixed self-assembled monolayers (SAMs) were produced in accordance with details given in chapter 2. "Adsorption of Self-Assembled Monolayers (SAMs)" resulting in monolayers with possibilities to tailor the concentration of polar hydroxyl groups as well as inert methyl groups.

Amine-terminated monolayers were also used for adhesion studies. In order to transform the hydroxyl groups into amine groups, the mixed monolayers were exposed to 1,4-phenylene diisocyanate (PDI) following the procedure in chapter 3. "Reactions of SAMs with Phenylenediisocyanate". Finally, the isocyanate terminated SAMs were hydrolyzed in neat water (for details, see section 4.3. "Reactions with Water") yielding amine groups in the monolayer. The reaction procedure is shown in Figure 5.2.

The wettability of the described mixed monolayers is shown in Figure 5.3. The higher wettability of the hydroxyl groups compared to the amine groups is evident at high surface fractions. In blank experiments with 0% amine groups (100% CH_3) the contact angle was 6° lower than prior to reaction with PDI. This is an effect of contamination from the solvent.

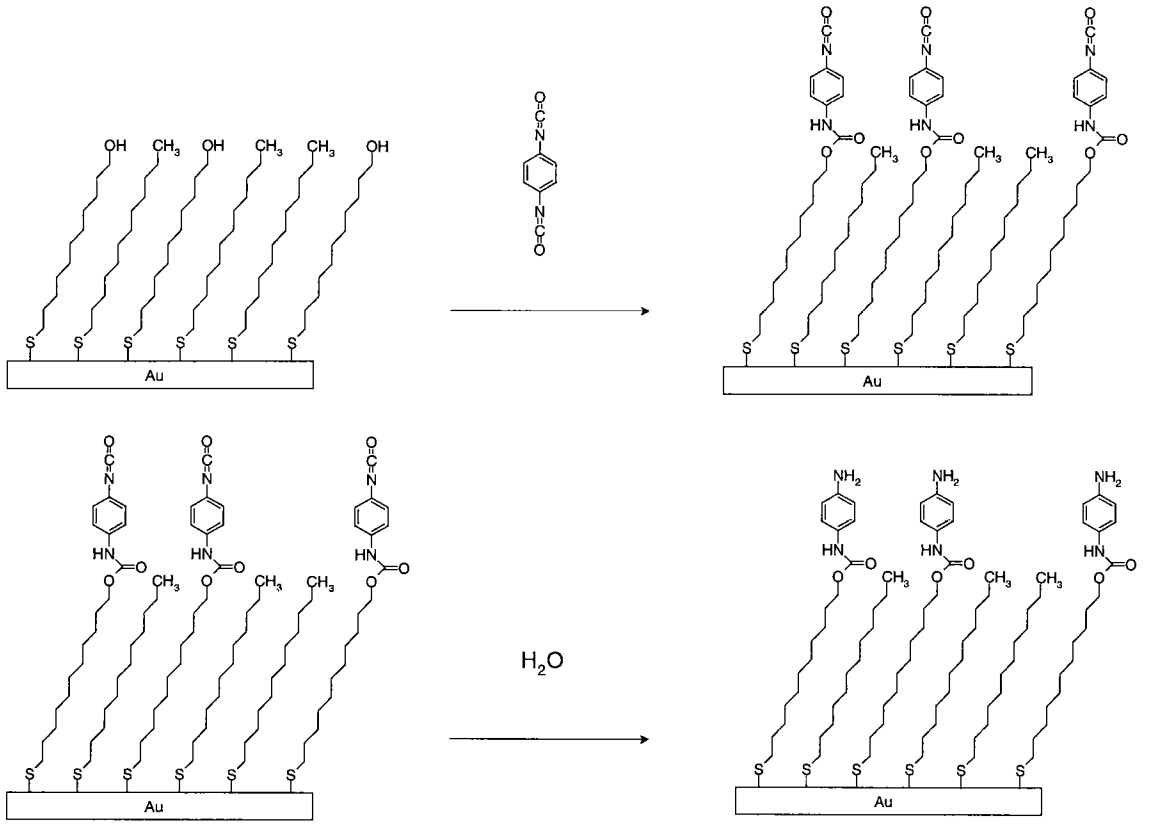

Figure 5.2. Schematic representation of the reactions to transform hydroxyl groups in the SAM into amines.

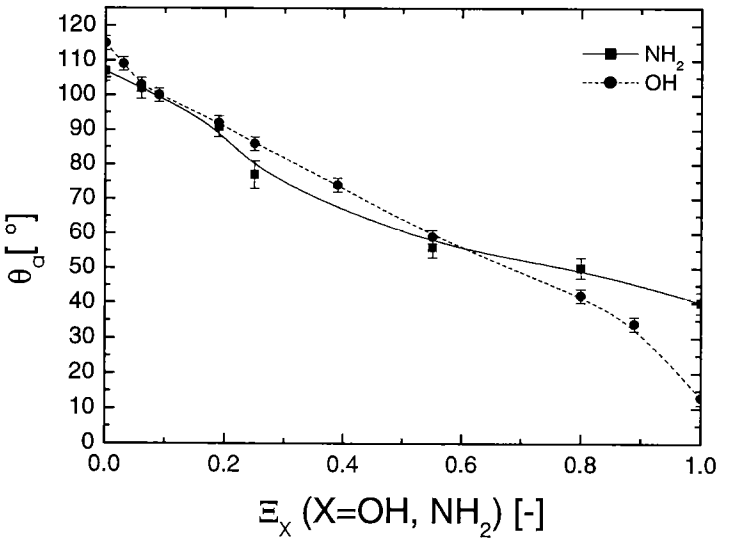

Figure 5.3. Contact angle of OH and NH_2-terminated SAMs as a function of their respective surface fraction. The indicated lines are guides to the eye.

For adhesion measurements the 90° peel-test was employed (Figure 5.4.). This test method involves peel or cleavage forces in the fracture. The test is accomplished by establishing a constant radius of curvature of the peeled layer after an initial failure and by monitoring the load required to promote peeling. However, there are also artefacts in the method. The peel force obtained can be a result of viscoelastic deformations in the adhesive. This can, depending on what kind of adhesive is used, sometimes correspond to more than 50% of the force measured. As a consequence, it is complicated to compare the peel force between different adhesive systems. Further, the peel force is also affected by the peel rate, which needs to be controlled throughout the measurement. Usually when a fracture is measured, variations between similar sample are considerable. This is also the case for the peel test. In order to reduce the fluctuations, several identical samples are measured, where the average peel force is monitored over a longer distance.

The test used in this work was performed in accordance to the european standard EN 28510-1 on a mechanical tensile testing machine with a special experimental set-up for the 90° peel-test in a climatised room at 23 °C and 50% relative humidity. Samples were equilibrated in the climatised room for at least 30 min. prior to testing. They were then mounted into the test compartment and exposed to a preforce of 0.1 N. The test rate was set to 50 mm/min. and the force was monitored as function of the peel distance. To avoid errors due to initial stresses in the samples, the first 15 mm of the peeling were not considered for evaluation. The distance evaluated was set to 20 mm. At least 4 samples (usually 6) were evaluated and the average peel force is presented in the data. Only samples where an obvious delamination occurred between the gold surface and the adhesive layer were followed. In some cases of high surface fractions of the functional groups, delamination occurred between the adhesive layer and the steel band. Thus, these results are not presented in the data.

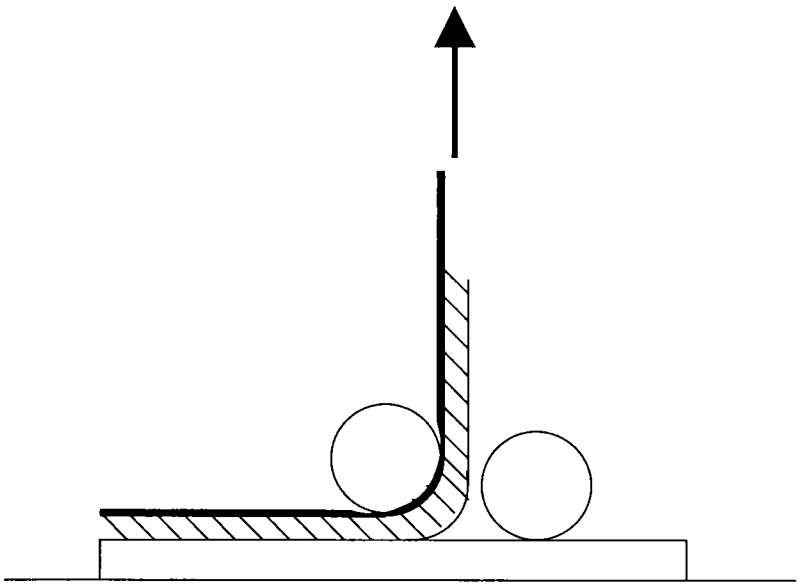

Figure 5.4. Schematic depiction of the peel-test.

Samples for peel-tests based on silicon (100) wafers (Powatech, Cham, Switzerland) cut into rectangles of dimensions 25×90 mm, which were used as substrates upon gold evaporation (described in section 7.2. "Preparation of Alkanethiol Monolayers"). The conversion of mixed monolayers into amine-terminated SAMs was made according to the description in section 7.3. "Surface Reactions". For the different adhesives tested, samples were glued and annealed as described below.

5.1. Experiments with an Epoxy Adhesive

Epoxy adhesives are usually two component adhesives which harden upon a chemical reaction between epoxy groups and nucleophiles such as amines. Due to a usual difunctionality in the epoxy component and a polyfunctionality in the nucleophiles, the adhesive will crosslink into a macromolecular network of very high molecular weight. The epoxy system used in this study was Araldite® Standard (Ciba Speciality Chemicals) consisting of the diglycidyl ether of bisphenol-A (DGEBA) as the main component in the resin. The crosslinking agent consisted of a mixture of various polyaminoamines such as triethylene-

tetraamine ($H_2NCH_2CH_2NHCH_2CH_2NHCH_2CH_2NH_2$) carrying both primary and secondary amines which can react with the epoxy resin. The principle of crosslinking of epoxy adhesives is shown in Figure 5.5., where the crosslinking agent is abbreviated as $H_2N\text{-}R\text{-}NH_2$. The resulting epoxy resin upon crosslinking with triethylene-tetraamine has a maximum glass transition temperature, T_g, of around 90 °C [234]. At room temperature, this will lead to a brittle fracture upon peeling. Hence, the viscoelastic component will be small and of little contribution to the obtained peel force.

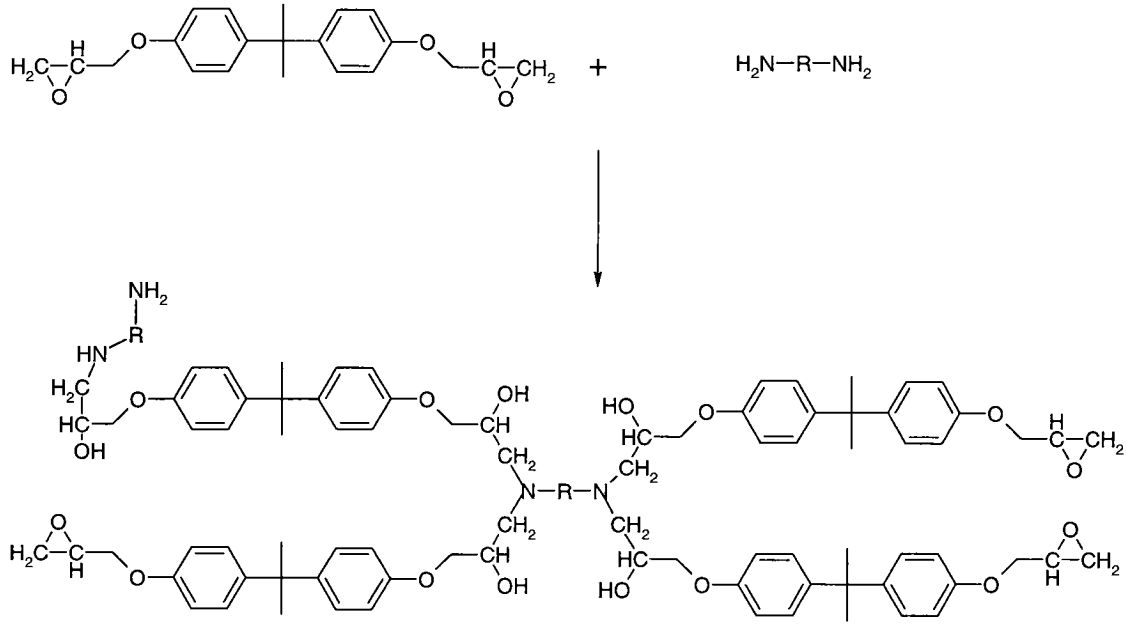

Figure 5.5. Schematic representation of the crosslinking of many epoxy adhesives.

This thesis deals with the influence of chemical interactions on adhesion. For the epoxy adhesive, it is suggested that the epoxy resin will be crosslinked not only with the crosslinking agent, but also with reactive functional groups present at the surface of a substrate. This will lead to interfacial chemical bonds between the substrate and the adhesive. The gain information of the influence of such interfacial bonds upon adhesion is the main goal of this work. The proposed reaction of the functionalised surfaces with the epoxy resin are schematically shown in Figure 5.6.

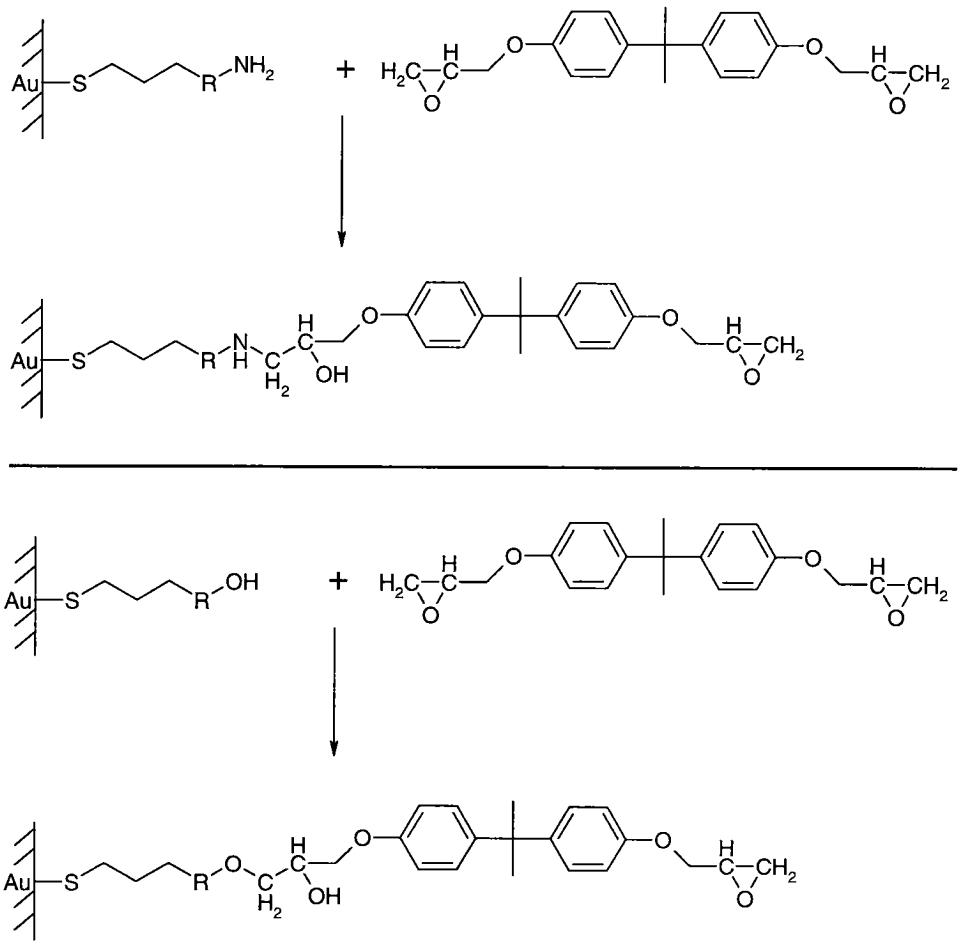

Figure 5.6. Schematic representation for the proposed reaction between the NH_2 functionalised surfaces and the epoxy adhesive (upper part). The lower part represents the possible reaction between the epoxy resin and SAMs terminating in OH.

For adhesion tests with epoxy based adhesive, a 100 μm thick adhesive layer was spread with a doctor blade onto 25 mm wide stainless steel bands previously rinsed with acetone. The samples with tailored surface composition were put in contact with the adhesive layer and were put under pressure by a 5 mm thick steel plate with the same dimensions as the sample. A schematic representation of the samples is shown in Figure 5.7. The samples were annealed for at 70° C, 45% relative humidity, for 16 hours prior to testing. The annealing temperature, 70° C, is well below the temperature where desorption of the self-

assembled monolayers in air have been observed (110° C) [104]. This implies that the sulphur-gold interaction should remain intact upon annealing.

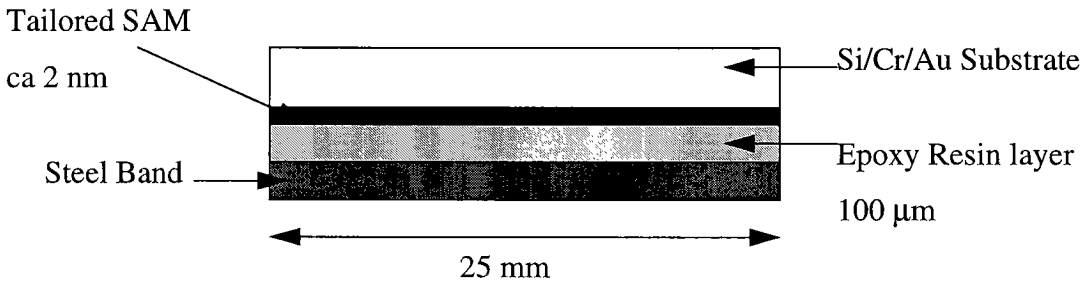

Figure 5.7. Schematic depiction of the samples used for adhesion tests with the epoxy system.

Typical results from the peel-test are shown in Figure 5.8. and a stick-slip behaviour, is observed. The stick slip behaviour is an artefact of the peel test, where the load builds up to a critical value at which the sample "unzips" and during which the load drops to a very low value. This process is then repeated several times. To avoid artefacts from initial stresses, only the peel distance from 15 to 35 mm is considered for each sample. However, residual stresses are still present in the sample throughout the peel testing.

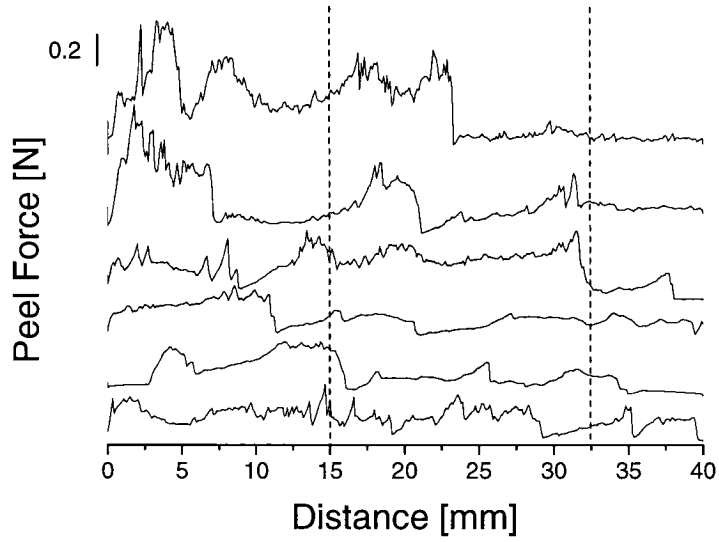

Figure 5.8. Peel-test results for the epoxy system. All samples shown are mixed SAMs terminating in OH at a surface fraction of 0.09.(Ξ_{OH}=0.09). The dashed lines represent the start and end point for evaluation.

For all different surface types evaluated, the average peel force is presented with standard deviations in Figure 5.9. For the amine-terminated SAMs, the resulting adhesion can only be measured up to a surface fraction of NH_2-groups of 0.25. Higher surface fractions in NH_2 result in a fracture of the adhesive layer followed by propagation at the steel-adhesive interface. For hydroxyl terminated samples, a visible delamination takes place between the adhesive layer and the substrate for all samples. The stronger linkages found for the NH_2-samples are most likely due to the higher reactivity of the amine group over the hydroxyl group regarding reactions with the epoxy ring. Lee & Neville [235] have described the reactions involved in the crosslinking of epoxy resins. They found that higher temperatures and longer times are needed for the crosslinking of epoxy resins with alcohols than with amines. The completion of cross linking is, however, complex. In general it can be said that for the faster reacting amines, the primary ones react about two times faster than secondary amines. For the slower reacting alcohols the preference for a reaction with an epoxy group can be written as primary > secondary > tertiary alcohols. Noteworthy is also that in our system the amines employed are aromatic which usually need higher temperature and a longer reaction time for crosslinking due to a lower mobility.

This argument can, however, be taken under less consideration due to the anchoring of all groups investigated onto the surface. Considering all observations by Neville & Lee and a comparison to our results, it seems reasonable to assume that the lower peel-forces of the hydroxyl-terminated samples observed in Figure 5.9. come from the lower reactivity. The amines present in the crosslinking agent react fast with the epoxy groups allowing only few hydroxyl groups to react with epoxy resin.

Another possible explanation of the higher peel forces observed for the amine-terminated surfaces could be the "difunctionality" in the amine group which would allow each "reactive nail head" to react twice over the monofunctionality found in the hydroxyl groups. This explanation is however less probable due to the detection of gold on the adhesive layer (see below).

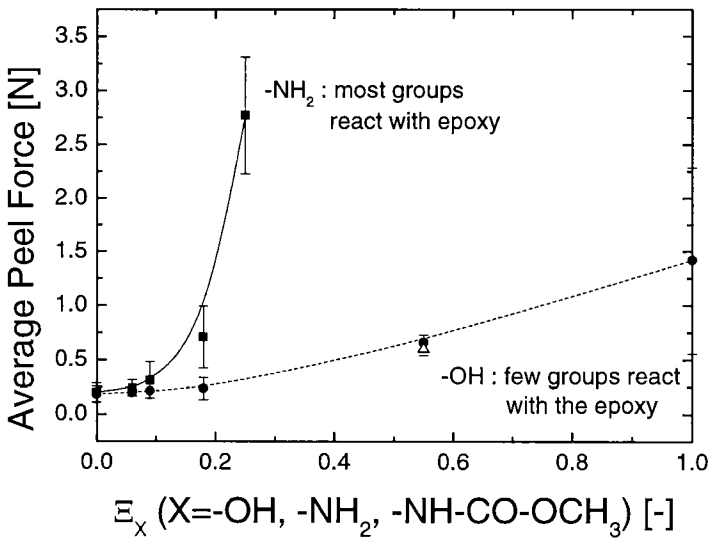

Figure 5.9. Average peel force of the epoxy system exposed to a surface with NH_2 (squares), OH (circles), or -NH-CO-OCH_3-terminated SAMs (open triangle) as a function of their respective surface fraction. The indicated lines are guides to the eye.

The delaminated adhesive layer was investigated with XPS and traces of gold and sulphur were found after peeling from both OH and NH_2-terminated samples. This is an indication that the "reactive" alkanethiol indeed have formed a covalent bond with the epoxy-resin

and are pulled out of the monolayer upon peeling. The sulfur-gold bonding seems to be strong enough to, at least in some cases, withstand the peeling process. For comparison of the bonding energies for the bonds at the gold-SAM interface, bonds incorporated in the SAM and those bonds obtained upon the crosslinking reaction with the epoxy layer (C-N and C-O, respectively) are listed in Table 5.1. [1][200][217]. The weakest of the listed bonds is the gold-gold bond. Of course, the gold atom has several partners in a metal bonding but still, the low bonding energy might suggest a priori that the failure during peel-testing occurs at this position, i. e. the failure occurs between gold atoms in the surface, and that gold atoms are actually pulled out of the surface upon peeling. In this context, it should also be mentioned that the force needed to break a chemical bond has little to do with the bonding energy (see also section 1.5.1. "Theories of Adhesion", $F = -dU/dr$).

Table 5.1. Typical bonding energies from the literature for some of the bonds incorporated in the self-assembled monolayers and those formed upon crosslinking with the epoxy-resin [1][200][217].

Bond	Energy [kJ/mol]
Au-Au	225
Au-S	418
S-C	259
C-C	343
C(ar)-C(ar)	518
C-O	351
C-N	291

Similar results where atoms are pulled out of one of the substrates have been found in a study of Wightman and coworkers [236]. They found evidence by XPS and IR spectroscopy for covalent bonding between an epoxy resin and thin polyphenylene sulfide films treated with oxygen and ammonia plasma. The covalent bonds at the interface were found to be C-O and C-N in the oxygen and ammonia-treated films, respectively. Bonds were

broken within the polyphenylene sulfide films and, hence atoms were pulled out of the substrate. These results agree well with our observations.

The gold peak from the high resolution XPS spectra is shown in Figure 5.14. and is of very low intensity (c. f. Figure 2.2.). This results in a low fraction in the atomic composition in the adhesive layer and was found to be as low as 0.1% (Table 2 on page 135). The gold peak appears around 85 eV but no shift correction of the binding energies with respect to the normal reference (Au at 84.0 eV) was made in this experiment. Usually the shifts are below 0.5 eV but in this experiment the measurement was performed on a thicker insulating layer (Adhesive layer ~100 μm compared to 1-3 nm for the SAMs). The insulating properties of the relatively thick layer is the probable cause of the high charging.

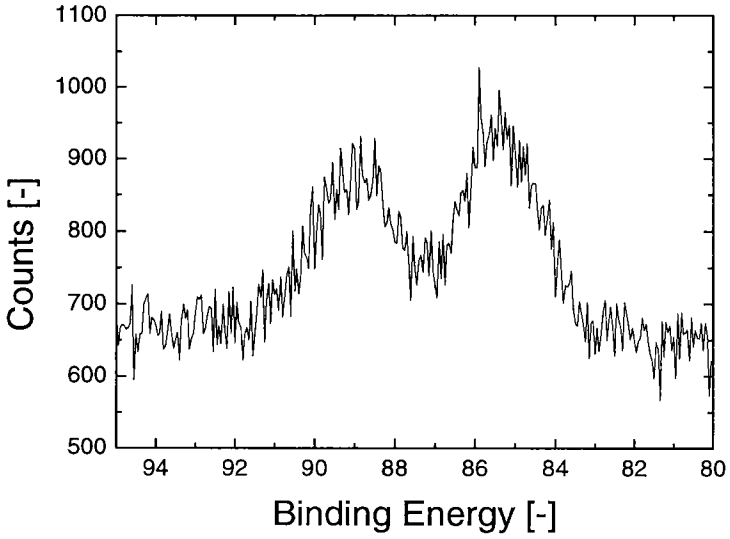

Figure 5.10. High resolution XPS spectra of the Au (4f) region after peeling (Ξ_{NH_2}=0.09).

Table 5.2. Atomic composition of the adhesive layer determined by XPS after peel-testing. The adhesive layer was glued with a monolayer terminated with NH_2 of a surface fraction of 0.09. the right column corresponds to a theoretical composition for the epoxy layer. .

Element	epoxy layer	pure epoxy layer
O	8.2	14
C	85.8	79
N	5.6	7
S	0.3	-
Au	0.1	-
Total	100.0	100

Sulphur was also detected on the adhesive layer after peel-testing (Figure 5.11.). The normal sulphur peak around 162 eV is found at a little higher binding energy (~ +1 eV) for the same reasons as for the gold peak. The normal sulphur peak is supplemented by an additional peak around 169 eV. Such peaks have also been found in some SAMs investigated in chapter 3 and 4. We believe that this peak originates in oxidized sulphur such as sulfate [167]. The amount of sulphur detected is higher (0.3%) than that of gold but at these low concentrations the differences are not significant since the signal-to-noise ratio of sulphur is very low. Abnormally high sulphur levels were also found in the oxidized SAMs in previous chapters.

The C(1s) spectra result in a broad peak at 285.8 eV (Figure 5.12.). The intensity of the urethane group stemming from the SAM is of too low intensity to be resolved as a specific peak. The N(1s) and the O(1s) spectra result in a single peaks at 400.4 eV and 533.8 eV, respectively (not shown). These two peaks as well as the carbon peak are an effect of the components of the epoxy resin. Hence, the very low contributions from the SAM can not be resolved.

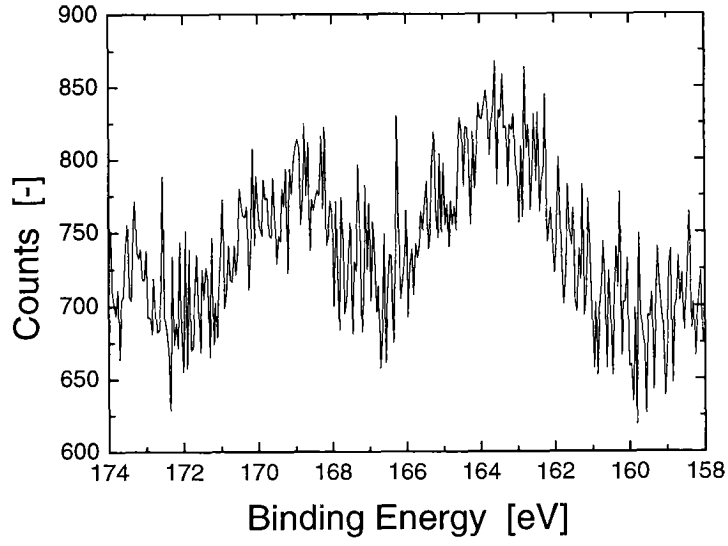

Figure 5.11. High resolution XPS spectra of the S (2p) region for the adhesive layer after peeling (Ξ_{NH_2}=0.09).

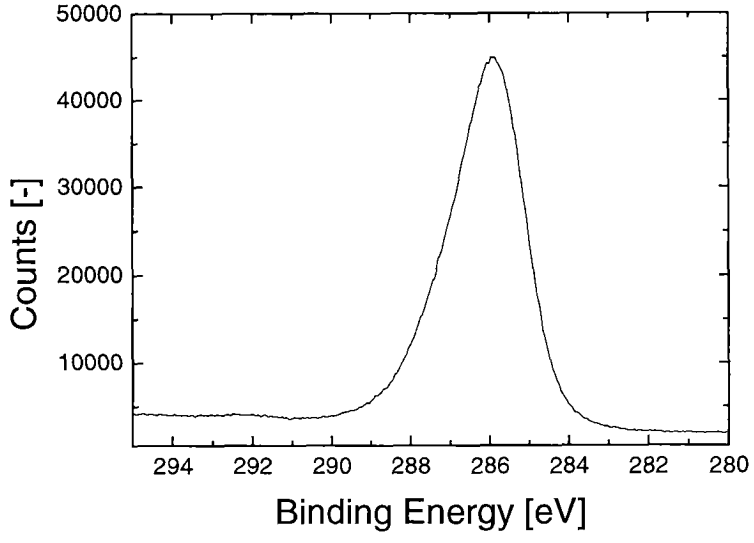

Figure 5.12. High resolution XPS spectra of the C (1s) region for the adhesive layer after peeling (Ξ_{NH_2}=0.09).

XPS-measurements of the gold substrate with remaining SAM showed little difference to samples prior to peeling. Hence, no change of the atomic composition upon peeling could be resolved.

For comparison of the reactivity of amine and hydroxyl groups, samples with Ξ_{OH}=0.55 were prepared and then derivatized with 1,4-phenylene diisocyanate as for the preparation of -NH_2 samples. However, instead of the normal hydrolysis the isocyanate bearing SAMs were exposed to a methanol solution resulting in surfaces terminating in -NH-CO-CH_3 as described in section 4.1. "Reactions with Alcohols". These surfaces exhibit carbamate groups susceptible to cross linking with the epoxy resin. However these are covered by -CH_3 groups. Peel testing of these samples resulted in an average peel force of 0.61±0.06 N. These results are comparable to those obtained for OH-terminated samples with Ξ_{OH}=0.55 (average peel force= 0.66+0.05 N). This suggest that no, or very few crosslinks are formed between the adhesive layer and the functionalised surfaces (slow reacting -OH groups and sterically hindered carbamate groups). In this case wetting and no (or few) chemical bond accounts for the adhesion. If chemical bonding accounts for the adhesive forces, this might suggest that carbamate groups, which are sterically hindered by the upper -CH_3 group form approximately the same amount of crosslinks as the slower reacting OH groups. In XPS, traces of gold where found in the adhesive layer upon peeling of the methanol modified sample but no sulphur was found. For the OH-terminated samples, neither gold nor sulphur could be detected in XPS. These results can be interpreted the following way: few chemical bonds are formed for the samples carrying carbamate groups, whereas pure wetting accounts for the adhesion for samples terminating in OH.

As a conclusion, both hydroxyl and amine-groups in the monolayer react in the epoxy system with the adhesive. For the same surface fraction of reactive groups Ξ_X (X = NH_2, OH) at the surface, there are less covalent bonds formed in the interphase with X=OH. Epoxy groups present at the interphase will rather react with primary amines present as crosslinking agent in the adhesive. For samples terminating in amines, the preference for a reaction between the cross linking agent and the epoxy resin is not plausible. Thus, more covalent bonds are formed across the interphase and resulting in joints stronger in the peel test.

5.2. Experiments with an Acrylic Acid Copolymer Adhesive

The acrylic acid copolymer adhesive (Figure 5.13.) employed in this study is a one-component contact adhesive where the polymer is dispersed in an aqueous phase. Contact adhesives are applied onto both objects that are to be joined. The adhesive layer is spread onto the substrates and interaction between the adhesive and the substrate are caused by physical adsorption (wetting) or electrostatic forces forming an electric double layer at the interface (for details, see 1.5.1. "Theories of Adhesion") [188]. A formation of hydrogen bonds across the interfacial layer is also a possible chance for adhesive interactions.

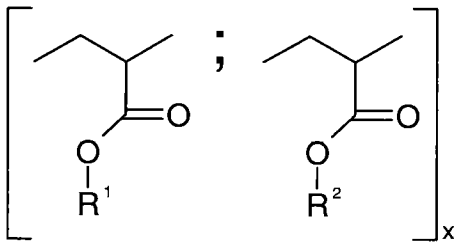

Figure 5.13. Depiction of the acrylic acid copolymer adhesive (R^1, R^2: unknown).

Upon evaporation of the solvent (in our case water), the viscosity of the adhesive increases and the parts to be joined are put in contact with each other and put under pressure. The adhesive joint is formed due to cohesion between the two adhesive layers. Since the glass transition temperature, T_g, of the adhesive is below room temperature, the fracture upon peeling will be ductile and the viscoelastic component measured will prevail the results. This should lead to, in general, higher peel forces for the copolymer system compared to the epoxy system, where the viscoelastic contribution will be of minor significance due to the higher glass transition temperature. Not only the viscoelastic contribution will influence the results, the results upon peeling will also depend on other factors. The time needed for evaporation of the solvent is crucial for the performance of the adhesive joint, and the thicker the adhesive layer, the longer the required evaporation time. In this study samples for peel-tests were prepared in the following way: 100 μm thick adhesive layers were spread with a doctor blade onto both stainless steel bands and tailored samples. After

evaporation of the solvent (water) for 20 min., the samples were put in contact with the steel band and then treated in the same way as the samples with epoxy-based adhesive.

A typical result from peel-testing with the copolymer system is shown in Figure 5.14.. An even stronger stick-slip behaviour than in the epoxy system is found. This is due to the flexibility within the adhesive layer. While the epoxy adhesive is rigid (below T_g), the acrylic acid copolymer, which is flexible (above T_g), will be deformed to a larger extent during peeling. When a critical deformation in the adhesive is built up, the adhesive slips of the surface and the peel force drops rapidly. The high amplitude in the stick-slip behaviour is most likely a result of viscoelastic deformation in the adhesive layer and also a cause of the high standard deviations obtained in the results (Figure 5.15.).

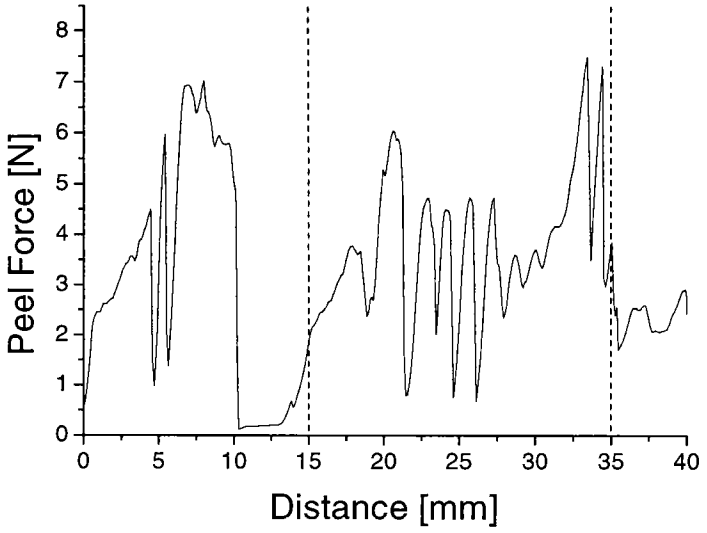

Figure 5.14. Peel-test result for the copolymer system. The curve refers to a sample terminating in methyl-groups (Ξ_{OH}=0.0).

For all the different surface fractions evaluated, the average peel force is presented with standard deviations in Figure 5.15. For both the hydroxyl- and amine-terminated surfaces a visual delamination between the gold substrate and the adhesive layer can be measured up to a surface fraction of 0.55. Surface fractions higher than 0.55 result in delamination between the adhesive layer and the steel band. The peel forces obtained for the copolymer system (Figure 5.15.) are significantly higher than for the epoxy system (Figure 5.9.),

most likely due to a higher viscoelastic deformation in the adhesive layer. In the copolymer system, the average peel force increases with the surface fraction of OH and NH_2, respectively. It seems that the SAMs terminating in OH-groups form marginally stronger adhesive joints, as measured by the peel test. However, the standard deviations are big, and no significant differences are found. This suggests precautions in the interpretation of the data.

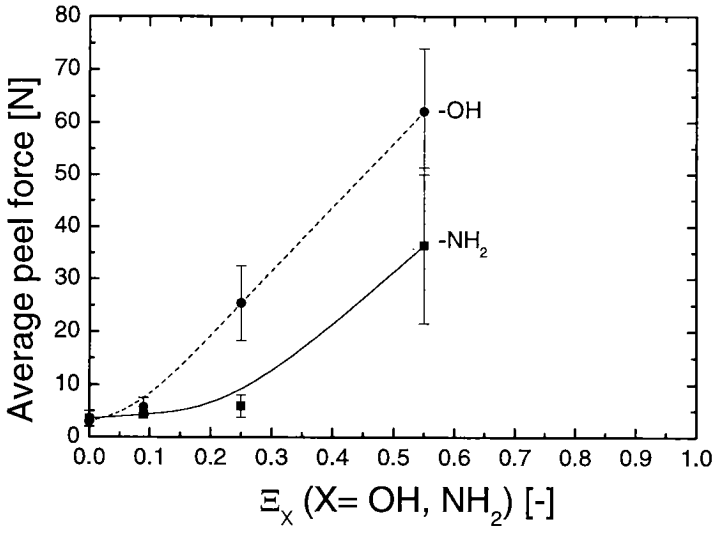

Figure 5.15. Average peel force of the copolymer system for NH_2 (squares) and OH-terminated SAMs (circles) as a function of their respective surface fraction. The indicated lines are guides to the eye.

The wetting behaviour (the physical interactions) is most likely almost alone responsible for the differences in the data although the OH- and NH_2-terminated surfaces show similar wetting behaviour (similar contact angles) at all the surface fractions where the delamination occurs between the adhesive and the substrate (c. f. Figure 5.3.).

The forces at the interface between the copolymer adhesive and the tailored surface will most likely relay on physical attraction forces such as van der Waals forces, chemical hydrogen bonds or a possible electric double layer as described in section 1.5.1. "Theories of Adhesion". Physical attraction forces as well as electrostatic forces at the interface will depend on the electronegativity of the elements present at the interface. If the adhesive

forces are originating in an electric double layer, these forces are, however only accounting for a fraction of the total adhesive strength as suggested in peel studies by Lee [190] and Possart [237][238].

The physical adsorption theory as well as the electrostatic theory would support higher adhesive forces for the OH-terminated monolayers due to the higher electronegativity in oxygen compared to nitrogen. If hydrogen bonds account for the adhesion at the interface, the situation is more complex and the strength will depend on several factors in the different established hydrogen bonds. Pauling has described the nature of hydrogen bonds [200]. He found that the strength of a hydrogen bond will depend on the orientation of the bond with the highest strength for a linear hydrogen bond as found for example in an α-helix of a protein (N-H·····O=C) [239]. When the hydrogen bonds are oriented with the same angle as their individual covalent bonds, they will also form strong interactions. Other orientations will lead to weaker interactions. Pauling also found a relation between the distance of the atoms in a hydrogen bond and the character of the bond. The closer the distance between interacting atoms, the more covalent character will the interaction have. Hence, the distance between the atoms in a hydrogen bond reflects the strength of the interaction. Stryer found the length of the O-H····O=C interaction and the N-H····O=C interaction to be 2.70 and 3.04 Å, respectively [239]. Pimentel [240] has described a qualitative inverse relation between the length of a hydrogen bond and its free enthalpy. He also cited the enthalpy of the O-H····O=C interaction and the N-H····O=C interaction in Carbon tetrachloride to be 5.4 and 3.9 kcal/mole, respectively. This suggest a stronger hydrogen bond for the O-H····O=C interaction.

If hydrogen bonds account for the adhesive forces at the interface of the studied system, the monolayers will act as a hydrogen donor through the functional groups at the surface, (O-H and N-H, respectively). The keto-oxygen in the adhesive will act as hydrogen acceptor in the established hydrogen interactions. According to the observations by Pauling, Stryer and Pimentel, this would result in stronger adhesion for the OH-terminated monolayers which is in accordance with our results. However, as already mentioned, the standard deviations are high which suggests caution in the conclusions. Since no evidences

for chemical bonding are found in the copolymer system (see below) it is suggested that the adhesion relies upon physical interactions, wetting.

The delaminated adhesive layer was investigated with XPS as already described for the epoxy system investigated. For the copolymer adhesive, no indications of either gold or sulphur were found in the adhesive layer. This might suggest that the delamination occurs between the monolayer and the adhesive layer as discussed above.

5.3. Conclusions

Self-assembled monolayers with tailored concentrations of functional groups were found to be suited substrates for adhesion studies. This was found by producing SAMs with different concentrations of functional groups, gluing the substrates onto a steel band with either an epoxy or an polyacrylic adhesive, and finally investigating the adhesion by the peel-test. For both systems investigated, a higher concentration of functional groups in the substrate results in stronger peel forces. Depending on the functional group and the adhesive investigated, high concentrations of OH or NH_2 groups, respectively, result in delamination between the adhesive layer and the steel band instead of delamination at the desired interface substrate-adhesive layer.

For the epoxy system studied, the monolayers terminating in NH_2 groups result in significantly stronger adhesive joints than those found for monolayers terminating in OH groups. This can be explained by the higher reactivity of amine-groups to form a covalent bond with the epoxy-ring. Hence, more covalent bonds between the adhesive and the substrate will be formed and these are accounting for the higher peel forces. The suggested formation of covalent bonds at the interface are supported by XPS investigations where traces of sulphur and gold were found on the adhesive layer after peeling.

In the studied copolymer system, the adhesion improves with the surface fraction of both amine- and hydroxyl- terminated monolayers up to a surface fraction of 0.55, and higher surface fractions result in delamination at the steel band-adhesive layer interface. Very strong peeling forces are found in the copolymer system due to large deformations of the

adhesive upon peeling. The adhesive forces at the interface are suggested to rely upon wetting, physical interactions such as van der Waals forces as well as hydrogen bonds. Little differences are found between the two functional groups investigated.

The absolute values of the peel forces between the epoxy and the acrylic acid copolymer systems can not be compared due to influence of the thickness of the adhesive layers. Thicker adhesive layers have been found to improve the peel strength [1]. In the copolymer system the adhesive layer is twice as thick as in the epoxy experiments and consequently higher peel forces are found. Further, the copolymer system is tested above T_g whereas the epoxy system is tested below T_g. This implies a higher mobility in the copolymer and resulting in more deformation and, as a consequence, in higher joint strength measured by peel-testing. The general practice [1] that rigid adhesives are strong in shear but weak in peel, whereas rubbery adhesives are resistant to peel but creep in shear can very much be applied to our peel results. This was also supported by initial studies of the epoxy system, where the epoxy system showed very good results in the lap-shear test. The test were, however, not followed further due to failures in the substrate.

6. General Discussion

Self-assembly of 1-mercapto-11-undecanol (MUD) and 1-dodecanethiol (DDT) from ethanolic solution results in densely packed monolayers. The surface fraction of MUD (Ξ_{MUD}), as determined by XPS, is below the related fraction in solution (y_{MUD}) if y_{MUD} is below 0.7-0.8. This effect is caused by the solvent used. At fractions of MUD above 0.7-0.8 in the solution the surface fraction is found to be similar as the fraction in solution ($\Xi_{MUD} \approx y_{MUD}$). This is believed to be due to hydrogen bonding between adjacent hydroxyl groups of adsorbed MUD molecules.

Comparison of the XPS measurements with results derived from contact angle measurements and interpreted by the Cassie as well as the Israelachvili and Gee equation suggests that the Israeleachvili and Gee equation describes the system better for $0.2 \leq y_{MUD} \leq 0.7$. This implies that the resulting monolayers are randomly mixed at the corresponding surface fractions. No difference was found between the Cassie and the Israelachvili and Gee equation when y_{MUD} is below 0.2. For $y_{MUD} > 0.7$ the system is probably separated into domains or patches according to the better fit to the Cassie equation. This can be interpreted as follows: at low concentrations the mixed SAMs are randomly mixed and that when the surface concentration gets high enough to allow hydrogen bonding between a substantial amount of MUD molecules, a phase separation takes place. Unfortunately, there are no available techniques to monitor such a phase separation for SAMs where the two components are of similar length. The sizes of such domains are an interesting matter in the study of self-assembled monolayers but still remains open.

The MUD monolayer and the mixed monolayers react under mild conditions with 1,4-phenylene diisocyanate (PDI) as confirmed by infrared spectroscopy, XPS, Ellipsometry and contact angle measurements. The optimal reaction conditions were found at a temperature of 40 °C, a MUD concentration of 0.1 M, and a reaction time of 2 h. Higher reaction temperatures result in desorption of the underlaying SAM. The derivatization of monolayers with PDI is accomplished by a reaction between hydroxyl groups in the SAM and one of the isocyanates in PDI. A carbamate group is formed, while the other isocyanate remains unaffected and reactive as confirmed by IR investigations. XPS measurements

lead to the conclusion that the surface hydroxyl groups have been converted to a high extent (93 (±10)%), independent of Ξ_{MUD}. The carbamate groups and, consequently also the residual phenylene isocyanate moieties, are preferentially oriented with the carbonyl group parallel and the 1,4-phenylene axis perpendicular to the surface.

The PDI-activated SAMs react under mild conditions with alcohols, amines, and water, as evidenced by XPS, IR reflection spectroscopy at grazing incidence, contact angle measurements, and layer thickness measurements by ellipsometry. The results from GIR spectroscopy imply high extents of reaction of the isocyanate groups under the reaction conditions applied here for all substances (water, methanol, hexanol, diethylamine, and 1,2-diaminoethane) except for 3,3-dimethylbutanol, where the IR-vibration of the isocyanate groups at 2278 cm^{-1} was still visible after a reaction time of 5 h. This is probably due to a slow intrinsic rate or the bulky side groups present in 3,3-dimethylbutanol, which cover some of the isocyanate groups at the surface and thereby obstruct a completion of the reaction. An accomplishment of the same reaction on a mixed SAM (Ξ_{MUD} <1), carrying less isocyanate groups after derivatization with PDI, would possibly result in desertion of the NCO-vibration, since steric hindrance of bulky side would not cause any problems. With less available and randomly mixed reaction sites (NCO-groups), there would be more space available for the bulky side groups in 3,3-dimethylbutanol. Derivatization of mixed SAMs resulting in tailored concentrations of isocyanate-groups would also allow the possibility of chemical anchoring of bigger macromolecules at the surface. These issues have, however, not been followed further in this thesis.

Self-assembled monolayers with tailored concentrations of functional groups were found to be useful for adhesion studies performed with peel-tests. For both adhesive systems investigated (an epoxy adhesive as well as an acrylic acid copolymer adhesive), a higher concentration of functional groups in the substrate results in stronger peel forces. For the epoxy system studied, the monolayers terminating in NH_2-groups result in significantly higher adhesive forces than those found for monolayers terminating in OH-groups. This can be explained by the higher reactivity of amine-groups to form a covalent bond with the epoxy-ring. Hence, more covalent bonds between the adhesive and the substrate will be formed and these are accounting for the higher peel forces found. For samples termi-

nating in OH, the adhesion is implied to relay on wetting. The suggested formation of covalent bonds at the interface of samples terminating in NH_2 are supported by XPS investigations where traces of sulphur and gold are found on the adhesive layer after peeling.

In the copolymer system studied, very strong peeling forces were found due to large viscoelastic deformations of the adhesive upon peeling. The large standard deviations make interpretation of the data complex. Reiteration of the measurements with bigger series of each sample might result in less standard deviations and data easier to interpret. Artefacts from viscoelastic deformations could possibly be avoided by the use of a different adhesive system also relying on wetting but with higher T_g, which would simplify the interpretation of the data. For the copolymer system studied, the adhesive forces at the interface are suggested to rely upon physical interactions such as van der Waals forces and hydrogen bonds. The difference between the two functional groups studied is believed to stem from the higher electronegativity of oxygen resulting in stronger hydrogen bonds and van der Waals forces at the interface between the adhesive layer and the self-assembled monolayer.

7. Experimental Methods

7.1. Sample Preparations

7.1.1. Materials

1-Mercapto-11-undecanol (97%), hexadecane (99%), nylon 6/6, 1,4-phenylene diisocyanate (purified by melting at 120 °C under argon atmosphere, cooling to room temperature and sublimation at a pressure of ca. 10^{-2} mbar prior to use) were purchased from Aldrich; dodecanethiol (97%), toluene (99.5% water-free over molecular sieve and 99.8% UV), 1-hexanol (99%), 3,3-dimethyl-1-butanol (98%), 1,2-diaminoethane (99.5%), diethylamine (99.5%) and phenyl-isocyanate(99%, purified in a similar way as for 1,4-phenylene diisocyanate) from Fluka; dichloromethane (99.5%) and methanol (99.8%) from Mallinckrodt Baker; and ethanol (absolute, deoxygenated prior to use by bubbling of argon for 15 min) from Merck. A two component epoxy adhesive, "Araldite® Standard" (17274) from Ciba Speciality Chemicals, an acrylic acid copolymer-based "Contact Adhesive" (78469) from Miocoll, and a methacrylate based "Multibond® Kit" (330) from Loctite were used for adhesion tests. If not otherwise mentioned above, the substances were used as received without any further purification.

7.1.2. Preparation of Alkanethiol Monolayers

Silicon (100) wafers (Powatech, Cham, Switzerland) cut into rectangles of dimensions 18×40 mm were used as substrates for evaporation. Wafers were cleaned from organic contaminants by immersion in toluene (99.8% UV) for 24 h prior to evaporation and followed by drying in a stream of argon. Gold substrates were prepared by evaporating ca. 2000 Å of gold (99.99%, Balzers, Liechtenstein) with a deposition rate of ca. 15 Å/s onto silicon (100) wafers, which had previously been covered with 60 Å of chromium (99.99%, Balzers, Liechtenstein) as an adhesion promoter. The evaporation procedure was carried out in a Balzers MED 010 coater, operating at a pressure of ca. 10^{-5} mbar. The thickness of the evaporated layers was controlled with a QSG 301 Vibration quartz

apparatus (Balzers, Liechtenstein). Consequently, the evaporation chamber was flushed with argon and the freshly prepared samples were immersed for 16 h in 0.1 mM solutions of the thiols in ethanol. The gold substrates were removed from the thiol solutions, washed with water-free ethanol and dried under an argon stream.

7.1.3. Surface Reactions

The SAMs were exposed to 0.01 or 0.1 M solutions of 1,4-phenylene diisocyanate (purified by sublimation as described above in the sub-section Materials 7.1.1) in water-free toluene at 40 °C for 2 h under an argon atmosphere, if not otherwise indicated in the text. The substrates were washed with toluene, dichloromethane, once again with toluene and finally dried in a stream of argon. In order to convert the isocyanate-terminated monolayers, the corresponding samples were placed into neat methanol, 1-hexanol, or 3-dimethyl-1-butanol for 2 h at 25 °C, unless otherwise indicated in the text. For the reaction of isocyanate-terminated monolayers with diaminoethane or diethylamine, the substrates were exposed to 0.1 M solutions of the amines dissolved in water-free toluene for (typically) 2 h at 25 °C. Reactions of isocyanate-terminated monolayers with water were carried out in neat water for 5 min at room temperature. All modified monolayers were washed with toluene, dichloromethane, and again toluene prior to drying under a stream of argon.

7.1.4. Sample Preparations for Adhesion measurements

Silicon (100) wafers (Powatech, Cham, Switzerland) cut into rectangles of dimensions 25×90 mm were used as substrates for evaporation and prepared in the same way as described in section See "Preparation of Alkanethiol Monolayers" on page 149.. The conversion of mixed monolayers into amine-terminated SAMs was made according to the description in section See "Surface Reactions" on page 150.. For adhesion tests with epoxy based adhesive, a 100 μm thick adhesive layer of Araldite® Standard (Ciba Speciality Chemicals, Basel, Switzerland) was spread with a doctor blade onto 25 mm wide stainless steel bands (Brütsch/Rüegger AG, Zürich, Switzerland) previously washed in acetone.

The samples with tailored surface composition were put in contact with the adhesive layer and were put under pressure by a 5 mm thick steel plate with the same dimensions as the sample. The samples were annealed for at 70° C, 45% relative humidity for 16 hours prior to testing. For adhesion tests with acrylic acid copolymer-based adhesive (Miocoll, Zürich, Switzerland), 100 μm thick adhesive layers were spread with a doctor blade onto both stainless bands and tailored samples. After evaporation of the solvent (water) for 20 min, the sample was put in contact with the steelband and then treated in the same way as the samples with epoxy based adhesive.

7.2. Analytical Methods

7.2.1. Contact Angle Measurements

Contact angles were quantified on a Ramé-Hart 100 goniometer at room temperature and ambient humidity. The advancing contact angles were obtained by forming a 3 μl drop of the applied liquid at the end of a needle attached to a 10 μl syringe, lowering the needle until the drop touched the surface, and raising the needle. A second droplet of 3 μl was centered on the first drop. As the drop detached itself from the needle tip, it advanced over the surface. The contact angles were measured typically within 30 s after the first contact of the liquid with the surface. Under these conditions, the contact angles were stable for several additional minutes, except for the case with the NCO-terminated monolayers, where the contact angles decreased with time as a consequence of the hydrolysis of the isocyanate groups; however, the contact angles were reproducible when measured within 20 s. Values were taken at minimally 6 different locations on the sample and averaged. The standard deviation of the mean was always within ±2°.

7.2.2. X-Ray Photoelectron Spectroscopy (XPS)

X-ray photoelectron spectra were measured at a pressure of ca. 10^{-9} mbar on a PHI 5700 gauge (Physical Electronics, USA) using Mg K_α radiation. The energy was calibrated for each sample to the Au($4f_{7/2}$) binding energy of 84.0 eV of the evaporated gold

substrates. The accuracy of the binding energies is estimated to be ±0.2 eV. Unless otherwise stated, a take-off angle of 15 ° from the surface was employed. Survey spectra were recorded with 187.85 eV pass energy, 0.8 mm spot size, and 350 W electron beam power and an acquisition time of 5 min. High-resolution spectra were recorded with 23.50 eV pass energy, 0.8 mm spot size, 350 W electron beam power, and an acquisition time of 30 min. All the high resolution spectra were fitted using symmetrical 90% Gaussian + 10% Lorentzian profiles and the minimum number of peaks consistent with a reasonable fit and the molecular structure of he adsorbates. Energy, intensity, and width of the fitted peaks were unconstrained.

7.2.3. IR-Spectroscopy

IR spectra were recorded at grazing incidence reflection on a Bruker IFS 66v spectrometer equipped with an MCT (mercury-cadmium-telluride) detector. The measurements were performed at an incident angle of 80° with a fixed-angle inset. To eliminate atmospheric bands of water and carbon dioxide, the pressure in the sample chamber was reduced below 1 mbar. Freshly prepared gold surfaces were used as references, i.e., the spectra of these surfaces were subtracted from those of the SAM-modified substrates. For comparison of samples that were not evaporated in the same batch as the gold sample used for background measurement, a baseline correction was performed using a manual "rubber band" guidance. Typically, 500 scans were averaged to yield spectra with excellent signal-to-noise ratios. A negative peak obtained in some spectra at around 1397 cm^{-1} descents from a gas adsorbed on the gold reference which is repressed upon immersion in thiol solutions [41].

7.2.4. Ellipsometry

Ellipsometric measurements were performed using a Plasmos SD 2300 ellipsometer, equipped with a He-Ne laser (λ = 632.8 nm), at an angle of incidence of 70°. The beam diameter was around 1 mm. The refractive index and the absorption coefficient of the gold substrates were determined before the samples were immersed in the thiol solutions.

The layer thickness was obtained from measurements at 20 spots spaced by 1 mm on a straight line. For the thickness calculation, refractive indices of 1.46 for the organic layers were used. Typical errors in thicknesses are ±1 to ±2 Å.

7.2.5. Peel Testing

Peel testing was performed in accordance to european standard EN 28510-1. Testing was performed on a mechanical testing machine (Zwick, Germany) with a special experimental set-up for the 90° peel test, where the substrate investigated can slide upon peeling in order to keep the peel angle at 90°. A photograph of the experimental set up is shown in Figure 7.1. Tests were performed in a climatised room at 23 °C and 50% relative humidity. Samples were mounted into test compartment and exposed to a preforce of 0.1 N. The test rate was set to a constant speed of 50 mm/min. and the force was monitored as function of the peel distance. To avoid errors due to initial stresses in the samples, the first 15 mm of the peeling were not considered for evaluation. The distance evaluated was set to 20 mm. At least 4 samples (usually 6) were evaluated and the average peel force is presented in the data. Samples with 0% functional groups at the surface were used as samples for blank measurements and are also presented as a reference in the data. To be able to compare different adhesive systems, it is necessary to normalize the data to the blank sample. This has, however, not been done for the adhesives studied here, in order to obtain information of the viscoelastic contributions for each adhesive. For a direct comparison between different adhesives, an identical thickness of the adhesive layers would also be necessary.

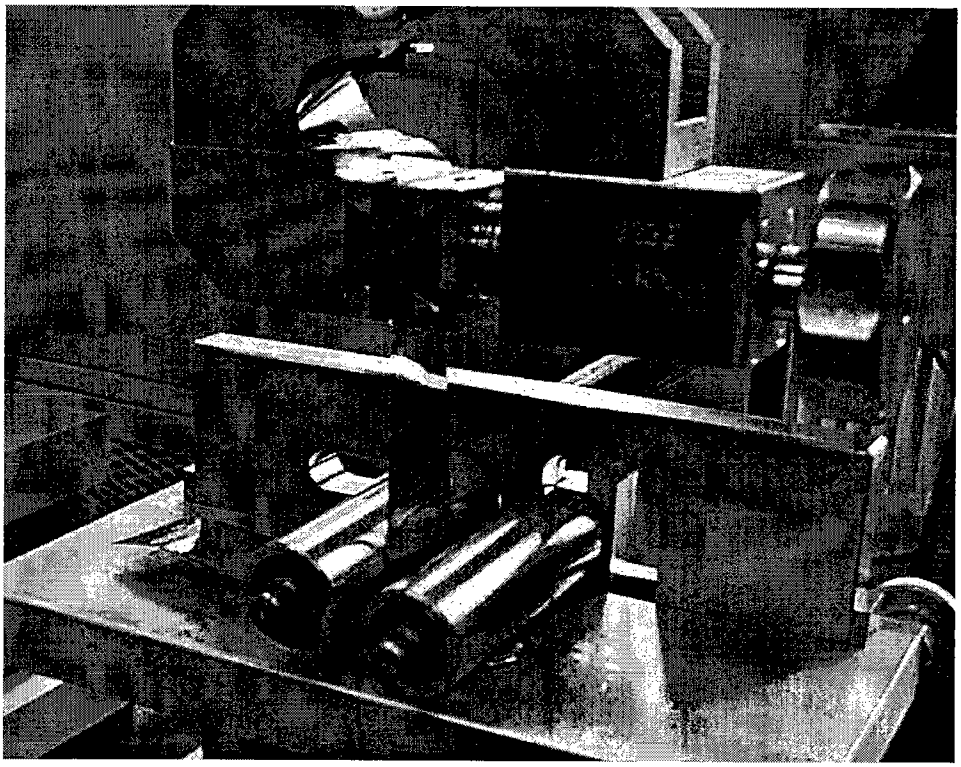

Figure 7.1. Photograph of the experimental set up for the peel test.

References

[1] Comyn, J; Adhesion Science, The royal Society of Chemistry, Cambridge 1997

[2] Stachowiak, E.; *Klebetechnik als Fügeverfahren*, VDI Verlag, Düsseldorf, 1998

[3] Ulman, A.; *Chem Rev.* **1996**, *96*, 1533

[4] Ulman A.; *An Introduction to Ultrathin Organic Films*, Academic Press, Boston, 1991

[5] Whitesides, G; Laibinis. P. E.; *Langmuir* **1990**, *6*, 87

[6] Laibinis, P. E.; Whitesides, G. M.; *J. Am Chem. Soc.* **1992**, *114*,1990

[7] Laibinis, P. E.; Whitesides, G. M.; Allara, D. L.; Tao, Y.-T.; Parikh, A. N.; Nuzzo, R. G.; *J. Am. Chem. Soc.* **1991**, *113*, 7152

[8] Laibinis, P. E.; Bain, C. D.; Nuzzo, R. G.; Whitesides, G. M.; *J. Phys.Chem* **1995,** *99* 7663

[9] Prime, K. L. Whitesides G. M. *Science* **1991**, *252*, 1164

[10] Singhvi R.; Kumar, A.; Lopez, G. P.; Stephanopolus, G. N.; Wang, D. I. C.; Whitesides, G. M.; Ingber, D. E.; *Science* **1994**, *264*, 696

[11] Wirth, M. J.; Fairbank, R. W.; Fatunmbi, H. O.; *Science* **1997**, *275*, 44

[12] Caseri, W.; *Solids with Organic-Inorganic Interfaces, a Contribution to Polymer Nanocomposites and Modified Inorganic Surfaces*, Inaugural Dissertation, ETH Zürich 1994

[13] Davis, G. D.; *Adhesive Bonding*, Ed. Lee, L.-H.; Plenum Press,New York 1991

[14] Xiao, X.; Hu, J.; Charych, D. H.; Salmeron, M.; *Langmuir* **1996**, 12, 235

[15] Feng, Y.; Teo, W.-K.; Siow, K.-S.; Gao, Z. J.; *Electrochem. Soc.* **1997**, *144*, 55

[16] Ramachandran, S.; Tsai, B. L.; Blanco, M.; Chen, H.; *Langmuir* **1996**, 12, 6419

[17] Woods, R.; *Modern Aspects of Electrochemistry*, Vol. 29, Bockris, J. O. M.; Con way, B. E.; White, R. E.; Eds., Plenum Press, New York, 1996

[18] Stewart, K. R.; Whitesides, G. M.; Godfried, H. P.; Silvera, I. F.; *Rev. Sci. Instrum.* **1986**, *57*, 1381

[19] Pluddemann, E. P.; *Silane Coupling Agents*, 2nd ed. Plenum Press, New York, 1991

[20] de Gennes P. G.; *Langmuir* **1996**, *12*, 4497

[21] Glodde, M.; Hartwig, A.; Henneman, O. D.; Stohrer, W. D.; *Int. J. Adhesion Adhesives*, **1998**, *18*, 359

[22] Zhuk, A. V.; Evans, A. G.; Hutchinson, J. W.; Whitesides, G. M.; *J. Mat. Res*, **1998**, *13*, 3555

[23] Choi, G. Y.; Kang, J. F.; Ulman, A; Zurawsky, W.; Fleischer, C.; *Langmuir* **1999**, *15*, 8783

[24] Lunt, S. R.; Ryba,G. N.; Santangelo, P.G.; Lewis N. S.; *J. Appl. Phys.* **1991**, *70*, 7449-7467

[25] Swalen, J. D.; Allara, D. L; Andrade, J. D.; Chandross, E. A.; Garoff, S.; Israelachvili, J.; McCarty, T. J.; Murray, R.; Pease, R. F.; Rabolt, J. F.; Wynne, K. J.; Yu, H.; *Langmuir* **1987**, *3*, 932

[26] Hirayama, M. K. N.; *Ph. D. Thesis Nr 12333*, ETH Zürich, 1997

[27] Mahan, J. E.; *Physical Vapor Deposition of Thin Films*, John Wiley & Sons, New York, 2000

[28] Dekker, J. P.; *Ph. D. Thesis*, Delft, NL, 1994

[29] Kinloch, A.J.; *Adhesion and Adhesives,* Chapman and Hall, London, 1987

[30] Schneider, H. G.; Ruth, V.; Kormany, T.; *Advances in Epitaxy and Endotaxy*, Elsevier, Amsterdam-Budapest 1990

[31] Younan, X., Rogers, J. A.; Paul, K. E.; Whitesides, G. M.; *Chem Rev.* **1999**, *99*, 1823

[32] Tabor, D,; *J. Colloid Interface Sci.* **1980**, *75*, 240

[33] Franklin, B.; *Phil. Trans. R. Soc.* **1774**, *64*, 445

[34] Pockels, A.; *Nature* **1891**, *43*, 437

[35] Pockels, A.; *Nature* **1892**, *46*, 418

[36] Pockels, A.; *Nature* **1893**, *48*, 152

[37] Pockels, A.; *Nature* **1894**, 50, 223

[38] Langmuir, I.; *J. Am. Chem. Soc.* **1917**, *39*, 1848

[39] Blodgett, K. A.; *J. Am. Chem. Soc.* **1935**, *57*, 1007

[40] Blodgett, K. A.; Phys. *Rev.* **1937**, *51*, 964

[41] Brunner, S.; *Ph. D. Thesis Nr 12831*, ETH Zürich 1998

[42] Bigelow, W. C.; Pickett, D. L.; Zisman, W. A.; *J. Colloid Sci.* **1946**, *1*, 513

[43] Shafrin, E. G.; Zisman, W. A.; *J. Colloid Sci.* **1949**, *4*, 571

[44] Schulman, F.; Zisman, W. A.; *J. Colloid Sci.* **1952**, *7*, 465

[45] Sagiv, J.; *J. Am. Chem. Soc.* **1980**, *102*, 92

[46] Bierbaum. K.; Kinzler, M.; Wöll, Ch.; Grunze, M.; Hähner, G.; Heid, S.; Effecberger, F.; *Langmuir* **1995**, *11*, 512

[47] Balachander, N.; Sukenik, C. N.; *Langmuir* **1990**, *6*, 1621

[48] Chaudhury, M. K.; Whitesides, G. M. *Science* **1992**, *255*, 1230

[49] Lee, Y. W.; Reeed-Mundell, J.; Sukenik, C. N.; Zull, J. E.; *Langmuir* **1993**, 9, 3009

[50] Chupa, J. A.; Xu, S.; Fischetti, R. F.; Strongin, R. M.; McCauley, J. P.; Smith, A. B.; Blaise, J. K. J. *J. Am. Chem. Soc.* **1993**, *115*, 4383

[51] Paulson, S.; Morris, K.; Sullivan, B. P. J.; *J. Chem. Soc. Chem. Commun.* **1992**, 1615

[52] Wasserman, S. R.; Biebuyck, H.; Whitesides, G. M.; *J. Mater. Res.* **1989**, *4*, 886

[53] Silberzan, P.; Léger, L.; Aussserré, D.; Benattar, J. J.; *Langmuir* **1991**, *7*, 1647

[54] Wasserman, S. R.; Tao, Y.-T.; Whitesides, G. M.; *Langmuir* **1989**, *5*, 1074

[55] Netzer, L.; Iscovichi, R.; Sagiv, J.; *Thin Solid Films* **1983**, *100*, 67

[56] Maoz, M.; Sagiv, J.; *Langmuir* **1987**, *3*, 1034

[57] Maoz, M.; Sagiv, J.; *Langmuir* **1987**, *3*, 1045

[58] Maoz, M.; Netzer, L.; Gun, J.; Sagiv, J.; *J. Chim. Phys. (Paris)* **1988**, *85*, 1059

[59] Netzer, L.; Iscovichi, R.; Sagiv, J.; *Thin Solid Films* **1983**, *99*, 235

[60] Netzer, L.; Sagiv, J.; *J. Am. Chem. Soc.* **1983**, *105*, 674

[61] Maoz, M.; Sagiv, J.; *Thin Solid Films* **1985**, *132*, 135

[62] Ogawa, K. Mino, N.; Tamura, H.; Hatada, M.; *Langmuir* **1990**, *6*, 851

[63] Ogawa, K. Mino, N.; Tamura, H.; Hatada, M.; *Langmuir* **1990**, *6*, 1807

[64] Pomerantz, M.; Segmüller, A.; Netzer,L.; Sagiv, J.; *Thin Solid Films* **1985**, *132*, 153

[65] Tillman, N.; Ulman, A.; Penner, T. L.; *Langmuir* **1989**, *5*, 101

[66] Li, D. Q.; Ratner, M. A.; Marks, T. J.; Zhang, C. H.; Yang, J.; Wong, G. K. J.; *J. Am. Chem. Soc.* **1990**, *112*, 7389

[67] Kakkar, A. K.; Yitzchaik. S.; Roscoe, S. B.; Kubota, F.; Allan, D. S.; Marks, T. J.; Xu, Z.; Zhang, C. H.; Lin, W.; Wong, G. K. J.; *Langmuir* **1993**, *9*, 388

[68] Yitzchaik. S.; Roscoe, S. B.; Kakkar, A. K.; Allan, D. S.; Marks, T. J.; Xu, Z.; Zhang, C. H.; Lin, W.; Wong, G. K. J.; *J. Phys. Chem.* **1993**, *97*, 6958

[69] Roscoe, S. B.; Kakkar, A. K.; Allan, D. S.; Yitzchaik. S.; Marks, T. J.; Lin, W.; Wong, G. K. J.; *Langmuir* **1994**, *10*, 1337

[70] Tidswell, I. M.; Ocko, B. M.; Pershan, P. S.; Wasserman, S. R.; Whitesides, G. M.; Axe, J. D.; *Phys Rev.* **1990,** *B 41*, 1111

[71] Wegner, G.; *Thin Solid Films* **1992**, *216*, 105

[72] Tripp, C. P.; Veregin, R. P. N.; Hair, M. L.; *Langmuir* **1993**, *9*, 3518

[73] Tripp, C. P.; Hair, M. L.; *Langmuir* **1992**, *8*, 1120

[74] Angst, D. L.; Simmons, G. W.; *Langmuir* **1991**, *7*, 2236

[75] Le Grange, J. D.; Markham, J. L.; Kurjian, C. R.; *Langmuir* **1993**, *9*, 1749

[76] Brandriss, S; Margel, S.; *Langmuir* **1993**, *9*, 1232

[77] Nuzzo, R. G.; Allara, D. L.; *J. Am. Chem. Soc.* **1983**, *105*, 4481

[78] Dubois, L. H.; Nuzzo, R. G.; *Ann .Phys. Chem.* **1992**, *43*, 437

[79] Bain, C. D.; Whitesides, G. M.; *Adv. Mater.* **1989**, *1*, 506

[80] Lee, T. R.; Laibinis, P. E.; Folkers, J. P.; Whitesides, G. M.; *Pure Appl. Chem.* **1991**, *63*, 821

[81] Whitesides, G. M.; Ferguson, G. S.; *Chemstracts-Org. Chem.* **1988**, *1*, 171

[82] Sellers, H.; Ulman, A.; Schnidman, Y.; Eilers, J. E. ; *J. Am. Chem. Soc.* **1993**, *115*, 9389

[83] Ulman, A.; *J. Mat. Ed.***1989**, *11*, 205

[84] Stewart, K.R.; Whitesides, G. M.; Godfried, H. P.; Silvera, I. F.; *Surf. Sci.* **1986**, *57*, 1381

[85] Blackman, L. C. F.; Dewar, M. J. S.; *J. Chem. Soc.* **1957**, 171

[86] Blackman, L. C. F.; Dewar, M. J. S.; Hampson, H.; *J. Appl. Chem.* **1957**, *7*, 160

[87] Troughton, E. B.; Bain, C.D.; Whitesides, G. M.; Nuzzo, R. G.; Allara, D. L.; Porter, M. D.; *Langmuir* **1988**, *4*, 365

[88] Somorjai, G. A.; *Chemistry in two dimensions- Surfaces*, Cornell University Press; Ithaca, 1982

[89] King, D. E.; *J. Vac. Sci Technol.* **1995**, *13*, 1247

[90] Nuzzo, R. G.; Zegarski., B. R.; Dubois, L. H.; *J. Am. Chem. Soc.* **1987**, *109*, 733

[91] Katz, E.; Itzhsk, N.; Wilner, I.; *J. Electroanal. Chem.* **1992**, *336*, 357

[92] Ihs, A.; Uvdal, K.; Liedberg, B.; *Langmuir* **1993**, *9*, 733

[93] Mielczarski, J. A.; Yoon, R. H.; *Langmuir* **1991**, *7*, 101

[94] Cooper, J. M.;Greenough, K. R.; McNeil, C. J.; *J. Electroanal. Chem.* **1993**, *347*, 267

[95] Uvdal, K.; Bodö, P.; Liedberg, B.; *J. Colloid Interf. Sci.* **1992**, *149*, 162

[96] Bain, C. D.; Evall, J.; Whitesides, G. M.; *J. Am. Chem. Soc.* **1989**, *111*, 7155

[97] Bain, C.D.; Troughton, E.B.; Tao, Y-T.; Evall, J.; Whitesides, G.M.; Nuzzo, R.G.; *J. Am. Chem. Soc.* **1989,** *111*, 321

[98] Ulman, A.; Tillman, N.; *Langmuir* **1989**, *5*, 1418

[99] Porter, M. D.; Bright, T. B.; Allara, D. L.; Chidsey, C. D. *J. Am. Chem. Soc.* **1987,** *109*, 3559-3568.

[100] Brust, M.; Walker, M.; Bethell, D.; Schiffrin, D. J.; Whyman, R.; *J. Chem. Soc., Chem. Commun.* **1994**, 801

[101] Thomas, R. C.; Sun, L.; Crooks, M.; *Langmuir* **1991**, *7*, 620

[102] Chailapakul, O.; Sun, L.; Xu, C.; Crooks, M.; *J. Am. Chem. Soc.* **1993**, *115*, 12459

[103] Strong, L. Whitesides G. M. *Langmuir* **1988**, *4*, 546-558

[104] Delamarche, E.; Michel, B.; Kang, H.; Gerber, Ch.; *Langmuir* **1994**, *10*, 4103.

[105] Schlenhoff, J. B.; Li, M.; Ly, H.; *J. Am. Chem. Soc.* **1995**, *117*, 12528

[106] Li, Y.; Huang, J.; McIver, R. T.; Hemminger, J. C.; . *Am. Chem. Soc.* **1992**, *114*, 2428

[107] Folkers, J. P.; Zerkowski, J. A.; Laibinis, P. E.; Seto, C. T.; Whitesides, G. M.; *ACS Symp. Ser.* **1992**, *499*, 10

[108] Zaugg, F.G.; *Ph. D. Thesis Nr 13182*, ETH Zürich 1999

[109] Ferris, M. M.; Rowlen, K. L.; ACS National Meeting, March 26-30, **2000**

[110] Cooper, E.; Leggett, G. J.; *Langmuir* **1998**, *14*, 4795

[111] Cooper, E.; Leggett, G. J.; *Langmuir* **1999**, *15*, 1024

[112] Laibinis, P.E; Palmer, B. J.; Lee, S-W.; Jennings, G. K; In *Thin films, Self-Assembled Monolayers of Thiols*, Ulman, A., Ed.; Academic Press, San Diego, Boston 1998; Vol 24

[113] Nuzzo, R. G.; Dubois, L.H.; Allara, D. L.; *J. Am. Chem. Soc.* **1990**, *112*, 558

[114] Chidsey, C. E. D.; Loiacono, D. N.; *Langmuir* **1990**, *6*, 682

[115] Carey, R. I.; Folkers, J. P.; Whitesides, G. M.; *Langmuir* **1994**, *10*, 2228

[116] Putvinski, T. M.; Schilling, M. L. Katz, H. E.; Chidsey, C. E. D. *Langmuir* **1990**, *6*, 1567

[117] Schilling, M. L. Katz, H. E.;Stein, S. M.; Shane, S.F.; Wilson, W. L.; Buratto, W. S.; Ungashe, S. B.; Taylor, G. N.; Putvinski, T. M.; Chidsey, C. E. D. *Langmuir* **1993**, *9*, 2156

[118] Lee, T. R.; Carey, R.I.; Biebuyck, H. A.; Whitesides, G. M.; *Langmuir* **1994**, *10*, 741

[119] Pale-Grosdemange, C.; Simon, E. S.; Prime, K. L.; Whitesides, G. M.; *J. Am. Chem. Soc.* **1991**, *113*, 12

[120] Prime, K. L.; Whitesides, G. M.; *J. Am. Chem. Soc.* **1993**, *115*, 10714

[121] Deng, L.; Mrksich, M.; Whitesides, G. M.; *J. Am. Chem. Soc.* **1996**, *118*, 5136

[122] Neogi, P.; Neogi,S.; Stirling C. J. M.; *J. Chem. Soc. Chem. Commun.* **1993**, 1134

[123] Robinson, G. N.; Freedman, A.; Graham, R. L.; *Langmuir* **1995**, *11*, 2600

[124] Graham, R. L.; Bain, C. D.; Biebuyck, H. A.; Laibinis, P. E.; Whitesides, G. M.; *J. Phys. Chem.* **1993**, *97*, 9456

[125] Xiao, S.-J.; *Tailored Organic Thin Films on Gold and Titanium*, Ph.D. Thesis, ETH-Zürich 1999

[126] Willner, I.; Riklin, A.; Shoham, B.; Rivenson D.; Katz, E.; *Adv. Mater.* **1993**, *5*, 912

[127] Arias, F.; Godinez, L. A.; Wilson, S. R.; Kaifer, A. E.; Ehegoyen, L.; *J. Am. Chem. Soc.* **1996**, *118*, 6086

[128] Duevel, R. V.; Corn, R. M.; *Anal. Chem.* **1992**, *64*, 337

[129] Dermody, D. L.; Crooks, R. M.; Kim, T.; *J. Am. Chem. Soc.* **1996**, *118*, 11912

[130] Kim, T.; Crooks, R. M.; Tsen, M; Sun, L.; *J. Am. Chem. Soc.* **1995**, *117*, 3963

[131] Yan, L.; Huck, W. T. S.; Zhao, X.-M.; Whitesides, G. M.; *Langmuir* **1999**, *15*, 1208

[132] Frey, B. L.; Corn, R. M.; *Anal. Chem.* **1996**, *68*, 3187

[133] Guiomar, A. J.; Guthrie, J. T.; Evans, S. D.; *Langmuir* **1999**, *15*, 1198

[134] Bertilsson, L.; Liedberg, B.; *Langmuir* **1993**, *9*, 141

[135] Pan, S.; Castner, D. G.; Ratner, B. D.; *Langmuir* **1998**, *14*, 3545

[136] Bent, S. F.; Schilling, M. L.; Wilson, W. L.; Katz, H. E.; Harris, A. L.; *Chem. Mater.* **1994**, *6*, 122

[137] Löfås, S.; Johnson, B.; *J. Chem. Soc. Chem. Commun.* **1990**, 1526

[138] Himmel, H.-J.; Weiss, K.; Jäger, B.; Dannenberger, O.; Grunze, M.; Wöll, Ch. *Langmuir* **1997**, *13*, 4943

[139] Spencer, N. D.; *Surfaces and Interfaces*, Lecture notes ETH Zürich, 1997

[140] Colthup, N. B.; Daly, L. H.; Wiberly, S. E.; *Introduction to Infrared and Raman Spectroscopy,* Academic Press, San Diego 1990

[141] Binnig, G.; AFM Paper *Phys. Rev. Mod.* **1986**, *56*, 930

[142] Tompkins, H. G.; *A Users Guide to Ellipsometry*, Academic Press, San Diego 1993

[143] Chapman, R. G.; Ostuni, E.; Yan, L.; Whitesides, G. M.; *Langmuir* **2000**, *16*, 6927

[144] Buttry, D. A.; Ward, M. D.; *Chem Rev.* **1992**, *92*, 1355-1379

[145] Buttry, D. A.; Ward, M. D.;*Science* **1990**, *249*, 1000-1007

[146] Fibbioli, M.; *Ph. D. Thesis Nr 13789*, ETH-Zürich 2000

[147] Zhao, X.-M.; Wilbur, J. L.; Whitesides, G. M.; *Langmuir* **1996**, *12*, 3257

[148] Suter, U. W.; *Polymer Chemistry I*, Lecture notes ETH Zürich, 1996

[149] Young, T.; *Miscellanous works*, Peacock, G., Ed.; Murray, London 1855

[150] Bikerman, J. J.; *Physical Surfaces*, Academic Press, New York , 1970

[151] Zisman ,W. A.; *Adv. Chem. Ser.* **1964**, *43*, 1

[152] Adamson, A. W.; *Physical Chemistry of Surfaces*, John Wiley & Sons, New York, 1990

[153] De Gennes, P.G.; *Rev. Mod. Phys.* **1985,** *57*, 827

[154] Bartell, F. E.; Shepard, J. W.; *J. Phys. Chem.* **1953**, *57*, 211

[155] Shepard, J. W.; Bartell, F. E.; *J. Phys. Chem.* **1953**, *57*, 458

[156] Cassie, A. B. D.; *Discuss. Faraday Soc.* **1948**, *3*, 11

[157] Israelachvili, J. N.; *Intermolcular and Surface Forces*; Academic Press: London, New York, 1990

[158] Israelachvili, J. N.; Gee, M. L.; *Langmuir* **1989**, *5*, 288

[159] Johnson, R. E. Jr.; Dettre, R. H.; In *Surface and Colloid Science*, Matijevic, E., Ed.; Wiley-Interscience New York, 1969; Vol 2

[160] Schwartz, L. W.; Garoff, S. J.; *Langmuir* **1985**, *1*, 219

[161] Schwartz, L. W.; Garoff, S. J.; *J. Colloid Interface Sci.* **1985**, *106*, 422

[162] Hähner, G.; *personal communication*

[163] Overney R.; Meyer, E.; *MRS Bulletin,* **1993**, *18*, 26

[164] Halliday, D.; Resnick, R.; *Fundamentals of Physics*, 3rd Ed.; John Wiley & Sons, New York 1988

[165] Siegbahn, K.; Nordling, C.; Fahlman, A.; Nordberg, R.; Hamrin, K.; Hedman, J.; Johansson, G.; Bergmark, T.; Karlsson, S.-E.; Lindgren, I.;Lindberg, B.; *ESCA* -

Atomic, Molecular and Solid State Structure Studied by Means of Electron Spectroscopy. Nova Acta Regiae Soc. Sci. Upsaliensis Ser IV, Vol. 20; North-Holland Publ. Comp., Amsterdam-London 1967

[166] Siegbahn, K.; Nordling, C.; Johansson, G.; Hedman, J.; Heden, P. F.; Hamrin, K.; Gelius, U.; Bergmark, T.; Werme, L. O.; Manne, R.; Baer, Y.; *ESCA Applied to Free Moelcules*, North-Holland Publ. Comp., Amsterdam-London 1969

[167] Moulder, J. F.; Stickle, W. F.; Sobol, P. E.; Bomben, K. D.; *Handbook of X-Ray Photoelectron Spectroscopy*, Chastain, J., Ed.; Perkin-Elmer Corporation, Minnesota,

[168] Siegbahn, K.; *Science*, **1982**, *217*, 111

[169] Ebel, M. F.; *Angewandte Oberflächenanalyse*, Grassbauer, M.; Dudek, H. J.; Ebel, M. F.; Eds.; Springer, Berlin 1986

[170] Tanuma, S.; Powell, C. J.; Penn, D. R.; *Surf. Interface Anal.*, **1991**, *17*, 911

[171] Chou, N. J.; *New Characterisation Techniques for Thin Polymer Films*, Tong, H.-M.; Nguyen, L. T., Eds.; John Wiley & Sons, New York 1990

[172] Beamson, G.; Briggs, D.; *High Resolution XPS of Organic Polymers*, John Wiley & Sons, Chichester, 1992

[173] Briggs, D.; Sheah, M. P.; *Practical Surface Analysis*, Vol 1, John Wiley & Sons Chichester, 1990

[174] Mårtensson, N.; *Analytical Techniques for Thin Films,* Tu, K. N.; Rosenberg, R.; Eds.; Academic Press, Boston 1988

[175] Castner, D. G.; *Functionalized Surfaces: Applications and Analytical Tools*, Keller, B.; Textor, M.; Eds.; ETH Zürich 1999

[176] Eischen, R. P.; Plisken, W. A.; Sims, M. L.; *J. Phys. Chem.*, **1954**, *22*, 1786

[177] Colthup, N. B.; Daly, L. H.; Wiberly, S. E.; *Introduction to Infrared and Raman Spectroscopy,* Academic Press, San Diego 1990

[178] Steiner, U. B.; *Ph. D. Thesis Nr 10428*, ETH Zürich 1994

[179]Hayden, B. E.; *Vibrational Spectroscopy of Molecules on Surfaces,* Yates Jr, J. T.; Madey, T. E.; Eds.; Plenum Press, New York 1987

[180] Suëtaka, W. ; *Methods of Surface Characterization vol 3: Surface Infrared and Raman Spectroscopy, Methods and Application*; Plenum Press, New York 1995

[181] Bradshaw, A. M.; Schweizer, E.; *Spectroscopy of Surfaces (Advances in Spectroscopy Vol. 16)*, Clark, R. J. H.; Hester, R. E.; Eds.; John Wiley & Sons, Chichester 1988

[182] Swalen, J. D.; Rabolt, J. F.; *Fourier Transform Infrared Spectroscopy*, Ferraro, J. R.; Basile, L. J.; Eds.; Academic Press, Orlando 1985

[183] Blanke, J. F.; Vincent, S. E.; Overend, J.; *Spectrochim. Acta, Part A*, **1976**, *32*, 163

[184] Hoffman, F. M.; *Surf. Sci. Reports*, **1983**, *3*, 109

[185] Tompkins, H. G.; *A Users Guide to Ellipsometry*, Academic Press, San Diego 1993

[186] Troughton, E. B.; Bain, C. D.; Nuzzo, R. G.; Allara D. L.; Porter, M. D.; *Langmuir*, **1988**, *4*, 365

[187] Kinloch, A. J.; *Adhesion and Adhesives, Science and Technology*, Chapman and Hall, London 1987

[188] Habenicht, G.; *Kleben: Grundlagen, Technologie, Anwendungen*, Springer-Verlag, Berlin 1997

[189] Lee, L.-H.; *Fundamentals of Adhesion,* Ed. Lee, L.-H; Plenum Press, New York 1991

[190] Lee, L.-H.; *Adhesive Bonding*, Ed. Lee, L.-H.; Plenum Press, New York 1991

[191] Atkins, P. W.; *Physical Chemistry*, 4th Edition, Oxford University Press, Oxford 1992

[192] Wu, S.; *Polymer Interface and Adhesion*, Marcel Dekker, New York, 1982

[193] Huntsberger, J. R.; *Treatise on Adhesion and Adhesives,* Vol. 1, (Ed. R. L. Patrick) Marcel Dekker, New York 1967

[194] Huntsberger, J. R.; *Adhesive Age*, **1970**, *13*, 43

[195] Orrowan, E.; *J. Franklin Inst.*, **1970** *290*, 493

[196] Tabor, D.; R*ep. Prog. Appl. Chem.,* **1951**, *36,* 621

[197] Klein, I. E.; Sharon, J.; Yaniv, A. E.; Dodiuk, H.; Katz, D.; Int. J. Adhesion Adhesives, **1983**, *3,* 159

[198] Miller, J. D.; Ishida, H.; *Fundamentals of Adhesion,* Ed. Lee, L.-H; Plenum Press, New York 1991

[199] Andrews, E. H; Kinloch, A. J.; *Proc. Roy. Soc.* **1973**, *A332*, 385

[200] Pauling, L.; *The Nature of the Chemical Bond,* Cornell University Press, New York 1960

[201] Good, R. J.; *Treatise on Adhesion and Adhesives,* Vol. 1, (Ed. R. L. Patrick) Marcel Dekker, New York 1967

[202] Fowkes, F. M.; *Physiochemical Aspects of Polymer Surfaces,* Vol 2. Ed. Mittal, K. L.; Plenum Press, New York 1983

[203] Klein, I. E.; Sharon, J.; Yaniv, A. E.; Dodiuk, H.; Katz, D.; *Int. J. Adhesion Adhesives*, **1983**, *3*, 159

[204] Shaw, D. J.; *Colloid and Surface Chemistry*, Butterworth Heinemann, Oxford 1989

[205] Anderson, G. P.; Bennett, J. S.; DeVries, K. L.; *Analysis and Testing of Adhesive Bonds*, Academic Press, New York 1977

[206] Goussev, O. A.; Zeman, K.; Suter, U. W.; *J. Adhesion*, **1996**, *56*, 45

[207] Bain, C. D.; Whitesides, G. M.; *J. Am. Chem. Soc.* **1988**, *110*, 6560

[208] Bain, C. D.; Whitesides, G. M.; *Angew. Chem. Int. Ed. Engl.* **1989**, *28*, 506

[209] Bain, C. D.; Whitesides, G. M.; *J. Am. Chem. Soc.* **1989**, *111*, 7164

[210] Persson, H. H. J.; Caseri, W.; Suter, U. W.; *Langmuir*, accepted for publication

[211] Lynch, D. W.; Hunter, W. R.; *Handbook of Optical Constants of Solids*, Palik, E. D.; Ed; Academic Press, New York 1985

[212] Wagner, P.; *Ph. D. Thesis Nr 11134*, ETH Zürich 1995

[213] Ulman, A.; Evans, S. D.; Shnidman,Y.; Sharma, R.; Eilers, J. E.; *Advances in Colloid and Surface Science*, **1992**, *39*, 175-224

[214] Arnold, R. G.; Nelson, J. A.; Verbanc, J. J.; *Chem. Rev.* **1957**, *57*, 47

[215] Waser, J.; Trueblood, K. N.; Knobler, C. M.; *Chem One (2nd Ed)*, McGraw-Hill, Singapore 1982

[216] Tillman, N.; Ulman, A.;Schildkraut, J. S.; Penner, T. L.; *J. Am. Chem. Soc.* **1988,** *111,* 6136

[217] Weast, R. C.; Ed; *Handbook of chemistry and Physics*; CRC; Boca Raton, FL **1995**

[218] Nissink, J. W. N.; *PhD Thesis*, **1999,** Utrecht, NL

[219] Andrade J. D.; *Surface and Interfacial Aspects of Biomedical Polymers (Volume 1, Surface Chemistry and Physics)*, Plenum Press, New York XXXX

[220] Laibinis, P. E.; Bain, C. D.; Whitesides, G. M.; *J. Phys. Chem.* **1991**, *95*, 7017

[221] Zisman, W. A.; *Adv. Chem. Ser.* **1964**, *43*, 1

[222] Carre, A.; Vial, J. In *Preprints EURADH '92*; Schultz, J.; Brockmann, W., Eds.; DECHEMA: Frankfurt am Main, 1992, p. 90.

[223] Hayes, W. A.; Kim, H.; Yue, X.; Perry, S. S.; Shannon, C.; *Langmuir* **1997**, *13*, 2511

[224] Bain, C. D.; Whitesides, G. M.; *J. Am. Chem. Soc.* **1988**, *110*, 5897

[225] Steiner, U. B.; Caseri, W. R.; Suter, U. W.; *Langmuir*, **1992**, *8*, 2771

[226] Steiner, U. B.; Caseri, W. R.; Suter, U. W., Rehahn, M.; Schmitz, L.; *Langmuir*, **1993**, *9*, 3245

[227] Steiner, U. B.; Caseri, W. R.; Suter, U. W., Rehahn, M.; Rau, I.; *Langmuir*, **1994**, *10*, 1164

[228] Yan, L.; Marzolin, C.; Terfort, A.; Whitesides, G. M.; *Langmuir* **1997**, *13*, 6704

[229] Hirayama, M.; Caseri, W. R.; Suter, U. W.; *J. Colloid Interface Sci.* **1998**, *202*, 167

[230] Brunner, S.; Caseri, W. R.; Suter, U. W.; Hähner, G.; Brovelli, D.; Spencer, N. D.; Vinckier, A.; Rau, I. U.; Galda, P.; Rehahn, M.; *Langmuir*, **1999**, *15*, 6333

[231] Folkers, J. P.; Laibinis, P. E.; Whitesides, G. M.; *Langmuir* **1992**, *8*, 133

[232] Tanahashi, M.; Matsuda, T,; *J. Biomed. Mater. Res.*,**1997**, *34*, 305

[233] Lee, J. H.; Park, J. W.; Lee, H. B.; *Biomaterials*,**1991**, *12*, 443

[234] Gruber, U.; Kramer, E.; *personal communication*

[235] Lee, H.; Neville, K.; *Handbook of Epoxy Resins*, McGraw-Hill, New York, 1967

[236] Webster, H. F.; Wightman, J. P.; *Acid-Base Interactions: Relevance to Adhesion Science and Technology,* Mittal, K. L.; Anderson, J. R.; Eds; VSP, Utrecht 1991

[237] Possart, W.; Müller, I.; *Phys. Status Solidi A*, **1988**, *106*, 525

[238] Possart, W.; *Int. J. Adhes., Adehes.*, **1988**, *8*, 77

[239] Stryer, L.; *Biochemistry*, 3rd Ed.,W. H. Freeman and Company, New York 1988

[240] Pimentel, G.; McClellan, A. L.; *The Hydrogen Bond*, W. H. Freeman and Company, San Francisco, 1960

Acknowledgement

I am very much indebted to Prof. Dr. Ueli Suter not solely for his confidence in entrusting me with an interesting research project but also for his scientific, educational, and personal wisdom which has been a continuous source of inspiration.

I would also like to express my deepest gratitude to PD Dr. Walter Caseri for his excellent experimental advice, thorough corrections of this thesis, and for his never ending enthusiasm regarding my ideas.

Further I would like to thank Prof. Dr. Nicholas D. Spencer for being my co-examiner and for allowing me to use his XPS-machines.

A special thanks to Dr. Samuel Brunner and Dr. Martina Hirayama for introducing me to experimental techniques, analytical tools as well as providing a most welcoming atmosphere in the lab.

I am very grateful to Dr. Olga Goussev for her skilful advice regarding adhesion measurements.

I thank all the people at the Laboratory for Surface Science and Technology (LSST) for teaching me the secrets of XPS, giving me helpful advice and supporting me in the accomplishment of the XPS-measurements.

Thanks also to Prof. Dr. Erich Kramer and Dr. Urs Gruber at Ciba Speciality Chemicals for their kind introduction to the world of epoxy adhesives.

I very much enjoyed the fruitful cooperation with Lydia Feller, Giona Kilcher and Rosalind Perrin who carried out some of their student projects within the frames of this thesis.

I also would like to thank all former and current colleagues at the Institute of Polymers for their support, friendship, and contribution to the nice atmosphere. They, as well as all other friends have made my stay in Zürich a most enjoyable and fruitful period in my life.

Finally, my very special thanks goes to those who shared with me the hard but memorable moments, either in the lab or during those wonderful early mornings in a rowing boat on lake Zürich. Those are things that I will not forget.

Curriculum Vitae

Personal Data

Name	Hans Johan Henrik Persson
Date of Birth	July 18th, 1970
Place of Birth	Halmstad, Sweden
Nationality	Swedish
Marital status	Single

Education

09/1996 –	Doctoral candidate Department of Material Science, ETH Zürich, Switzerland Advisor: Prof. U.W. Suter, Institute of Polymers
08/1996	Master of Science in Chemical Engineering, Lund University, Sweden Diploma thesis "Surface Modifications of Polyetylene for Medical Implants" under supervision of Prof B. W. Wesslèn and Prof. L.-M. Bjursten, Institute of Technology
10/1994 – 07/1995	Exchange student, ETH Zürich, Switzerland
08/1991 – 08/1996	Undergraduate student in chemical engineering, Institute of Technology, Lund University, Sweden
07/1989 – 01/1991	Reserve officer education at Airforce Academy, Halmstad and Stockholm, Sweden
08/1986 – 06/1989	High School, Kristianstad, Sweden
08/1977 – 06/1986	Primary School, Kristianstad, Sweden

Professional Experience

03/1997 –	Teaching assistant in the courses "Polymere: eine Einführung, Polymere I, Makromolekulare Chemie I"and "Werkstoffpraktikum II" at ETH Zürich, Switzerland

06/1994 – 08/1994	Internship at TSE Industries Inc. Clearwater FL, USA Development of polyester-polyols
06/1993 – 08/1993	Program director at Maine State YMCA camp, Winthrop ME, USA
06/1992 – 08/1992	Unit leader at Maine State YMCA camp, Winthrop ME, USA
06/1991 – 08/1991	Campleader at Maine State YMCA camp, Winthrop ME, USA
03/1991 – 05/1991	Temporarary teacher in german, mathematics and chemistry, Kristianstad, Sweden

Languages

Swedish	mother tongue
English	fluent
German	fluent